University Transportation Research Center - Region 2

FINAL REPORT

Experimental Study on Pre-stressed Concrete Box Beams From a Decommissioned Bridge Strengthened with Carbon Fiber Reinforced Polymer Anchors and Laminates

Seyedsina Yousefianmoghadam, Ph.D. and Andreas Stavridis, Ph.D.

November 2023

Performing Organization

University at Buffalo

Prepared for

NEW YORK STATE OF OPPORTUNITY. Department of Transportation

DISCLAIMER

This report was funded in part through grant(s) from the Federal Highway Administration, United States Department of Transportation, under the State Planning and Research Program, Section 505 of Title 23, U.S. Code. The contents of this report do not necessarily reflect the official views or policy of the United States Department of Transportation, the Federal Highway Administration or the New York State Department of Transportation. This report does not constitute a standard, specification, regulation, product endorsement, or an endorsement of manufacturers.

ACKNOWLEDGEMENTS

The authors would like to thank the New York State Department of Transportation for funding this study. The guidance of Jonathan Kunin, the NYSDOT Project Manager was crucial for the successful completion of this study. Moreover, Ryan Lund provided thoughtful feedback. James Troise and Perry Gernold provided valuable support in the field and addressed many challenges beyond those anticipated, as this phase took place in Spring 2020, during the initial outbreak of Covid-19. The support of Scott Arnold, Serge Roux, and Bill Alexander, all of Fyfe Co., is gratefully acknowledged. The study would not have been possible without the material contributions as well as their assistance with the design and application of the retrofit schemes. The authors would also like to thank Jorge Miguel Romero Loyola, Rohit Singh, Rohan Tanna, and Juan Carlos Singaucho Armas, graduate students at the University at Buffalo, for their help with the installation of the anchors and laminates. The cooperation of Lynn Gorski and the staff at CatCo during the demolition of the bridge on J.J. Audubon Parkway and the transportation of the beams to and from the Structural and Earthquake Engineering Laboratory at the University at Buffalo is also appreciated. Moreover, the authors would like to thank Mr. Lawrence Matthews and Mr. Jerry O'Connor for bringing to the attention of the principal investigator the prospect about the bridge replacement and for their assistance in initiating the discussions about the project with NYSDOT and the other stake holders. Finally, the support of UTRC and Professor Camille Kanga in addressing all logistical challenges due to the timing of this study is gratefully acknowledged. The opinions expressed in this report are those of the authors and do not necessarily represent those of the sponsor or the collaborators.

USDOT Form DOT F 1700.7 Technical Report Documentation Page

1. Report No. C-17-13	2. Government Accession No.	3. Recipient's Catalog No.	
4. Title and Subtitle Experimental Study on Pre-tressed Concrete Box Beams from a Decommissioned Bridge Strengthened with Carbon Fiber Reinforced Polymer Anchors and Laminates		5. Report Date November, 2023 6. Performing Organization Code	
7. Author(s): Seyedsina Yousefianmoghadam and Andreas Stavridis		8. Performing Organization Report	
9. Performing Organization Name and Address: University at Buffalo 224 Ketter Hall, Buffalo NY 14260-1660		10. Work Unit No. 11. Contract or Grant No.	
12. Sponsoring Agency Name and Address: NYS Department of Transportation 50 Wolf Road Albany, New York 12232		13. Type of Report and Period Covered Final Report 14. Sponsoring Agency Code	
15. Supplementary Notes: Project funded in part with funds from the Federal Highway Administration.			
16. Abstract This report discusses the findings of an experimental program involving the tests to failure of three 57-ft long pre-stressed concrete box beams strengthened with Carbon Fiber Reinforced Polymer (CFRP) laminates and CFRP anchors. The beams were obtained from a highway bridge, located in Buffalo, NY, which was replaced after 37 years in service due to extensive deterioration. The goal of the study was to investigate the effectiveness of the strengthening method and the influence of design variations of the strengthening when applied to deteriorated beams. The beams were extensively instrumented with displacement transducers and strain gauges and were subjected to four-point bending tests. The tests were conducted at the service- and capacity levels prior to and after the retrofit. Service-level tests simulated the vehicular load as per AASHTO specifications. The capacity-level tests examined the behavior of the retrofitted beam under extreme loads until failure. As discussed in this report, the capacity of the beams increased up to 50% compared to the strength of the unretrofitted beam.			
17. Key Words: Bridge retrofit, Prestressed concrete box beams, FRP laminate, FRP anchorage, Full-scale testing.	18. Distribution Statement No Restrictions		
19. Security Classif. (of this report) Unclassified	20. Security Classif. (of this page) Unclassified	21. No. of Pages 97	22. Price

EXECUTIVE SUMMARY

This study, conducted at the University at Buffalo (UB), addresses the need to increase the flexural capacity of deteriorated pre-stressed concrete box beams through an experimental campaign involving the design, application, and testing of a retrofit scheme. The retrofit methodology considered here involves the use of carbon fiber reinforced polymer (CFRP) laminates which are attached to the beams using epoxy and CFRP anchors. As part of the study, three 57-ft long beams were cautiously extracted during the demolition of a bridge on J.J. Audubon Parkway in Buffalo, NY and were transported to the SEES Laboratory at UB.

When delivered in the lab, the beams were cleaned, and their bottom surface was prepared for the application of the CFRP retrofit. Besides cleaning, the surface preparation involved patching of cavities with epoxy, and grinding to increase the roughness according to Technical Guideline No 310.2 of the International Concrete Repair Institute. Holes were also drilled to allow the installation of the CFRP anchors. The layout of the anchors, as well as the thickness of the CFRP laminates, varied between the three specimens to investigate their effect on the structural performance. All beams were tested under service loads before they were retrofitted to evaluate their structural condition prior to the retrofit application. Once strengthened, they were tested to failure with a four-point bending test set up using two 440-kip actuators.

The first beam included three layers of laminate, an anchor-to-laminate ratio of 0.5, and 14 anchors distributed at the ends and the two quarter-length points of the beam where the sections were solid concrete. The beam reached a moment 22% higher than the capacity of the unretrofitted beam. At that load, the anchors and laminate pulled away due to the failure of the concrete cover, which exposed the beam reinforcement.

The second beam included two layers of CFRP laminate, an anchor-to-laminate ratio of 0.8, and 14 anchors, distributed as in the case of the first beam on one end, but in three cross sections on the other end. The beam reached a moment 46% higher than the capacity of the unretrofitted beam. Its damage pattern included debonding of the laminate and failure of the concrete cover.

The third beam included a single layer of laminate, an anchor-to-laminate ratio of 1.2, and 14 anchors located near the ends of the beam, but within the hollow section. This beam reached a moment 50% higher than the moment capacity of the unretrofitted beam. The damage pattern was dominated by the debonding and the subsequent fracture of the CFRP laminate. This beam exhibited the largest ductility, as it reached a beam end rotation of 3.4 degrees, which corresponded to a displacement of 16 in. at the beam midspan.

The research presented in this report provides much needed experimental data for the behavior of deteriorated beams retrofitted with CFRP laminates and anchors. The tests on the beams obtained from an actual bridge after 37 years of service indicate the feasibility and effectiveness of the retrofit scheme. They also demonstrate that differences in the design of the retrofit scheme, i.e. the thickness of the laminate and the distribution of the anchors can lead to drastically different failure patterns. However, in all cases the adopted retrofit scheme increases the stiffness, and mainly the strength, and ductility of the beams. The increase in strength and ductility was larger after the application of smaller thickness of FRP laminates.

TABLE OF CONTENTS

LIST OF FIGURES

LIST OF TABLES

CHAPTER 1
INTRODUCTION

1.1 Problem Statement

The replacement of concrete bridges that are deteriorated due to harsh climate conditions, years before they reach the end of their design service life, is financially and environmentally costly. The severity of this problem becomes more evident when considering the large inventory of deteriorated bridges in the United States. According to the National Bridge Inventory database (NBI 2020) there are 66,000 box-girder concrete highway bridges, over 12% of which are structurally deficient. The development of reliable and efficient retrofit schemes, that can extend the service life of these bridges, is a considerably less demanding alternative to the replacement of such structures. Generally, this process includes i) the selection of appropriate retrofit method among the different available options considering the condition of the bridge and any possible access constraints, ii) the design of the optimal retrofit scheme considering the design objectives, and iii) the application of the proposed scheme in the field.

This report presents the research conducted at the University at Buffalo focusing on the strengthening of existing bridge girders. The research program involved the tests of three girders obtained during the demolition of a deteriorated nearby bridge, 36 years after it was constructed.

This chapter reviews the available background and knowledge in these areas and highlights the current shortcomings with respect to applications for prestressed concrete box-beam bridges. Chapter 2 discusses important design details for the bridge and its condition prior to the tests. Chapter 3 presents the retrofit design and method of application. In Chapter 4 the test set up is presented. Chapter 5 discusses the test results, and Chapter 6 summarizes the findings and conclusions of the tests.

1.2 Retrofit Schemes

Bridges are typically retrofitted to restore or increase the flexural or shear capacity of their structural elements, and/or to limit the deflection and crack sizes during their continued use. There are a variety of retrofit methods using Fiber Reinforced Polymers (FRP) or similar materials that have been considered in the past. These include non-prestressed and prestressed carbon fiber reinforced polymers (CFRP), unbonded and bonded post-tensioned CFRP, and near-

surface mounted (NSM) reinforcement (Fathelbab et al., 2014; Harries et al. 2009; Klaiber et al., 2004; Obaidat et al., 2011; Shahawy & Beitelman, 1999). Retrofit schemes that utilize CFRP have been found to increase the cracking moment, restore a portion of the original flexural strength, and extend fatigue life (Kim et al., 2008; Larson et al., 2005). The application of NSM reinforcement can be challenging, but it can improve the flexural and shear strength (De Lorenzis & Nanni, 2001; Dias & Barros, 2005; Parretti & Nanni, 2004). Experiments in the past have been conducted to determine the feasibility of using Fiber-Reinforced Polymers (FRP) in place of steel plates and other methods to repair bridges (Parretti & Nanni, 2004; Rahimi & Hutchinson, 2001; Ritchie, 1989).

The use of epoxy to adhere the FRP to the concrete beams is one of the most common methods used in retrofit schemes (Ritchie, 1989). However, this installation method usually suffers from a premature failure mode known as debonding. This phenomenon occurs when the FRP reinforcement pulls away from the structure and can no longer transfer loads. A number of studies have focused on evaluating the bond behavior of an FRP reinforced member (Hassan & Rizkalla, 2003; Rosenboom, 2006). Some ways to mitigate the debonding failure are to add U-wraps to hold the FRP to the beam or wrap the entire beam. However, such mitigation strategies cannot be implemented in the case of box beams where there is not sufficient space to go around an individual beam. In such cases, the use of anchors has proven beneficial in reducing and/or delaying the debonding of FRP laminates from concrete members (Ceroni et al., 2008; Martin & Lamanna, 2008; Panchacharam & Belarbi, 2002). By incorporating anchors into the design, the beam can achieve failure modes related to concrete crushing or steel yielding.

1.3 Testing Setups

Three- or four-point-bending test setups have been typically used to test prestressed concrete beams with and without retrofit schemes. (Avendano et al., 2013; Brecht et al., 1965; Harries, 2009; Naito et al., 2008). The former testing method requires a considerably simpler test setup compared to the latter one. On the other hand, the four-point bending setup provides a region of constant maximum moment, allowing for the development of the flexural failure over a segment of the retrofitted system rather than a single section. Also, the distance between the loading points in the four-point-bending tests can be adjusted to emulate the vehicular load patterns. As

discussed in Chapter 3, in this study the four-point bending setup is adopted, despite its complexity, as it is more realistic and allows for a better understanding of the structural behavior. Instrumentation schemes used to measure engineering response quantities, such as strains and deflections may include a variety of sensor types, such as strain gauges, displacement transducers (e.g. linear variable differential transducers (LVDTs), linear potentiometers, and string pots), as well as optical sensors (e.g. fiber optic sensors and laser devices). In this study strain gauges were applied on the concrete and FRP surface, while string pots were used to measure the deflection of the concrete beams.

CHAPTER 2

TEST STRUCTURE

2.1 Test Structure Description

The focal point of this project was a pair of deteriorated highway bridges which were slated for demolition. Each bridge, shown in Figure 2-1, had three spans and a total length of 193 ft. The two bridges served the northbound and southbound traffic on JJ Audubon Parkway in Amherst, NY. Both structures were built in 1983 to cross the Ellicott Creek stream. The bridge coordinates were 43°00'30.4"N, 78°46'49.6"W.

a) Northbound structure

b) Southbound structure

Figure 2-1 Overall view of the bridge

2.1.1 Design Overview

The plan view of the superstructures, including the overall dimensions and layout of the box beams as well as the typical cross sections are shown in Figure 2-2a and Figure 2-2b, respectively. The northbound and the southbound superstructures were comprised of 14 and 11

adjacent prestressed box beams, respectively. Two types of AASHTO box-beam cross sections were used in the deck construction, namely, Type BI-36 (3-ft. wide) and Type BI-48 (4-ft. wide) (AASHTO, 2017). The deck also included a concrete slab, shown in Figure 2-2b, which had a thickness varying from 6 in. to 7 7/8 in.

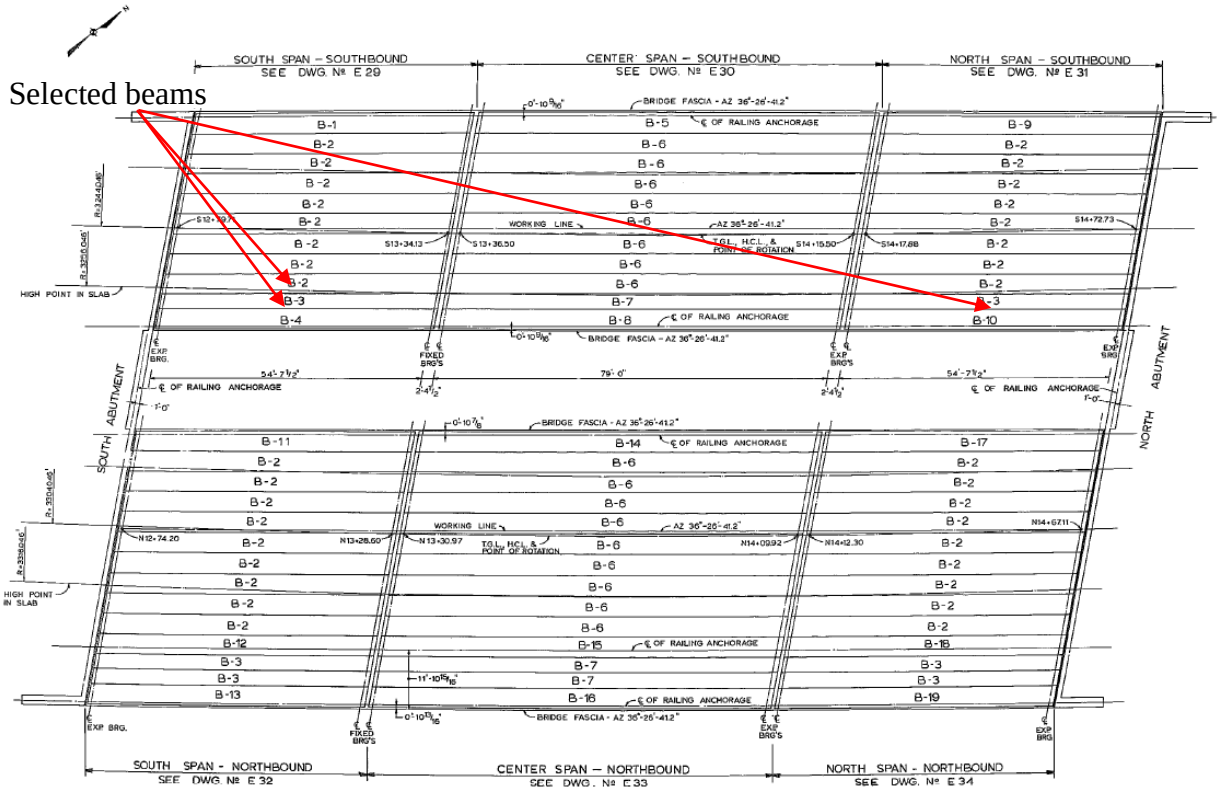

a) Superstructure plan view

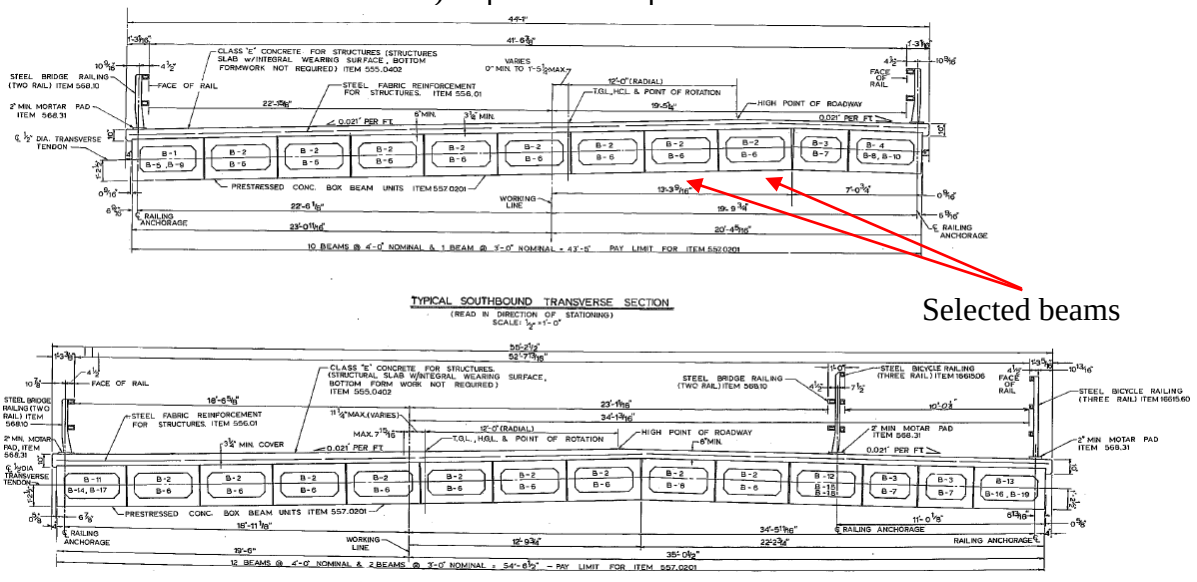

b) Superstructure typical sections

Figure 2-2 Overall layouts and geometry of the bridge

2.1.2 Observed Deterioration

Since their construction, the bridges were subjected to severe winter conditions and consequently. Hence, they deteriorated mainly due to freeze and thaw cycles and the significant use of deicing chemicals. The deteriorated condition was documented during regular site inspections conducted by NYSDOT. The results indicated extensive surface concrete spalling with exposed stirrup bars in facia girders. The spalling covered more than 30% of the vertical face of the exterior beams. Also, concrete spalling was observed at the end block of the prestressed beams, exposing the stirrups and prestressing tendons. Figure 2-3 presents examples of observed deterioration. A Yellow Flag was issued by NYSDOT prior to 2016 for some of the abovementioned deficiencies which were not repaired.

a) Spalled concrete and corroded reinforcement at a facia beam

b) damage at the pier support

c) damage at the abutment

Figure 2-3 Examples of observed deterioration

2.2 Selected Beams

According to the scope of this study, as outlined in the project proposal, three prestressed concrete box beams were sought from the bridge to be repaired and tested at the Structural and Earthquake Engineering (SEES) laboratory at the University at Buffalo.

2.2.1 Selection Strategy/Limitations

The beam selection process was governed by the following considerations:

- For the test results of the beams to be comparable, beams with the same dimensions and apparent deterioration level were sought.
- Due to the lab dimensions, space available at the SEES laboratory, the beams from the 79-ft long span were not considered and only the beams located from the 57-ft spans were considered.
- Lighter beams were preferred by both the demolition contractor and the SEES laboratory to facilitate the transportation, delivery, and maneuvering within the laboratory.

The demolition schedule of the contractor, the testing schedule of the SEES laboratory, and issues related to shutdowns due to COVID-19 also influenced the beam selection process.

The southbound bridge was slated for demolition and replacement before the northbound bridge, and therefore, all the beams were selected from this bridge to avoid delays in the project. This structure included only two 3-ft.-wide (lighter) beams in its shorter spans while the rest were 4-ft.-wide beams. Therefore, two 3-ft.-wide and one adjacent 4-ft.-wide beam with similar level of deterioration, as indicated Figure 2-2, were selected for further studies.

2.2.2 Condition of the Selected Beams

To minimize the disturbance of the beams, and also test the beams under conditions similar to the field, the cast-in-place concrete slab on top of the beams was maintained during the tests. To achieve that, a saw was used by the demolition contractor to cut the part of the slab corresponding to each beam. Another issue that needed to be addressed in the demolition process was that the beam ends were connected to the bridge piers and abutments using pins passing through the beam. The pins consisted of 1-in. anchors surrounded by cast-in-place grout. Hence it was not possible to remove the beams without damaging them. Figure 2-44 presents a sample of the anchorage detailing. To allow the beam removal with minimal damage, the concrete deck slab above each anchor was carefully removed and a core drill was used to cut through the concrete surrounding the anchor to release it, as shown in Figure 2-5. This process was repeated for both ends of the selected beams.

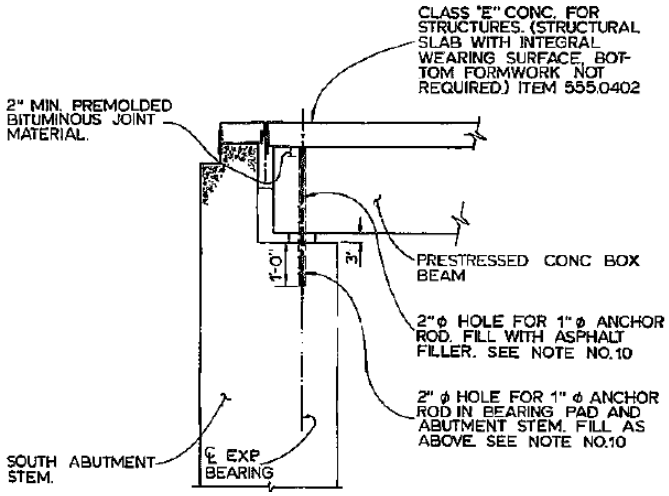

Figure 2-4 Elevation view of the end-beam anchorage detailing

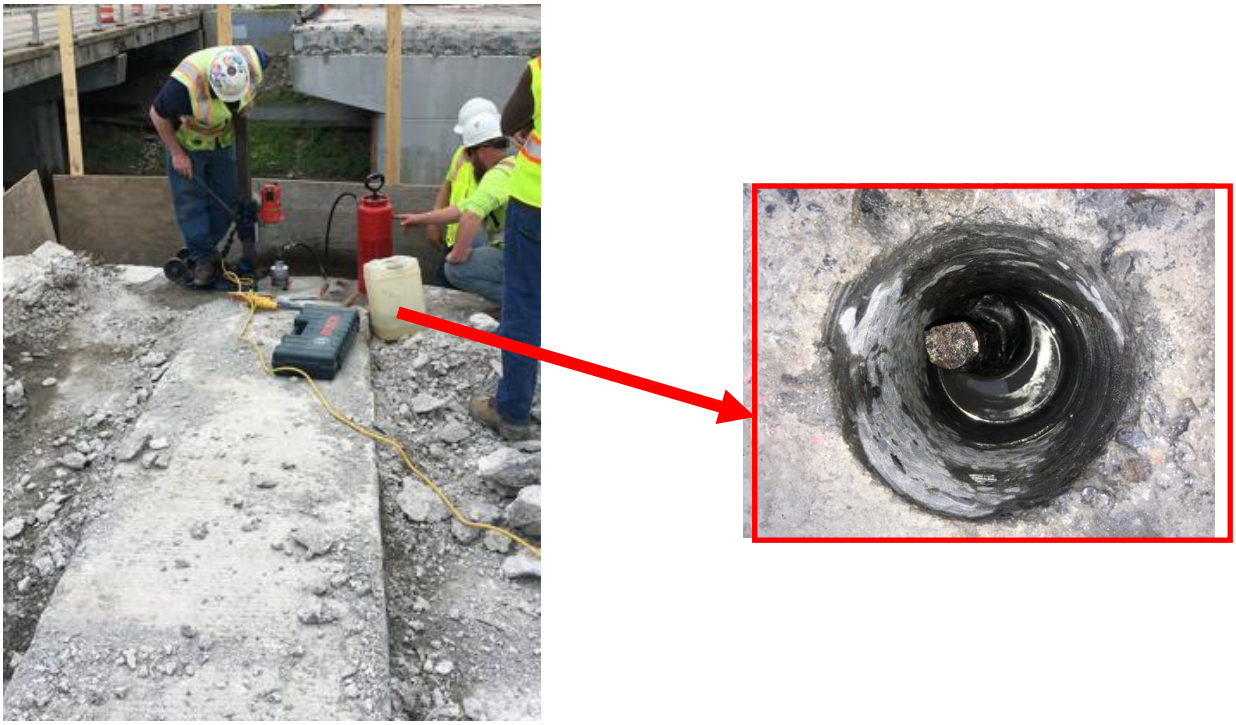

Figure 2-5 Sample of core drilling around the anchors at the beam ends

The condition of each beam before the repairs was also investigated prior to and after the beam removal and the findings are summarized as follows.

2.2.2.1 Beam 1 (3-ft.-wide)

Beam 1 is shown in Figure 2-6. As discussed before, the concrete deck slab on both ends of the beam was removed prior to delivery. Except for minor concrete spalling and steel corrosion at

the west end, shown in Figure 2-6d, no other sign of damage or deterioration was observed. It should be noted that the cardinal coordinates, based on the beam orientation during testing at the SEES laboratory, are used in this report to refer to the various locations along their length. For instance, the "west end" refers to the end of the beam that is closer to the west side of the laboratory which remains the same for the entire testing period.

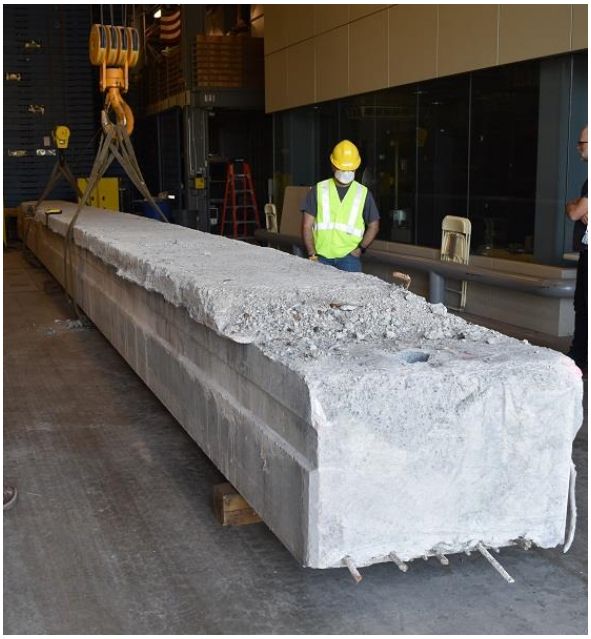

a) Delivered beam

b) West end of the flipped beam

c) East end of the flipped beam

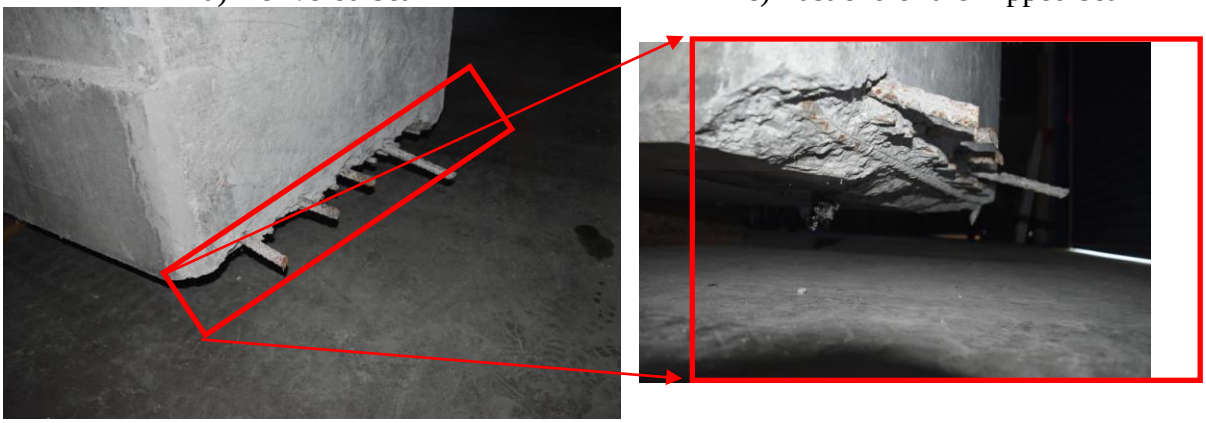

d) Steel reinforcement and concrete condition at the west end of the beam

Figure 2-6 Overall condition of Beam 1 upon delivery to the SEES laboratory

2.2.2.2 Beam 2 (3-ft.-wide)

The overall condition of Beam 2 is shown in Figure 2-7. Similar to Beam 1, the concrete deck slab on both ends of Beam 2 was removed prior to removal from the bridge site and delivery to

SEESL. Corrosion of transverse steel and concrete spalling were observed on both ends as shown in Figure 2-7b, and c. No visible shear or flexural crack was observed.

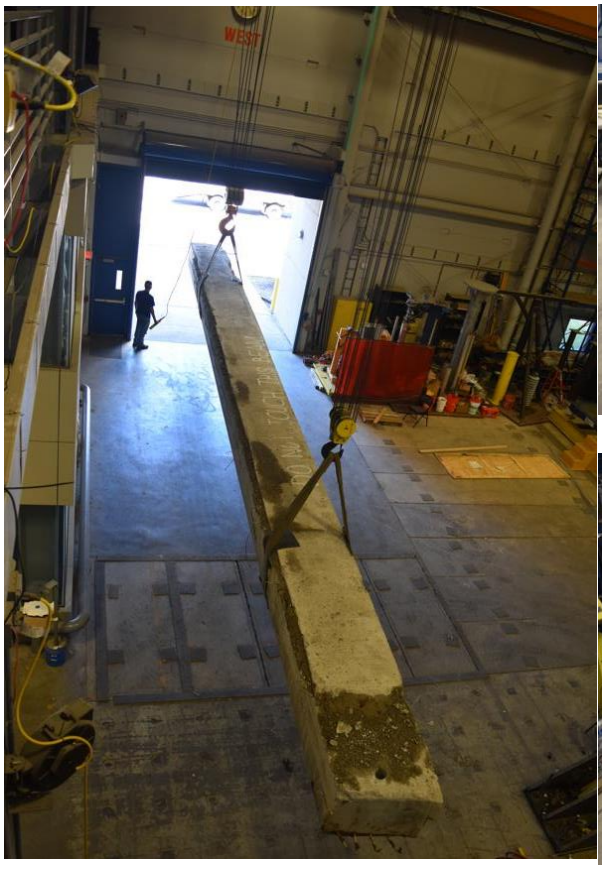

a) delivered beam (view from the east)

b) West end of the beam

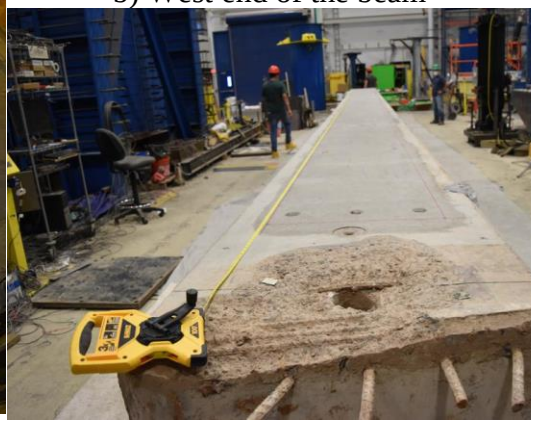

c) East end of the beam (flipped 180 degrees)

Figure 2-7 Overall condition of Beam 2 after delivery to the SEES laboratory

2.2.2.3 Beam 3 (4-ft.-wide)

The overall condition of Beam 3 is shown in Figure 2-8. Similar to the other two beams, the deck slab was removed at both ends of Beam 3. However, more severe damage was observed in Beam 3 at its ends, when compared to Beams 1 and 2, in terms of concrete spalling and corrosion of the transverse steel as shown in Figure 2-8a and b. Also, concrete spalling at the beam substrate occurred at several locations along the length of the beam due to the forceful beam removal using the excavators. Examples of the demolition-induced damage are presented in Figure 2-8c and d. This damage did not affect the load carrying capacity of the beam; however, it would reduce the bonding area and the effectiveness of the FRP retrofit. Hence, as discussed in Chapter

3, the beam was patched prior to the application of the FRP layer. As with Beams 1 and 2, no visible shear or flexural cracks were observed prior to the FRP application.

a) West end of the beam (flipped 90 degrees) b) East end of the beam (flipped 90 degrees)

c) Damaged beam substrate d) Damaged beam substrate

Figure 2-8 Overall condition of Beam 3 upon delivery to the SEES laboratory

2.2.3 Beam Detailing

The dimensions and the reinforcement detailing of the 3-ft.-wide and 4-ft.-wide beams are presented in Figure 2-9 and Figure 2-10, respectively. Both beam types included closely spaced transverse reinforcement at the beam ends. Besides the ends of the beams which had solid sections, the box section was interrupted by solid sections at three locations along the length; located approximately every 14 ft. These sections were 8-in.- wide at the quarter spans and 18-in. wide in the middle.

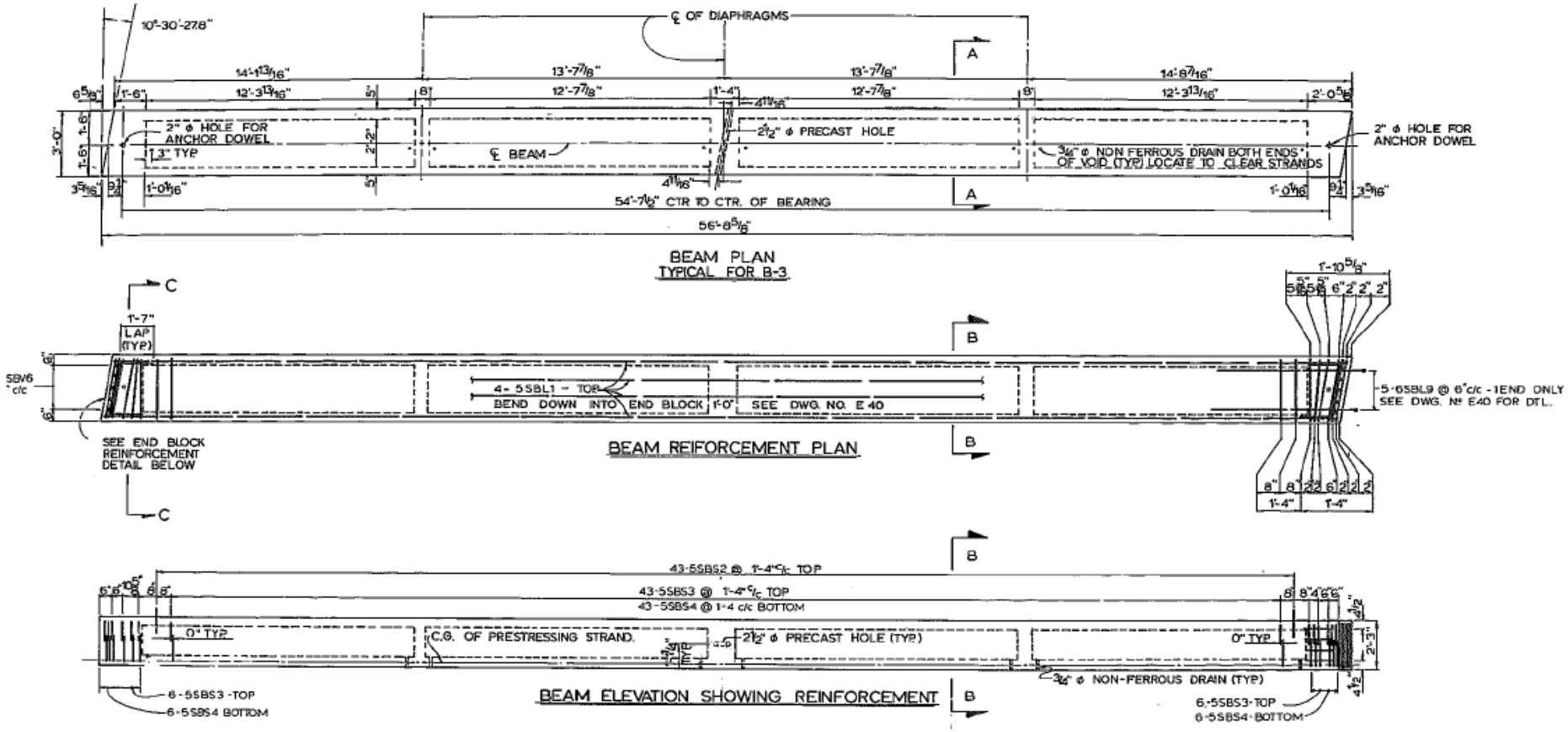

Figure 2-9 Design detailing of the 3ft.-wide beams (Beam 1 and Beam 2)

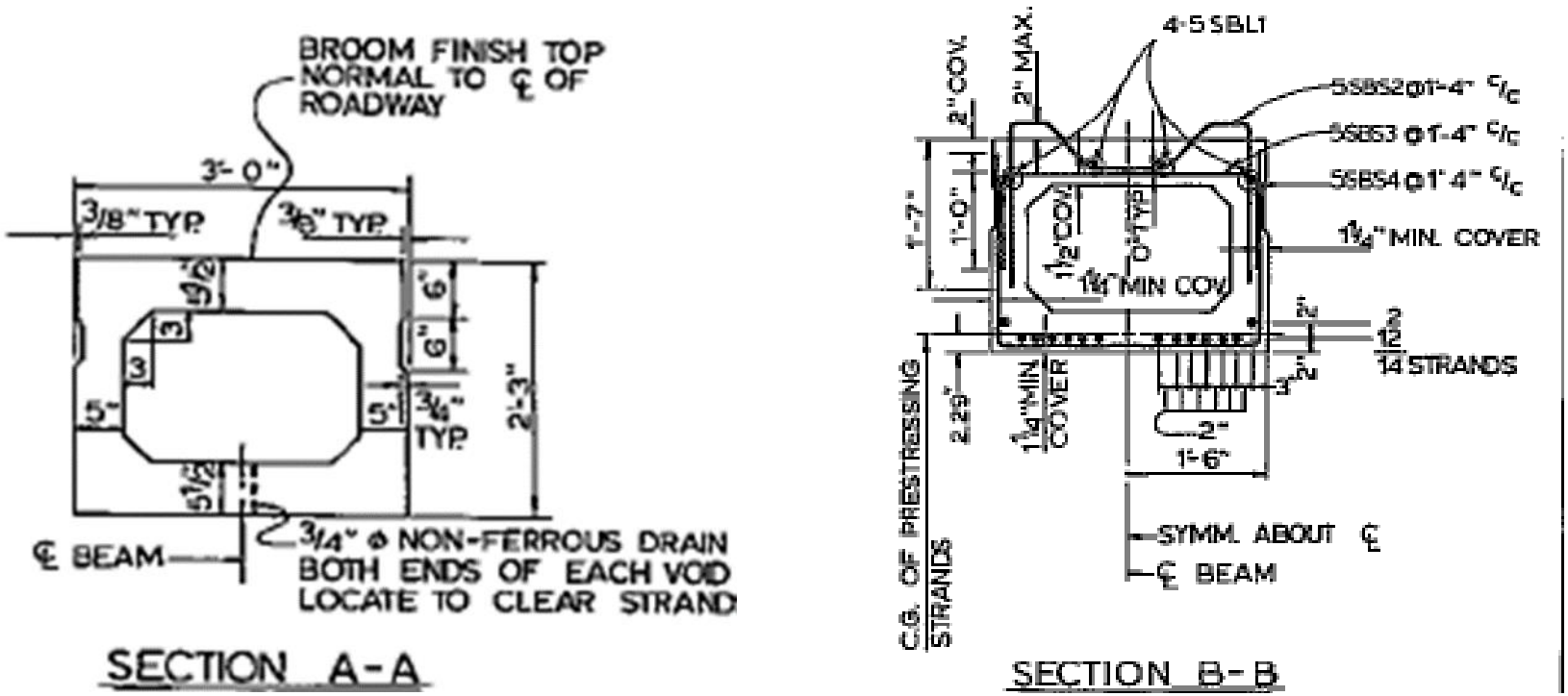

Figure 2-9 Design detailing of the 3ft.-wide beams (Beam 1 and Beam 2) (cont'd)

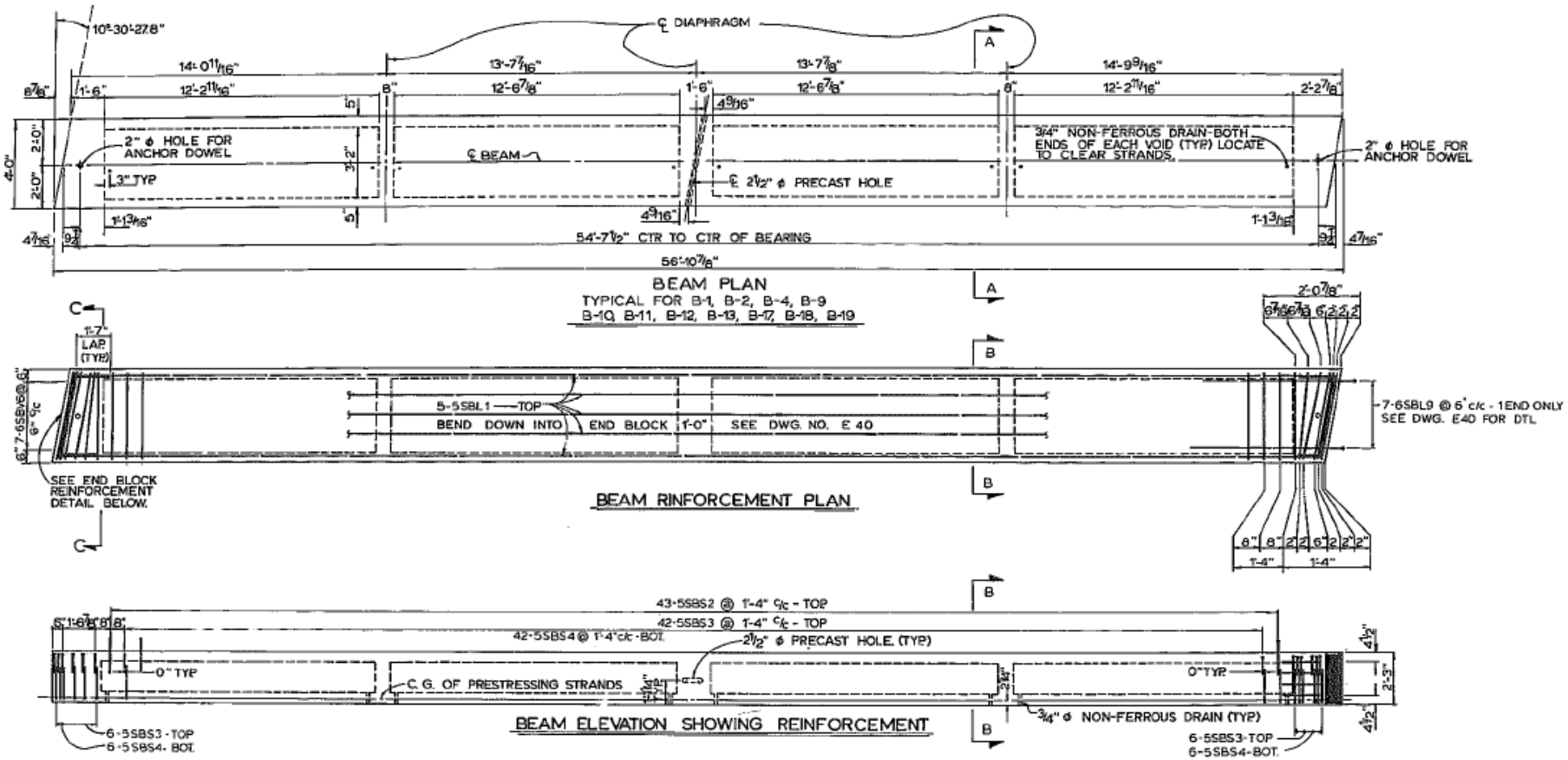

Figure 2-10 Design detailing of the 4ft.-wide beam (Beam 3)

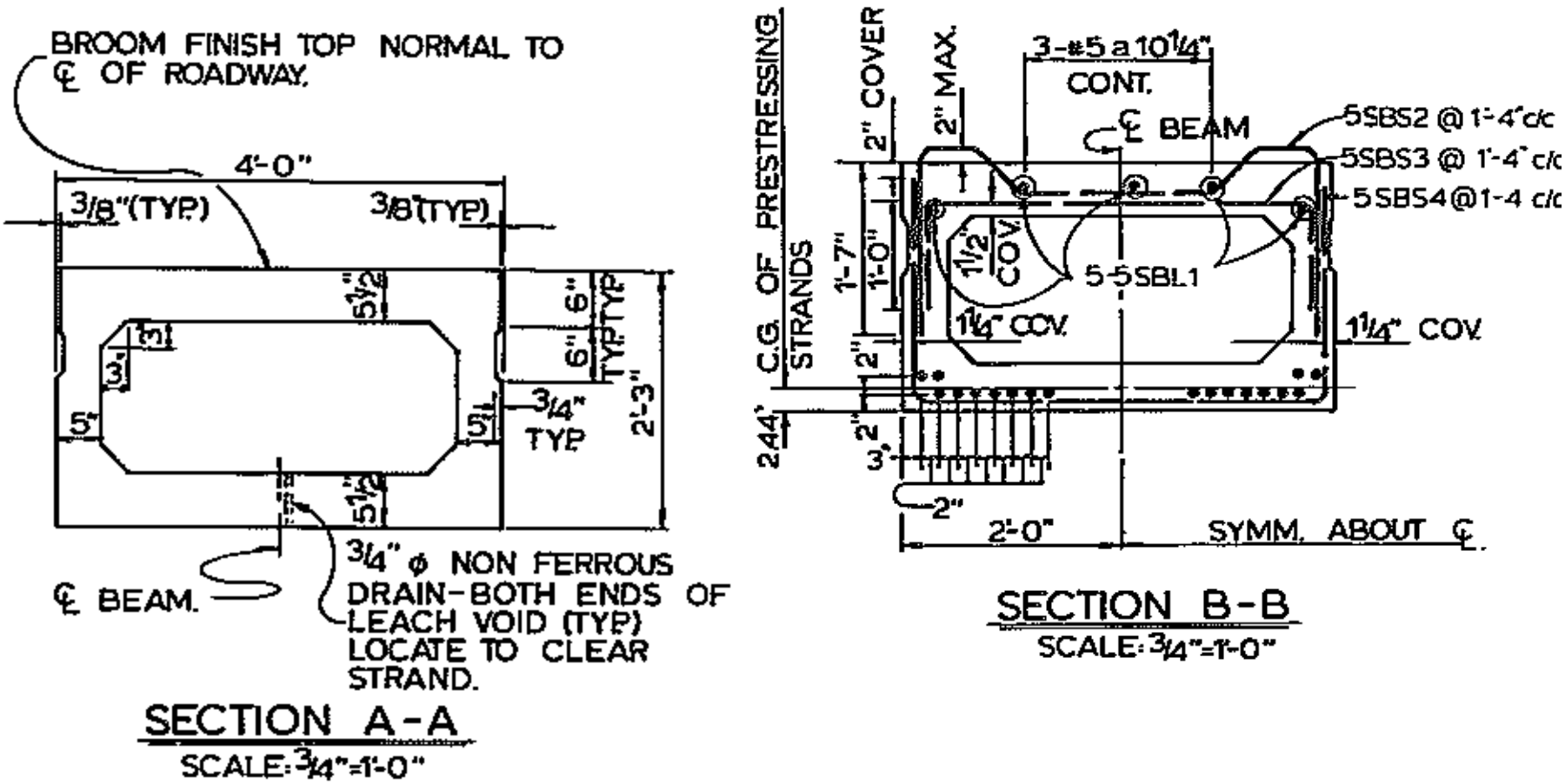

Figure 2 10 Design detailing of the 4ft.-wide beam (Beam 3) (cont'd)

The key design information provided in the figures is also summarized in Table 2-1. The table includes the dimensions of the concrete sections, as well as the area of the reinforcing strands.

Table 2-1 Overall geometry and section properties of the selected beams

Beam ID	Length (Center to the center of bearings)	Width	Height	Cross-sectional area	Moment of inertia (major axis)	Prestressed strand diameter	Total prestressed strand area
	in.	in.	in.	sq. in.	in.^{4}	in.	sq. in.
Beam 1 and 2	655.5	36	27	560.5	50,334	0.5	2.142
Beam3	655.5	48	27	692.5	65,941	0.5	2.754

2.3 Material Properties

2.3.1 Concrete

Concrete cores were extracted from the 4-ft.-wide beam and subjected to compressive and split-cylinder tests according to the ASTM standards (ASTM, 2013) at the SEES laboratory to obtain the relevant material properties of the concrete beam and slab. The results are presented in Figure 2-11 and
Table 2-2. The compressive strength of the beams exceeds the 28-day prescribed design values (6,000 psi) by 38%. On the contrary, the modulus of elasticity and the tensile strength of the concrete are lower than those prescribed in building codes such as ACI318-14 (ACI 2014).

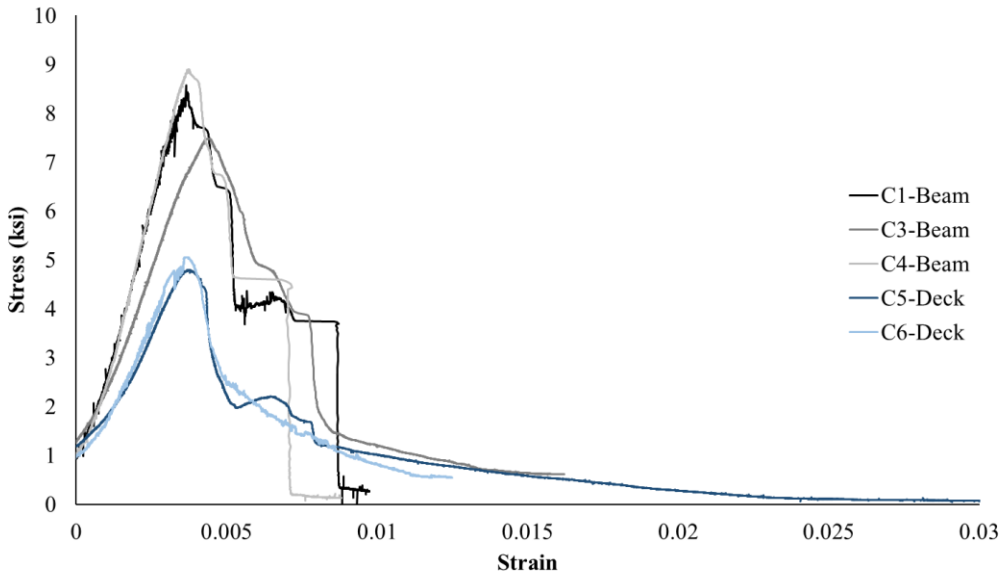

Figure 2-11 Compressive behavior of concrete cores

Table 2-2 Mechanical properties of concrete cores

Structural Element	Number of tested samples	Modulus of elasticity	Compressive strength	Strain at peak	Tensile strength
		ksi	ksi		ksi
Beam	Compression: 3 Split cylinder: 2	2253	8.27	0.0040	0.595
Deck slab	Compression: 2 Split cylinder: 2	1440	4.93	0.0038	0.505

2.3.2 FRP Laminates, Anchors, and Epoxy

During the application of the retrofit on each beam, 12×12 inch samples of CFRP laminates were made from the same fibers and epoxy that was installed on the beams. Coupons were then cut out of the sample panels and tested according to ASTM D3039 standard (ASTM, 2000) to obtain their strength under uniaxial tensile load. The results are summarized in Table 2-3. The measured mechanical properties of the bonding epoxy are also summarized in Table 2-4.These properties reflect the properties of the FRP laminates and anchors since the same fibers and epoxy were used in both cases.

Table 2-3 Mechanical properties of FRP laminates

Beam ID	Number of tested samples	Number of laminate layers	Width[1]	Thickness[1]	Modulus of elasticity (curve fitting)[1]	Ultimate tensile strength[1]	Ultimate strain[1]
			in	in	ksi	ksi	
Beam 1	2	1	0.761	0.113	9542	140.4	0.0111
Beam 2	2	2	0.768	0.208	10740	N/A[2]	N/A[2]
Beam 3	2	1	0.776	0.099	9429	110.6	0.0199

[1]Based on the average values of the tests.
[2]Ultimate capacity was not reached due to slippage at the supporting elements of the coupons.

Table 2-4 Mechanical properties of the bonding epoxy

Type	Tensile Modulus	Compressive Modulus	Flexural Modulus	Tensile Strength	Compressive strength	Flexural Strength	Tensile Elongation
	ksi	ksi	ksi	ksi	ksi	ksi	
Tyfo® S Epoxy	461	465	452	10.5	12.5	17.9	5%

CHAPTER 3
RETROFIT DESIGN AND CONSTRUCTION

3.1 Introduction

The goal of this study, as discussed prior to the tests with NYSDOT engineers, was to restore the flexural capacity of the beams and increase to 1.2 times their nominal capacity prior to any damage via the application of the selected retrofit scheme. The retrofit scheme selection and design calculations are discussed in this chapter.

3.2 Selected Retrofit Option

The access to in-service beams in a box beam bridge is limited to the bottom surface of the beams for all but the two facia beams. According to the discussion of the available strengthening methods in Chapter 1, the retrofit options applicable to this type of bridge beams are i) FRP laminates and ii) Near Surface Mounted (NSM) reinforcement. The application of the latter system is more complicated as it requires more preparation and higher level of precision for the application of the retrofit since grooves should be cut along the length of the beams to place the strands. Therefore, in discussions with the engineers at NYSDOT, FRP laminates were selected as the retrofit method that is investigated in this study. Also, prestressing or post tensioning the laminates were also not considered as the would limit the applicability of the strengthening method in the field.

3.2.1 Repair Design Considerations

The retrofit system aimed at improving the performance of the beam as well as addressing the challenges observed in previous similar strengthening studies as described in Chapter 1. The main objectives include i) increasing the flexural capacity by approximately 20% of the nominal capacity of the undamaged beams, ii) avoiding or delaying the FRP-concrete debonding failure mode to achieve higher ductility, and iii) utilizing the full tensile-strength capacity of the FRP laminates to optimize the material and labor costs associated with the retrofit. The first objective is a function of the area of the laminate, while the next two mainly depend on the bond between the concrete and FRP laminates. The amount of laminate used was varied between the beams to

investigate its effect on the structural performance of the retrofitted beams. Furthermore, in addition to applying an adhesive between the FRP laminates and concrete, the use of FRP anchors with various layouts was considered to improve the bond.

3.2.2 Design Calculations

Carbon Fiber Reinforced Polymer (CFRP) laminates and CFRP anchors were selected for the retrofit application. More specifically, 0.08-in.-thick Tyfo SCH-2X laminates and ¾ in.-diameter Tyfo SCH composite anchors were acquired for this project. Also, Tyfo S Epoxy was used as an adhesive, bonding the CFRP elements and the concrete.

To facilitate the application of the FRP in the laboratory each beam was flipped upside down. With the beam flipped any amount of FRP layers could have been applied. However, this would not be realistic in the field in the case of an actual bridge. Hence the actual limitations encountered in the field were considered in the design. Therefore, it was deemed that no more than three layers of laminates would be applied at the beam as this is considered a realistic upper limit indicated by the field professionals. For the width of the laminates, the standard 2-ft wide rolls were considered to avoid customizations unlikely to occur in a field application. Hence, for the first beam, it was decided to install three layers of laminates. Considering the diagram of the moment demand occurring from a four-point bending testing setup, as the setup employed to test the beams in this project, the number of laminates was reduced to two at the ends of the beam. Practically, this meant that the first two layers of laminates were applied from end to end of the beam, while a shorter third layer was applied between the two loads where the maximum moment was anticipated. Extending the third layer to the ends would not be meaningful considering the diagram of the moment demand.

Following the decision on the number of laminates, the numbers and locations of the anchors were selected. For the locations of the anchors, the solid sections at the two ends of the beam and the quarter lengths were selected. The number of anchors at each section was decided based on the width of the beam and the need to sufficiently overlap the fans of the anchors.

In this section, the calculations for the design of the retrofit scheme for Beam 1 are presented.

- **Nominal material properties assumed before the tests):**

Tyfo SCH-41-2X System:

$E_f := 11900ksi$ design tensile modulus

$\varepsilon_{fu} := 0.0085$ design ultimate strain

$t_f := 0.08in$ thickness per layer

Tyfo SCH Composite Anchors:

$E_{fa} := 11900ksi$ design elastic modulus

$f_{fa} := 121ksi$ design ultimate tensile strength

$A_{fa} := 0.44in^2$ area of 3/4". diameter composite anchor

Slab Properties:

$f'_c := 6000psi$ assumed compressive strength of concrete

Reduction Factors:

$\psi := 0.85$ FRP reduction factor

$\alpha_{ar} := 0.59$ anchor failure design calibration factor

$\phi_t := 0.9$ tension reduction factor

- **Reinforcement Design:**

Tensile Capacity of FRP at midspan:

$w_f := 24in$ width of FRP

$n_f := 3$ number of layers of FRP

$$\varepsilon_{fd} := \min\left(0.083\cdot\sqrt{\frac{f'_c}{n_f\cdot\frac{t_f}{in}\cdot E_f}},\ 0.9\cdot\varepsilon_{fu}\right) = 0.0038$$ debonding FRP strain

$\varepsilon_{fe} := \varepsilon_{fd}$ effective FRP strain

$f_{fe} := \varepsilon_{fe}\cdot E_f = 45.3\cdot ksi$ effective FRP design stress

$A_f := n_f\cdot t_f\cdot w_f = 5.76\cdot in^2$ effective cross-sectional area of FRP

The calculation of the design capacity in tension includes a 0.9 tension reduction factor. Typical 0.85 FRP reduction factor not included.

$\phi T_n := \phi_t\cdot f_{fe}\cdot A_f = 234.69\cdot kip$ factored tension capacity provided by FRP

Anchor Capacity at Midspan:

(Typical 0.59 anchor reduction factor not included)

$T_{fa} := A_{fa} \cdot f_{fa} = 53.2 \cdot kip$ — anchor capacity, anchor rupture failure

$n_{fa} := 4$ — number of anchors to be used

$T_{anc} := n_{fa} \cdot T_{fa} = 212.96\,kip$ — factored tension capacity provided by anchors

$A_{ratio} := \frac{A_{fa} \cdot n_{fa}}{A_f} = 0.31$ — ratio of composite anchor area to FRP sheet area

$T_{transfer} := \frac{T_{anc}}{\phi T_n} = 0.91$ — percent of tension transfered through composite anchors

$\varepsilon_{fe.2} := \frac{T_{anc}}{A_f \cdot E_f \cdot \phi_t} = 0.0035$ — effective strain of FRP sheets at anchor rupture

Tensile Capacity of FRP at end spans:

$w_f := 24in$ — width of FRP

$n_f := 2$ — number of layers of FRP

$\varepsilon_{fd} := \min\left(0.083 \cdot \sqrt{\frac{f'_c}{n_f \cdot \frac{t_f}{in} \cdot E_f}}, 0.9 \cdot \varepsilon_{fu}\right) = 0.0047$ — debonding FRP strain

$\varepsilon_{fe} := \varepsilon_{fd}$ — effective FRP strain

$f_{fe} := \varepsilon_{fe} \cdot E_f = 55.4 \cdot ksi$ — effective FRP design stress

$A_f := n_f \cdot t_f \cdot w_f = 3.84 \cdot in^2$ — effective cross-sectional area of FRP

Tension capacity includes a 0.9 tension reduction factor. The typical 0.85 FRP reduction factor not included.

$\phi T_n := \phi_t \cdot f_{fe} \cdot A_f = 191.62 \cdot kip$ — factored tension capacity provided by FRP

Anchor Capacity at Midspan:
(Typical 0.59 anchor reduction factor not included)

$T_{fa} := A_{fa} \cdot f_{fa} = 53.2 \cdot kip$ — anchor capacity, anchor rupture failure

$n_{fa} := 3$ — number of anchors to be used

$T_{anc} := n_{fa} \cdot T_{fa} = 159.72\,kip$ — factored tension capacity provided by anchors

$A_{ratio} := \frac{A_{fa} \cdot n_{fa}}{A_f} = 0.34$ — ratio of composite anchor area to FRP sheet area

$T_{transfer} := \frac{T_{anc}}{\phi T_n} = 0.83$ — percent of tension transfered through composite anchors

$\varepsilon_{fe.2} := \frac{T_{anc}}{A_f \cdot E_f \cdot \phi_t} = 0.0039$ — effective strain of FRP sheets at anchor rupture

3.2.3 Retrofit Design

. In summary, the following configurations were designed and implemented for each beam.

3.2.3.1 Beam 1:

- Laminates: As discussed in a previous section, and shown in Figure 3-1, two 24-in.-wide Tyfo SCH-2X layers were used to cover the beam length between the supports, while a third layer with the same width was used to cover only the center half of the beam length, where higher moment demand was anticipated based on the test setup.
- Anchors: Three anchors were embedded into each solid section of the beam close to the supports. Moreover, four anchors were embedded into each solid section of the beam located at its quarter length as shown in Figure 3-1. This arrangement resulted in a total of 14 anchors, seven on each side of the beam. All the anchors were 16-in. long, with a design embedment depth of 4 inches. Those at the quarter sections were embedded perpendicularly with respect to the bottom surface of the beam while those at the ends of the beam were embedded with an angle of 45 degrees. All the anchors were sandwiched between the first and second layers of the laminates, with their fans overlapping by 6 inches and covering the full width of the laminates.

3.2.3.2 Beam 2:

- Laminates: The same layout as that of Beam 1 was used except for the third layer which was not included in the design, resulting in two layers of laminates spanning between the supports as shown in Figure 3-2.
- Anchors: Seven anchors were designed to be placed at each half of the beam. The anchor layout on one side of the beam was kept the same as that of Beam 1, while for the other side the anchors were distributed further within the first quarter of the beam as shown in Figure 3-2.
-

3.2.3.3 Beam 3:

- Laminates: Only one layer of laminate spanning between the supports was designed as shown in Figure 3-3.
- Anchors: Seven anchors were placed at each half of the beam. All the anchors were concentrated at the ends of the beam and were patched using FRP laminates as shown in Figure 3-3.

The quantity of materials used to retrofit each beam is summarized in Table 2-1. The area of laminates per unit width of beams indicates a 33.3 percent reduction between beam 1 and Beam 2 and a 66.7 percent reduction between Beam 1 and Beam 3. Also given that the quantity of anchors remained unchanged, the ratio between the area of the anchors and laminates increased by 50.1 percent between Beam 1 and Beam 2 and by 126.4 percent between Beam 1 and Beam 3.

Table 3-1 CFRP materials used for each beam.

Specimen	Beam width (ft)	Laminate area at midspan	Anchor area on each side	Laminate area per beam width	Anchor/laminate area ratio
	ft.	Sq. in.	Sq. in.	Sq. in./ft.	
Beam 1	3	5.76	3.08	1.92	0.53
Beam 2	3	3.84	3.08	1.28	0.80
Beam 3	4	2.56	3.08	0.64	1.20

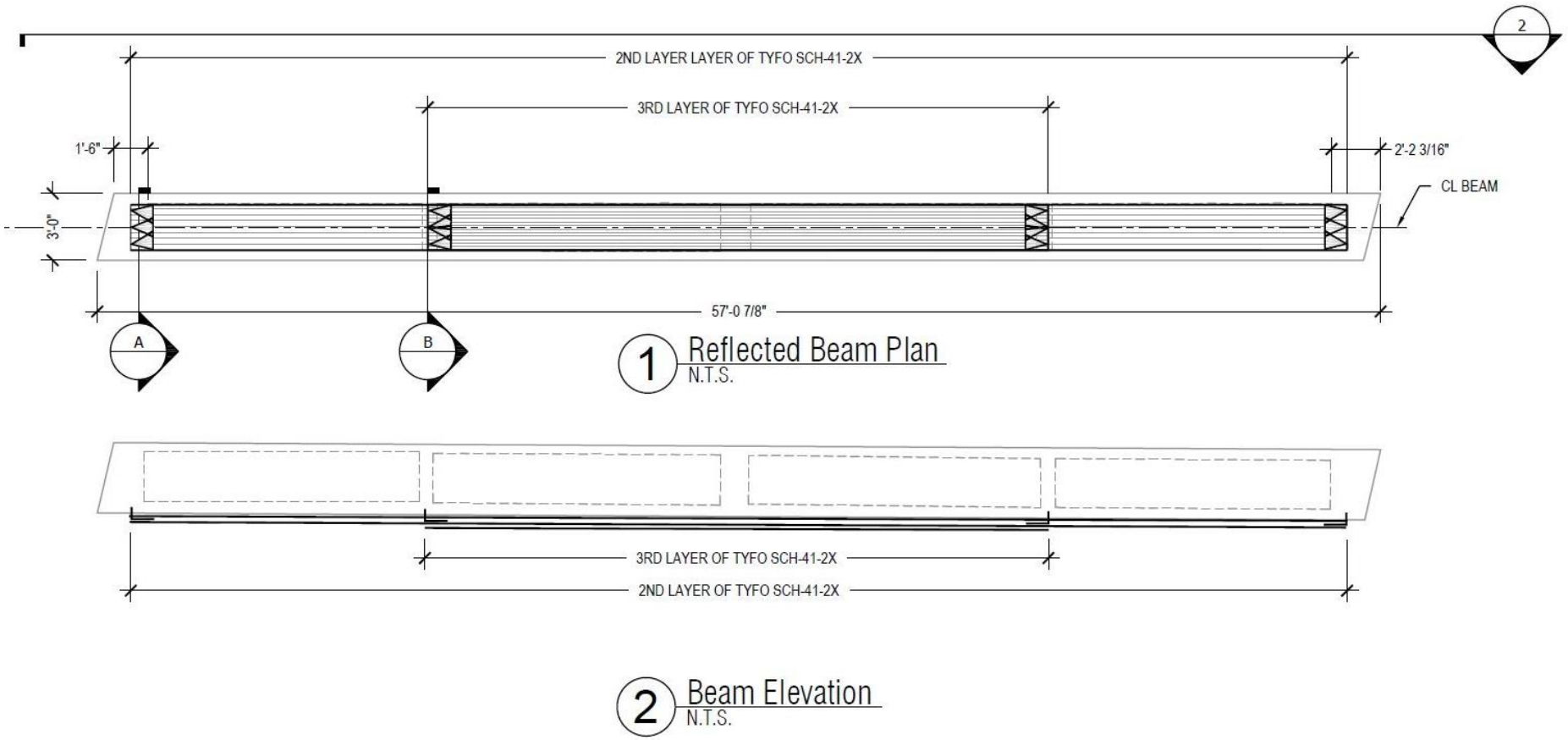

Figure 3-1 Beam 1 retrofit detailing

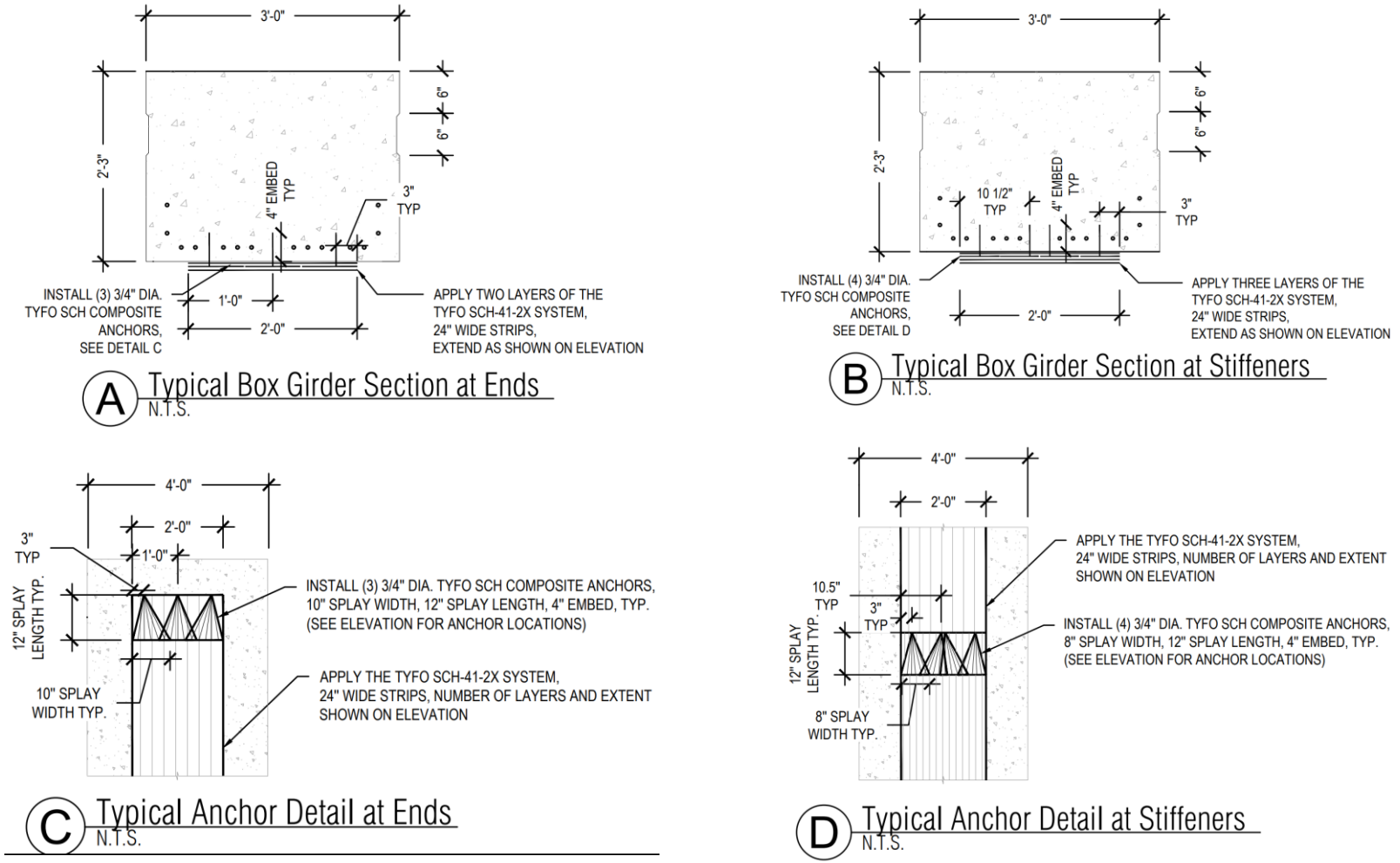

Figure 3 1 Beam 1 retrofit detailing (cont'd)

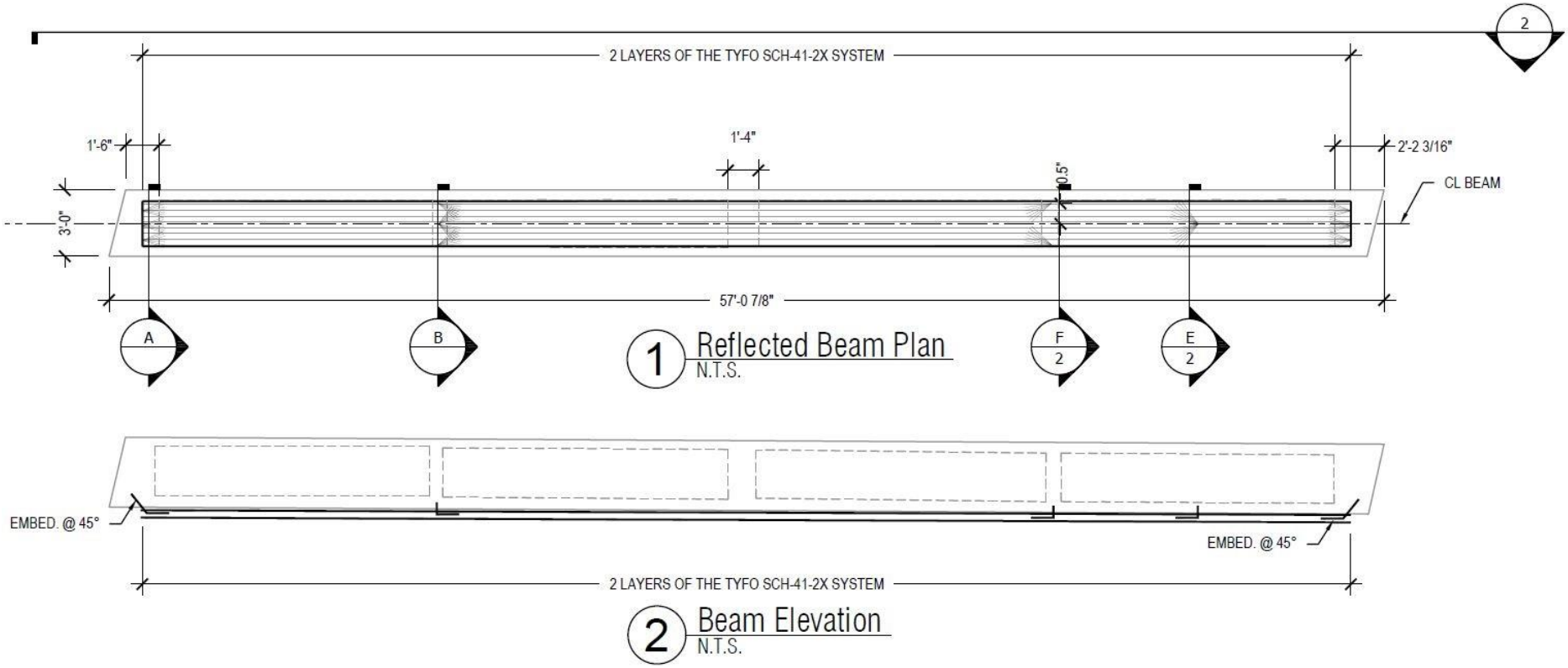

Figure 3-2 Beam 2 retrofit detailing

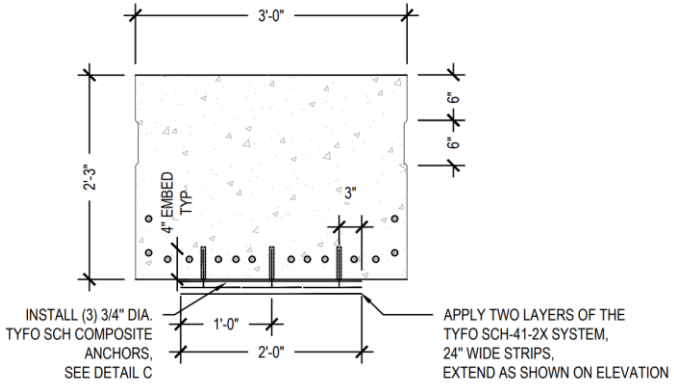

A Typical Box Girder Section @ Ends
N.T.S.

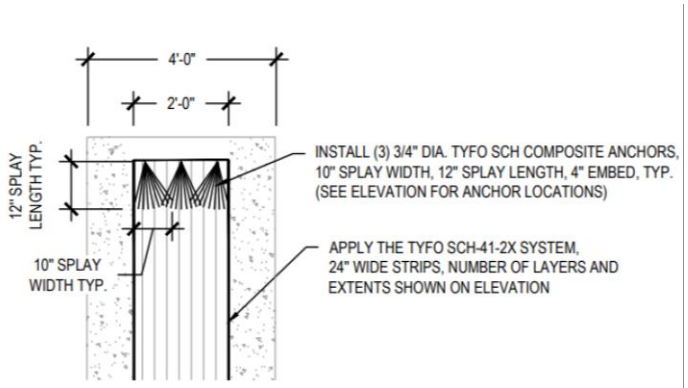

A Typical Anchor Detail at Ends
N.T.S.

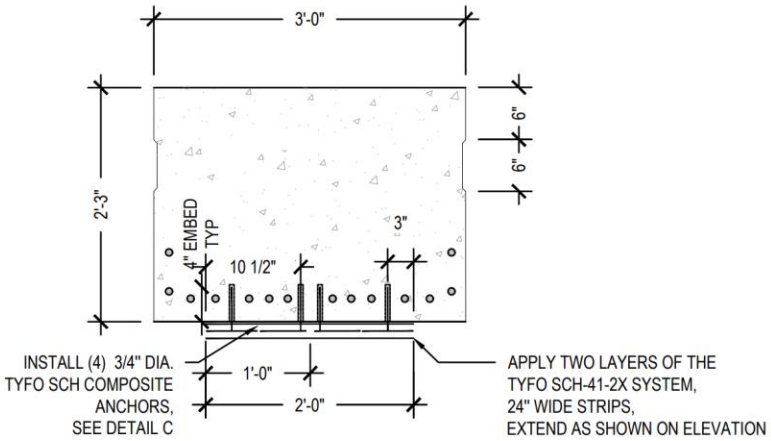

B Typical Box Girder Section @ Stiffeners
N.T.S.

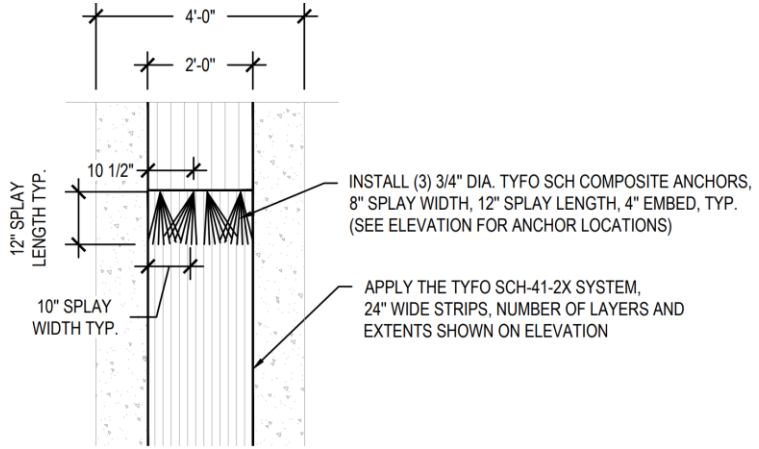

B Typical Anchor Detail at Stiffeners
N.T.S.

Figure 3-2 Beam 2 retrofit detailing (cont'd)

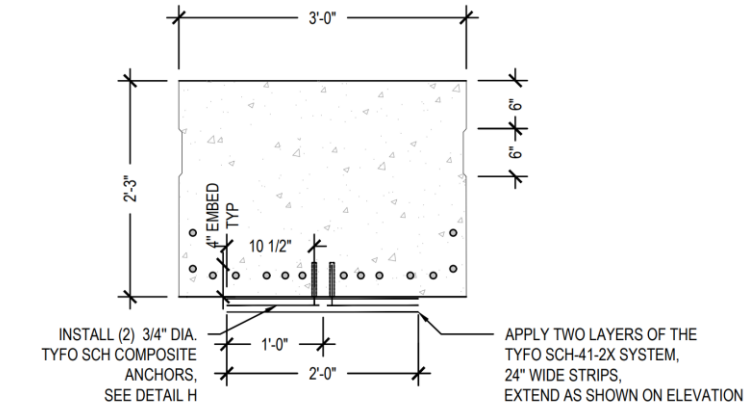

E Typical Box Girder Section @ Stiffeners
N.T.S.

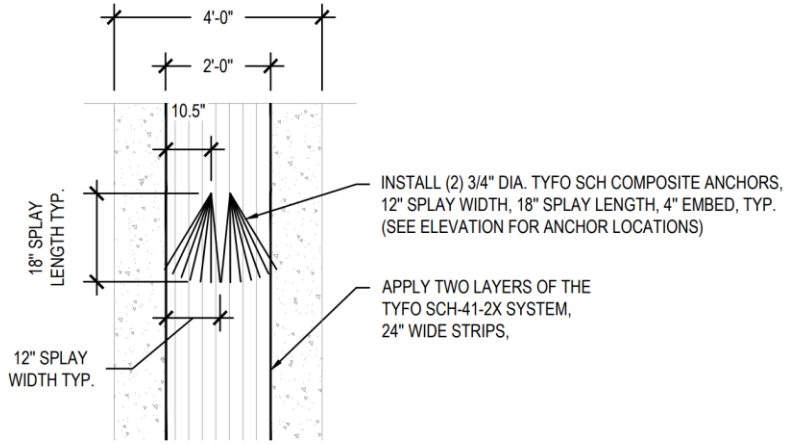

E Typical Anchor Detail at Stiffeners
N.T.S.

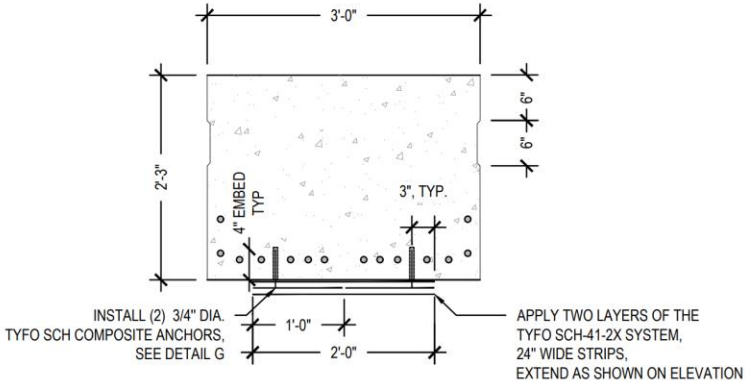

F Typical Box Girder Section @ Stiffeners
N.T.S.

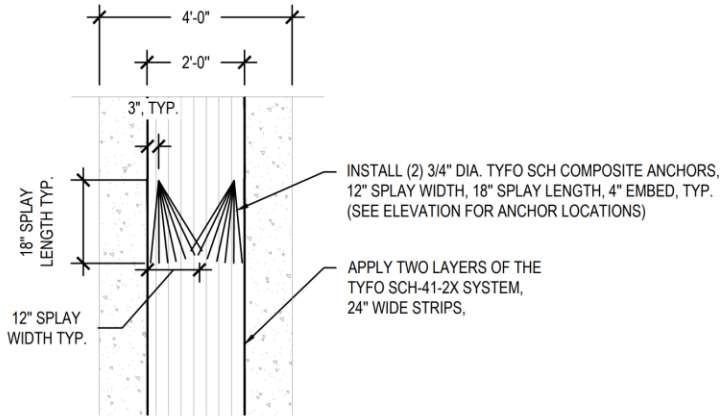

F Typical Anchor Detail at Stiffeners
N.T.S.

Figure 3-2 Beam 2 retrofit detailing (cont'd)

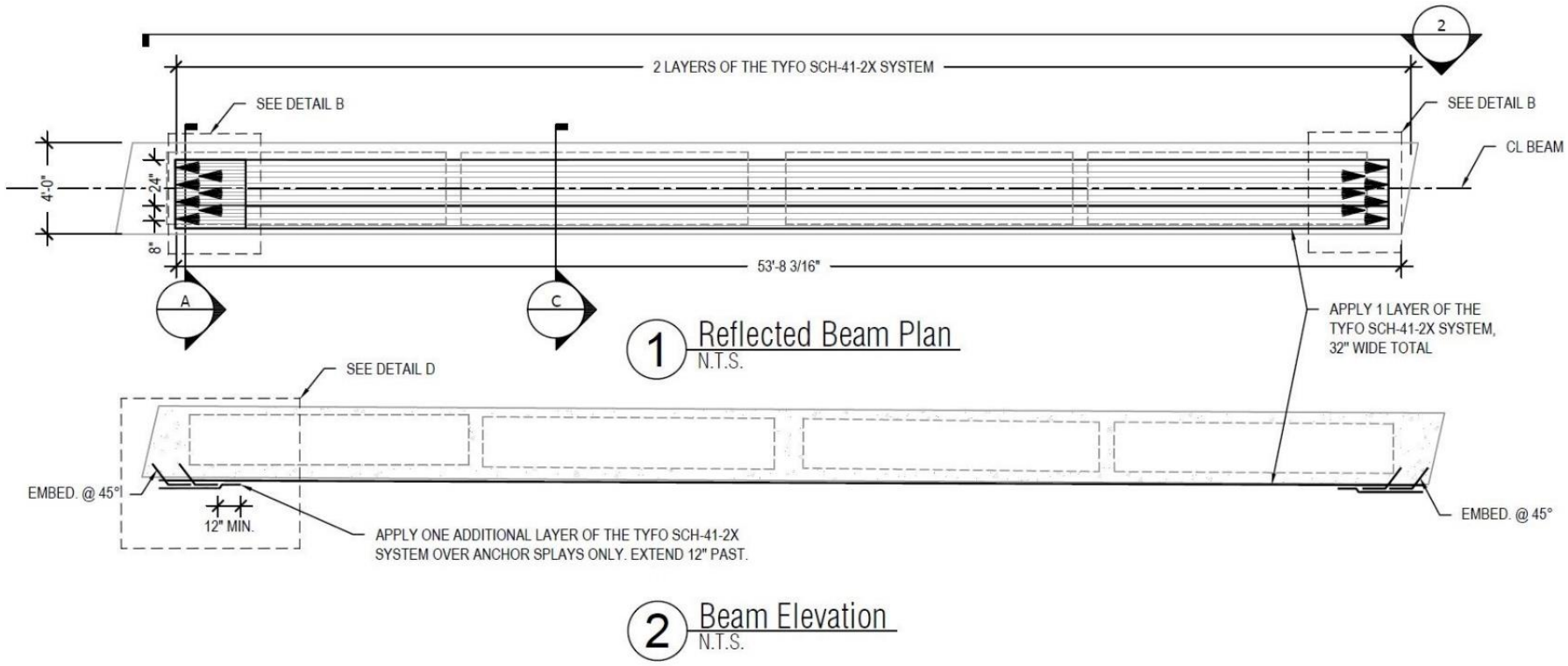

Figure 3-3 Beam 3 retrofit detailing

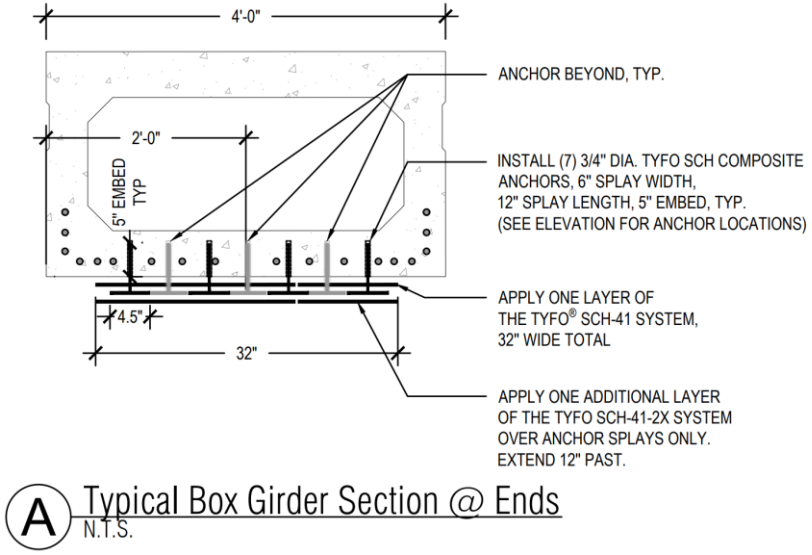

A Typical Box Girder Section @ Ends
N.T.S.

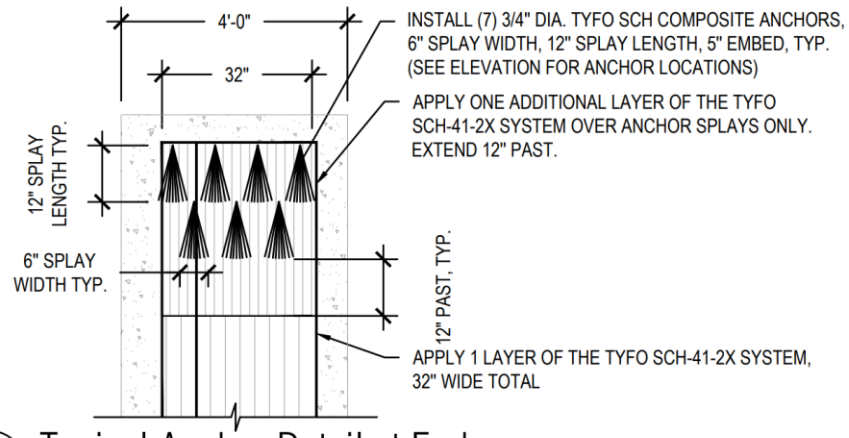

B Typical Anchor Detail at Ends
N.T.S.

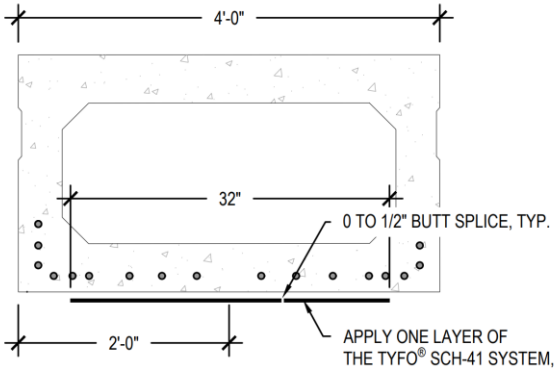

C Typical Box Girder Section
N.T.S.

Figure 3 3 Beam 3 retrofit detailing (cont'd)

3.3 Retrofit Implementation

This section discusses the procedure that was followed to retrofit the beams. In all cases, the beams were flipped in the lab using two cranes to bring their bottom side up to facilitate the installation of the laminates and anchors. Clearly, this is not possible in the field, and alters the strains in the concrete section. However, once the beams were brought in the laboratory, it was not possible to lift the beams and allow the application of the retrofit scheme in a safe and cost-effective manner from underneath.

3.3.1 Surface Preparation

The concrete surface where the FRP laminates and anchors are installed must be clean, dry, and free of cavities that may cause voids behind the laminates. A diamond wheel grinder was used to clean the concrete surface as well as to increase roughness and enhance the bond between the CFRP laminates and the concrete. The roughness of the grinded surface, shown in Figure 3-4, was close to the Concrete Surface Profile 3 (CSP 3), as defined by the International Concrete Repair Institute (ICRI) Technical Guideline No 310.2 (ICRI, 2013). It should be noted that the surface cleaning and roughening can be completed in the field using other methods such as sandblasting and water blasting which are more efficient options for in-situ applications. However, these could not be applied within a laboratory setting for practical reasons. In addition to this step, the surface cavities of Beam 3, which resulted from concrete spalling during the demolition, as discussed in Chapter 2, were also patched by the same epoxy used to provide a bond between concrete and CFRP laminates. This was done a few days before the application of the CFRP laminates to allow the epoxy to harden. Patched surfaces were also roughened after hardening using sandpaper. Other methods could also be employed for patching the concrete depending on the extent of the damage.

a) Before grinding b) After grinding

Figure 3-4 Change in the surface profile due to grinding

3.3.2 Hole Drilling

After the surface was prepared, 1-in.-diameter 4.5-in.-deep holes were drilled according to the design layout for each beam. The holes were ¼ in. wider and ½ in. deeper than the anchor diameter and embedment depth, respectively. This is standard application practice as it allows for the epoxy to surround the anchor and provide a strong bond between the anchor and concrete. The top ½ in. of each hole was also widened by ¼ of an inch in diameter towards the side of the anchor spread on the beam surface, as shown in Figure 3-5. This was done to prevent the anchor from bending 90 degrees and reduce the bearing stress concentration between concrete and the anchor at the bent segment of the anchors.

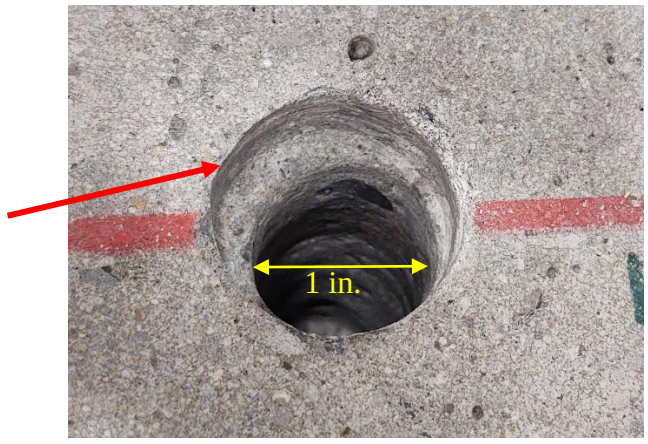

Figure 3-5 Example of the drilled holes

3.3.3 Application of CFRP Laminates and Anchors

This step involved i) saturating the concrete surface by spreading the epoxy, ii) unrolling the first laminate layer on the beam, iii) saturating the laminate, iv) rolling the saturated laminate, v) repeating steps ii through iv for all laminates, vi) unrolling the first layer of the saturated laminate for the final installation, vii) cutting 1 in. by 1 in. holes in the first layer of laminate to allow the installation of the anchors, viii) saturating and installing the anchors, ix) installing the next layer of laminates (if there is only one laminate in the location of the anchors, to better protect them, patches of laminates can be used to cover them), and x) applying a layer of thickened epoxy after the last aminate has been applied. This process needs to be completed before the epoxy hardens and requires qualified and trained personnel, as the performance of the retrofit heavily depends on the quality of its implementation. Properly trained personnel are

crucial to achieving the design objectives. In the case of the beams discussed in this report, the retrofit for the first beam was applied by professionals of Fyfe Inc. The professionals trained a group of researchers at the University at Buffalo who applied the retrofit to the following two beams.

3.3.4 Curation

The curing time for the epoxy used in this project is a function of the ambient temperature as presented in Table 3-2 and Figure 3-6. Since these beams were cured inside the laboratory, the curing of the epoxy was not a concern. However, the fluctuation of the temperature and humidity was measured during the curation of Beam 2 and the results are presented in Table 3-3. All the retrofitted beams went through the curing process in the same temperature-controlled condition as that of Beam 2, and according to Table 3-3, 85 percent curation was achieved in approximately 4 days.

Table 3-2 Tyfo S epoxy cure time as a function of temperature

Cure Temperature	Time to 85% Curation
°F	Hours
50-65	Cannot be achieved
73	96
80	48
90	20
110	12

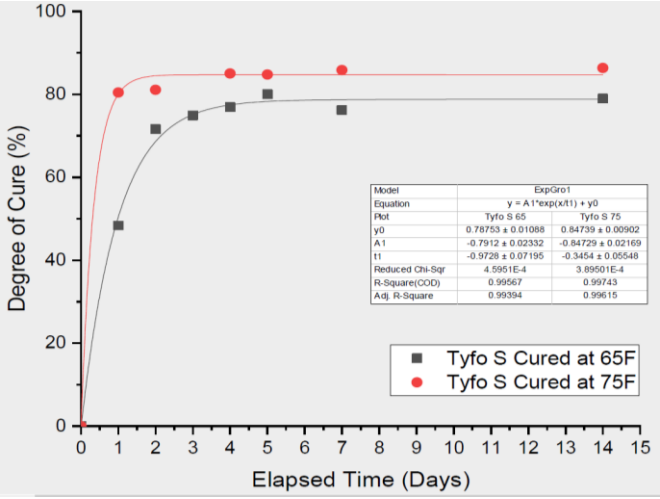

Figure 3-6 Tyfo S degree of cure progression

Table 3-3 Variation of temperature during the curing of Beam 2

Date	Time	Instant temperature	Instant humidity	Min temperature*	Max temperature*	Min humidity*	Max humidity*
		°F	%	°F	°F	%	%
8/8/2020	12:04 PM	79	50	79	79	50	52
8/9/2020	10:11 PM	73	64	73	79	47	78
8/10/2020	1:16 PM	72	63	72	73	56	73
8/10/2020	4:33 PM	72	62	72	73	56	73
8/11/2020	10:35 PM	72	67	72	73	56	73
8/11/2020	12:37 PM	72	62	72	73	59	70
8/11/2020	4:53 PM	72	64	72	72	64	66
8/12/2020	5:55 PM	73	48	70	73	46	66
8/13/2020	12:28 PM	72	52	70	73	46	66

*The reported temperature and humidity ranges are valid for the time intervals between the times reported in this table.

CHAPTER 4
TESTING OF THE BEAMS

4.1 Introduction

This chapter discusses the test setup, instrumentation, and testing protocols implemented to investigate the behavior of the unretrofitted and retrofitted beams under service and extreme loads.

4.2 Test Setup

A four-point-bending test setup was selected to simulate the behavior of the beams under vehicular loads. This type of test provides a region of constant maximum moment between the loading points which is beneficial for the performance evaluation of the flexural retrofit system implemented in this project. Also, two points of loading along the length of the beam provide similar load distribution induced by vehicles.

4.2.1 Test-Setup Design and Considerations

The available testing equipment and fixtures at the SEES laboratory, including the supporting plates for the actuators and the specimens, are mainly designed for the application of horizontal loads. Although supports for the specimen could have been assembled, allowing enough space for inspection under the beam, the placement of the actuators over the beam to apply the load in combination with gravity required steel towers that are not available and would be rather costly to build. Therefore, the actuators were placed to apply loads horizontally, and the beams were flipped 90 degrees about their longitudinal axis and loaded horizontally. Figures 4-1 through 4-3 present the test setups for Beam 1, Beam 2, and Beam 3, respectively. The beams were simply supported at both ends, similar to their support condition while in service.

The weight of the beams is transferred to the laboratory floor at multiple support locations to prevent the development of bending and shear moments perpendicular to the loading plane that would not be realistic in the case of an actual bridge. The overall setup is similar between all tests, however, following the tests of Beam 1, modifications were made to the fixture that transferred the weight of the beam to the floor. Following observation during the tests on Beam 1, a rolling system was introduced to replace the use of Teflon sheets and lumber used in the tests

of Beam 1, as shown in Figures 4-2 and 4-3. This modification resulted in less friction, and therefore, less resistance to the horizontal motion of the beams.

Finally, it can be noted that the distance between the actuators was reduced in the tests of Beam 3 which was wider and thus stronger than Beams 1 and 2. This adjustment reduced the force required to reach the anticipated failure moment, ensuring the safety of the test setup.

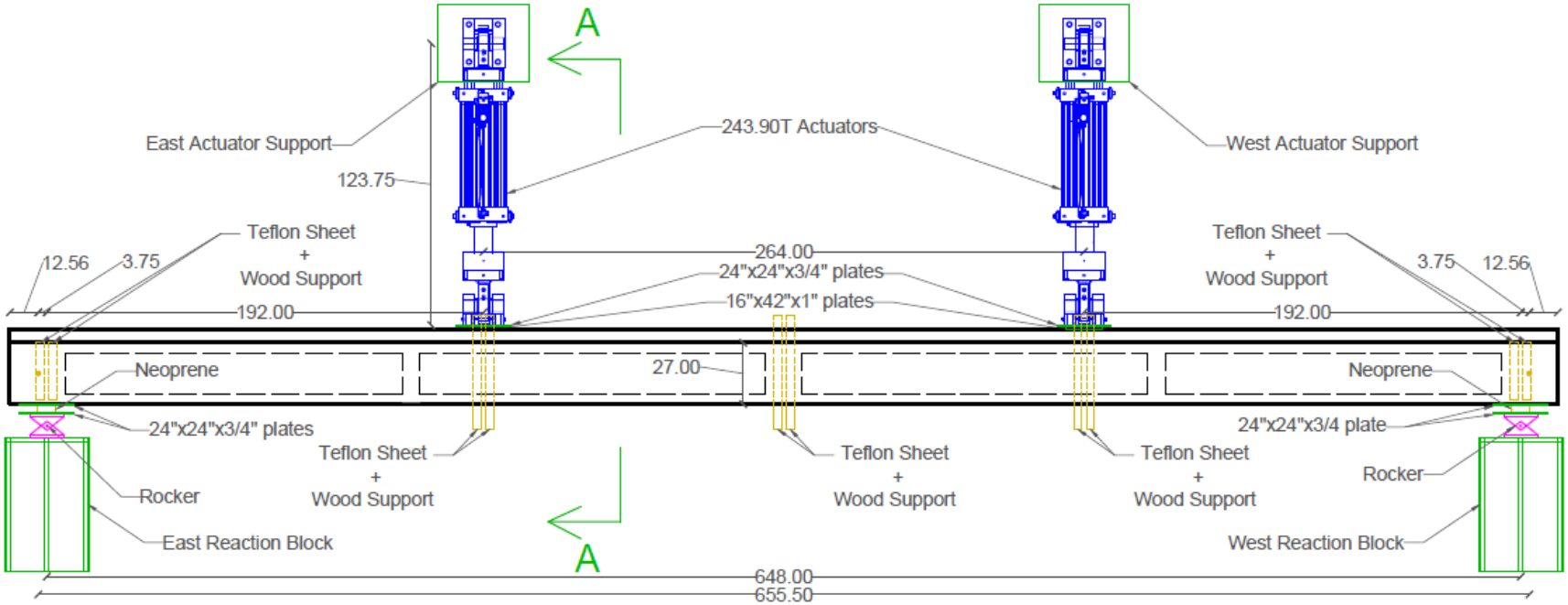

a) Plan view

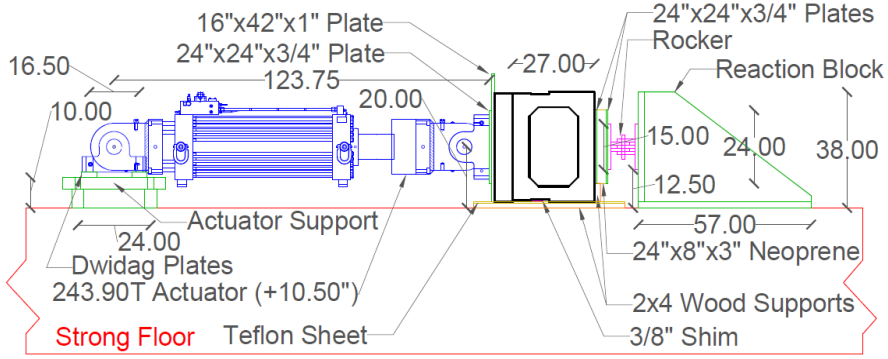

b) Section A-A

Figure 4-1 Beam 1 test setup (units are inches unless stated otherwise)

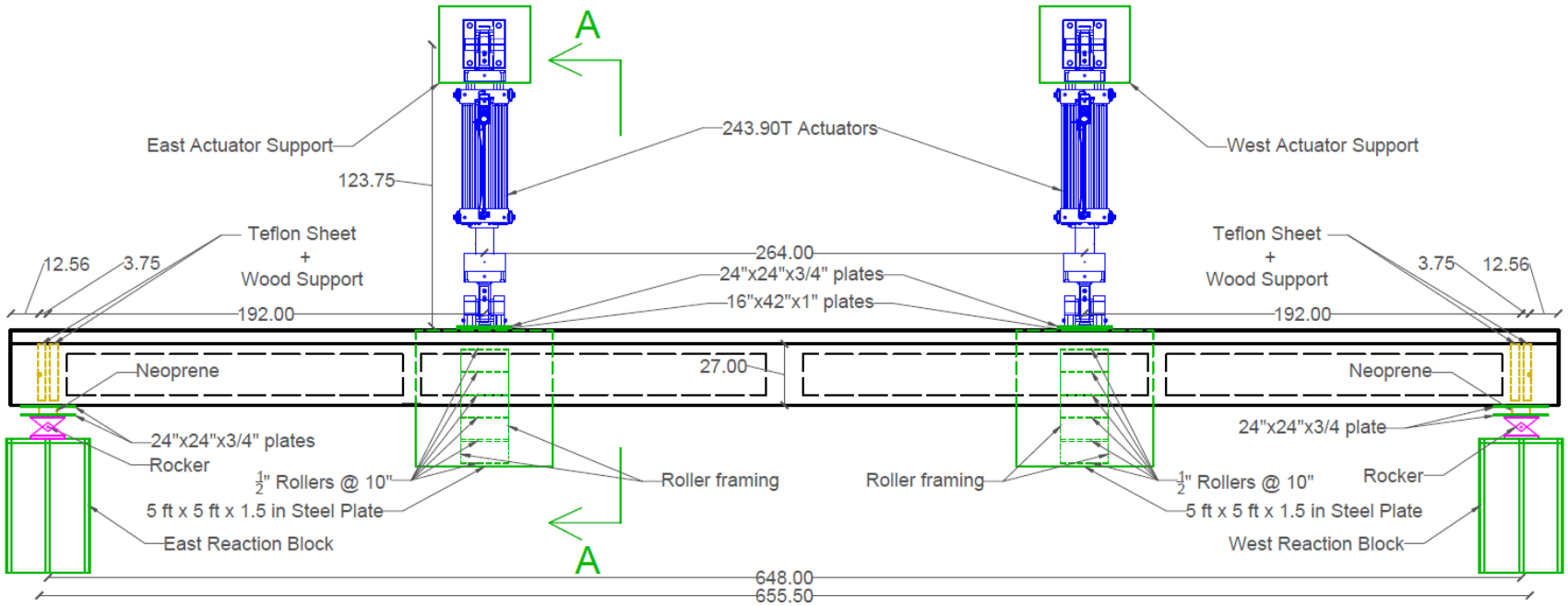

a) Plan view

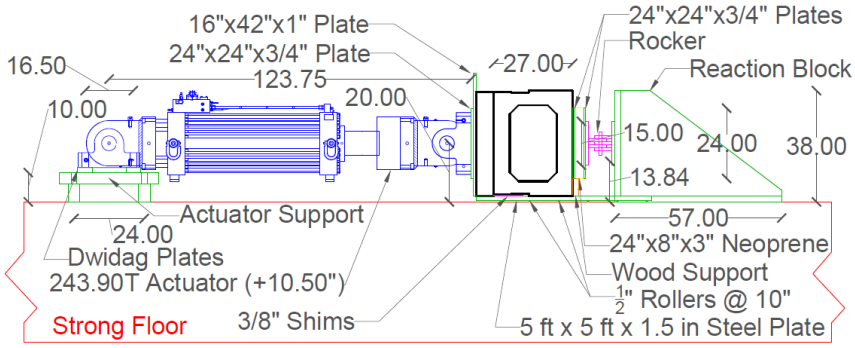

b) Section A-A

Figure 4-2 Beam 2 test setup (units are inches unless stated otherwise)

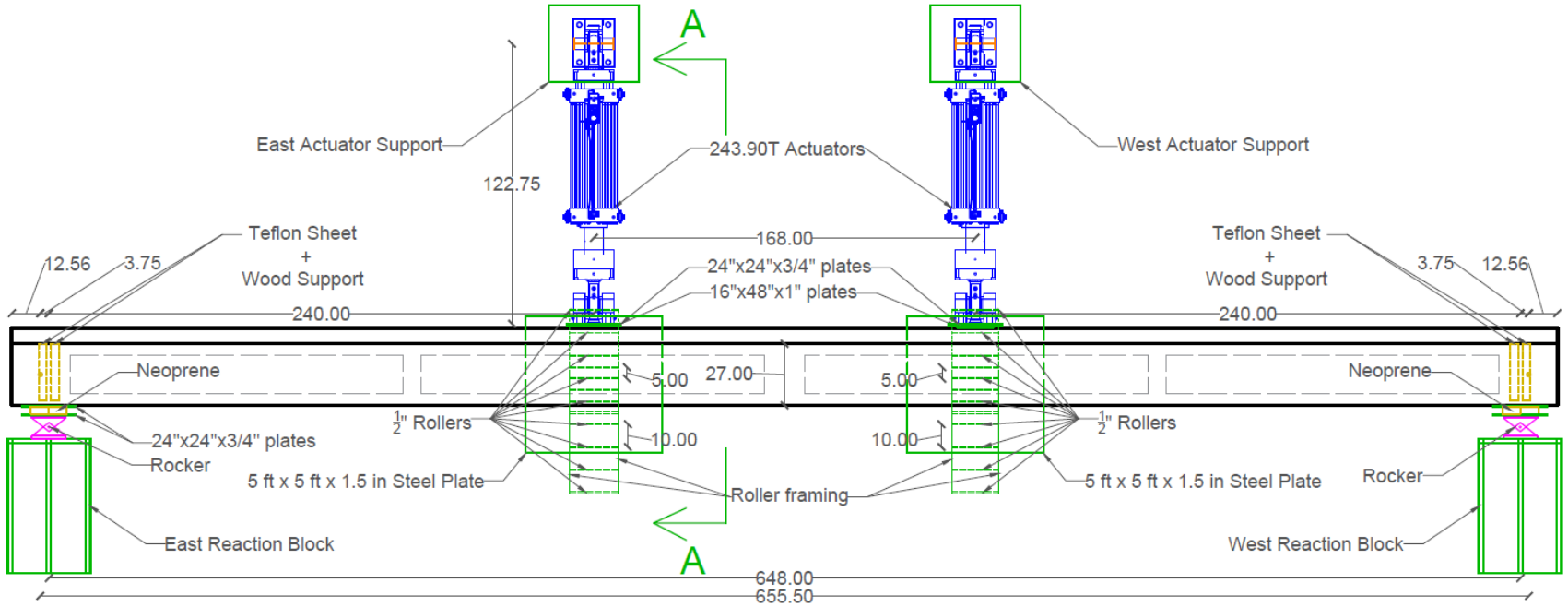

a) Plan view

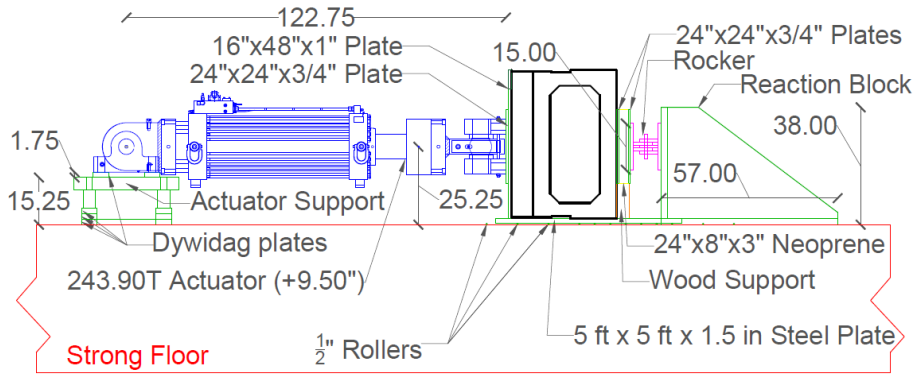

b) Section A-A

Figure 4-3 Beam 3 test setup (units are inches unless stated otherwise)

4.3 Testing Protocol

Two types of tests were conducted on each beam. Forced-controlled tests to obtain the service-level behavior of the beams. These tests were conducted prior to the application of the retrofit, as well as after the FRP laminates and anchors were applied. The tests prior to the FRP application provide a baseline to compare the initial condition of the beams, while the comparison of the behavior before and after the application of the retrofit scheme provides a measure of its effect on the handling of everyday loads. Then displacement-controlled tests were conducted to investigate the behavior of the retrofitted beams until failure. The development of the loading protocol is explained in the following sections.

4.3.1 Service-Level Tests

The vehicular-load demand on the beams during service was estimated according to the guidelines of AASHTO LRFD Bridge Design Specifications, 8th Edition (AASHTO, 2017) on bridge loads and distributions. Hence, a moving-load analysis was performed on models of the beams in SAP 2000 V21 (CSI, 2020) to obtain the maximum moment demand. The analysis included the HL-93 vehicular live load in combination with the self-weight of the beams and the deck. It should be noted that the HL-93 loading scenario consists of three elements, namely the Truck, Tandem, and Lane loads. The applicable load cases and amplification factors, including "1.33 Truck + Lane" and "1.33 Tandem + Lane" were considered in the analysis.

The distribution of the estimated maximum demand between the box beams was obtained from the live-load distribution factors, g, as recommended by AASHTO Article 4.6.2.2. Table 4-1 summarizes the estimation of the share of each beam from the maximum moment demand and the corresponding actuator force required to achieve the estimated demand. The target force was estimated to be 23.0 kips for the two 3-ft wide beams and 23.4 kips for the 4-ft wide beam with the different actuator location. The maximum force used for the service-level tests was increased to 25 kips per actuator to account for the friction at the gravity-load support mechanisms. The load was applied at a slow loading rate of 4.8 kips per minute. Each test consisted of two loading cycles as the first cycle involved the closing of gaps that were introduced during the placement of the beams within the test setup between all the loading and reaction components of the test setup. These small gaps were created due to imperfections of the beams, but also due to their large weight that made the manipulation with the cranes rather challenging.

Table 4-1 Calculation of maximum actuator force for the service-level tests

Specimen	Span length	Beam depth	Maximum moment from analysis	Tables used from AASHTO	live-load dist. factor g	Share of each beam	Distance between actuators	Force required at each actuator	Force applied by each actuator
	ft.	in.	kip-ft			kip-ft	in	kips	kips
Beam 1	54.625	34	1496.1	4.6.2.2.2b-1 4.6.2.2.1-1	0.235	351.0	288	23.4	25
Beam 2									
Beam 3	54.625	34	1579.5	4.6.2.2.1-3	0.292	460.6	168	23.0	25

4.3.2 Capacity-Level Tests

Preliminary analysis was conducted to estimate the flexural and shear capacities of the selected beams using the applicable methods as per ACI 318-14 (ACI, 2014) so that the most suitable actuators could be selected. The strength calculations were performed based on the information from the available drawings, as well as the recommendations found in the literature:

- Strand type: ½" diameter seven-wire stress-relieved Grade 270 (sectional area: 0.153 sq. in).
- Jacking force for each strand: 28700 lbs. (187.6 ksi prestress).
- Approximately 80 percent strain relaxation is assumed, leading to a prestress level of 150 ksi.
- The compressive strength of concrete is assumed to be equal to 6000 psi.
- Compressive non-prestressed reinforcement is not included.

The results of the analytical calculations are summarized in Table 4-2. As it can be seen in the table, the force required to achieve failure was 84 kips for Beams 1 and 2, and 86 kips for the unretrofitted beams, which led to the selection of two MTS 243.90T actuators with a maximum capacity of 450 kips and a stroke of 40 inches. Also, the calculated stress levels in strands at failure were used to inform the retrofit design in terms of the tension force required from the retrofit system.

Table 4-2 Strength calculations of the unretrofitted beams

Specimen	Total strand area	Strand stress level at beam failure[1]	Total force produced by strands at failure	Predicted nominal moment capacity	Approximate concrete shear capacity[2]	Distance between actuators	Total force required for failure	Force required at each actuator
	Sq. in.	ksi	ksi	kip-ft	kips	in	kips	kips
Beam 1	2.142	257.4	551.4	1340.3	87	264	168	84
Beam 2								
Beam 3	2.754	257.9	710.2	1729.3	107	168	173	86

[1]ACI 318-14 section 20.3.2.3.1 is used to calculate the stress levels in strands at the nominal strength condition.
[2]ACI 318-14 section 22.5.5.1 is used to estimate the concrete shear capacity. Total cross-sectional area of the beams was used instead of term $b_w.d$ in equation 22.5.5.1.

4.4 Instrumentation

In order to monitor the behavior of the beams during the tests and the interaction between the concrete and CFRP laminates and anchors, the following instrumentation layout was deployed.

1. Displacement transducers were placed at multiple locations along the beam length to measure the overall deformation of the beam and the possible rotation along its longitudinal axis. The latter was important to confirm the setup acted as intended without introducing any undesired deformation modes.
2. Strain gauges were installed at selected sections on the concrete and FRP surfaces, to monitor the strain compatibility between the concrete and FRP.
3. An accurate 3D Coordinate Measuring Machine (CMM) known as Krypton was used to track 45 to 54 locations on each beam near one of the two loading zones, to obtain the local deformations and track possible delamination.

In addition to instrumenting the beams, the possible slippage/rotation of the reaction blocks was monitored using an array of displacement transducers.

Figures 4-4 through 4-6 present the instrumentation details of Beams 1, 2, and 3, respectively during the service-level tests prior to the retrofit application. Figures 4-7 through 4-9 present the instrumentation of the same beams during the tests after the beams were retrofitted. The type, location, and measurement direction of instrumentation are identified by an eight-character name in the drawings.

The first character indicates the instrument type which can be “D”, “G”, or “A” (denoting the Displacement transducers, strain Gauges, or Accelerometers, respectively).

The second character indicates the sensor location with respect to the middle of the beam which can be “W”, “E”, or “M” (referring to the West side of the mid span, East side of the mid span, and the Mid span, respectively). As stated in a previous chapter, the cardinal coordinates are based on the beam orientation at the SEES laboratory which remains unchanged for the entire testing period.

The third and fourth characters identify the distance of the instrument from the mid-span of the beam in feet (in case of closely-spaced sensors of the same type, this two-digit number increases by 1 ft. between those sensors to distinguish between the names. The accurate location of all sensors is provided in the drawings).

The fifth character provides the side of the beam on which the sensor is installed which can be “T”, ”B”, or “S” (corresponding to the Top, Bottom, and Side surfaces of the beam, respectively as shown on the cross section of the beam provided in the upper left of the instrumentation drawings) for the beam instrumentation. In the case of the instruments used to monitor the test setup, the fifth character can be “A” or “R” (Actuator or Reaction blocks, respectively).

The sixth and the seventh characters provide the location of the sensors within their corresponding section, measured in inches from the upper edge (after the beam is flipped to its testing position) of the corresponding surface for the top and bottom surfaces and the South edge of the side surface as shown in the drawings. These two characters take the value of “0” for the sensors monitoring displacements of the reaction blocks or actuator supports.

The eight and last character indicates the sensor measurement direction which can be “X”, “Y”, “Z” (based on the coordinate system shown in the drawings) or “D” (identifying the orientation of the Diagonal displacement transducers installed at 45 degrees angle in the horizontal plane). The summary of the nomenclature for the instrumentation is provided in Figure 4-10.

In addition to the abovementioned sensors, the tests were video recorded from different angles using 6 to 8 cameras.

4.5 Data Acquisition

The response of the beams was recorded throughout all tests using a data acquisition system, acquiring data from the sensors at the rate of 25 Hz.

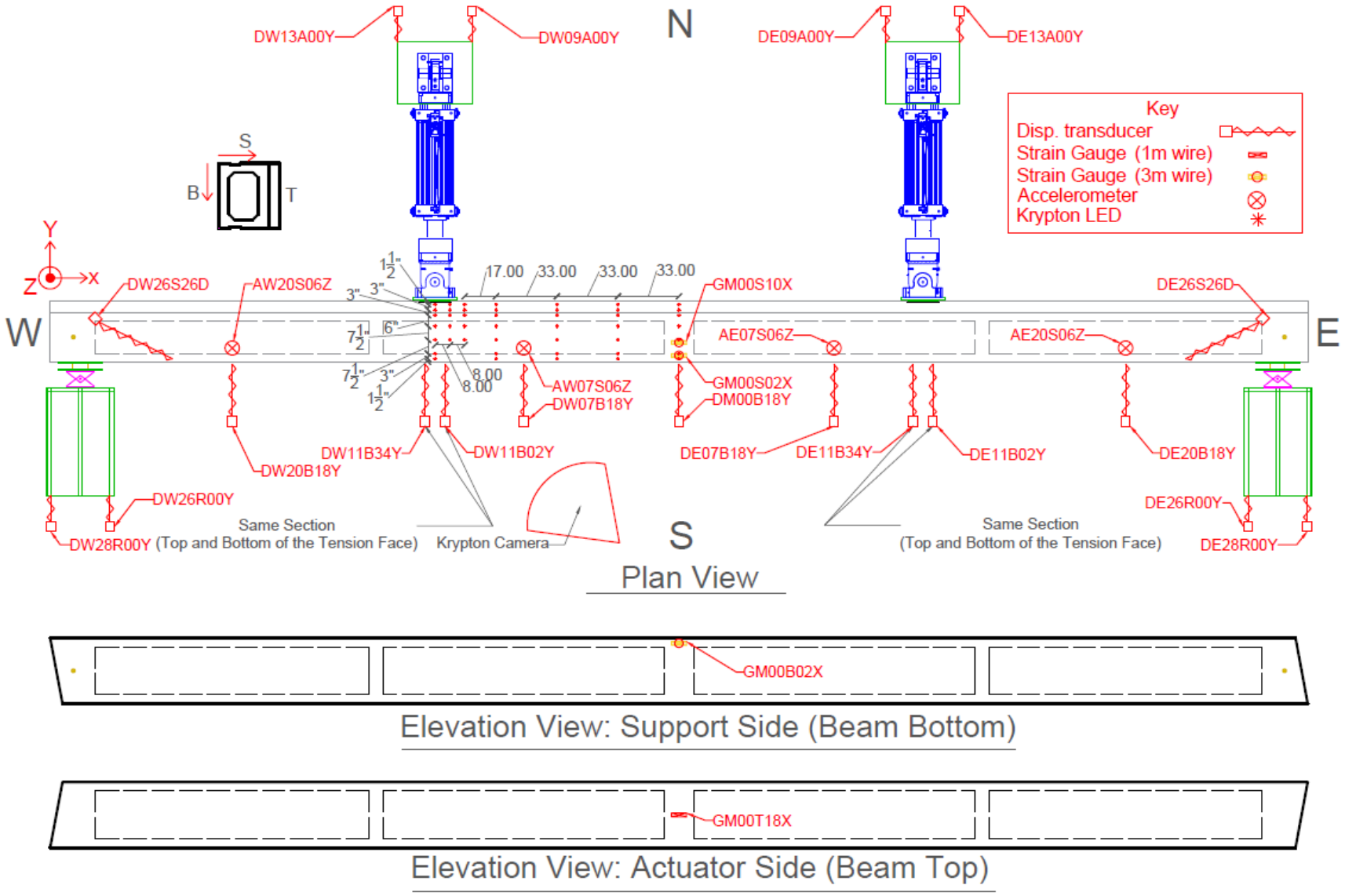

Figure 4-4 Beam 1 Instrumentation (service-level tests)

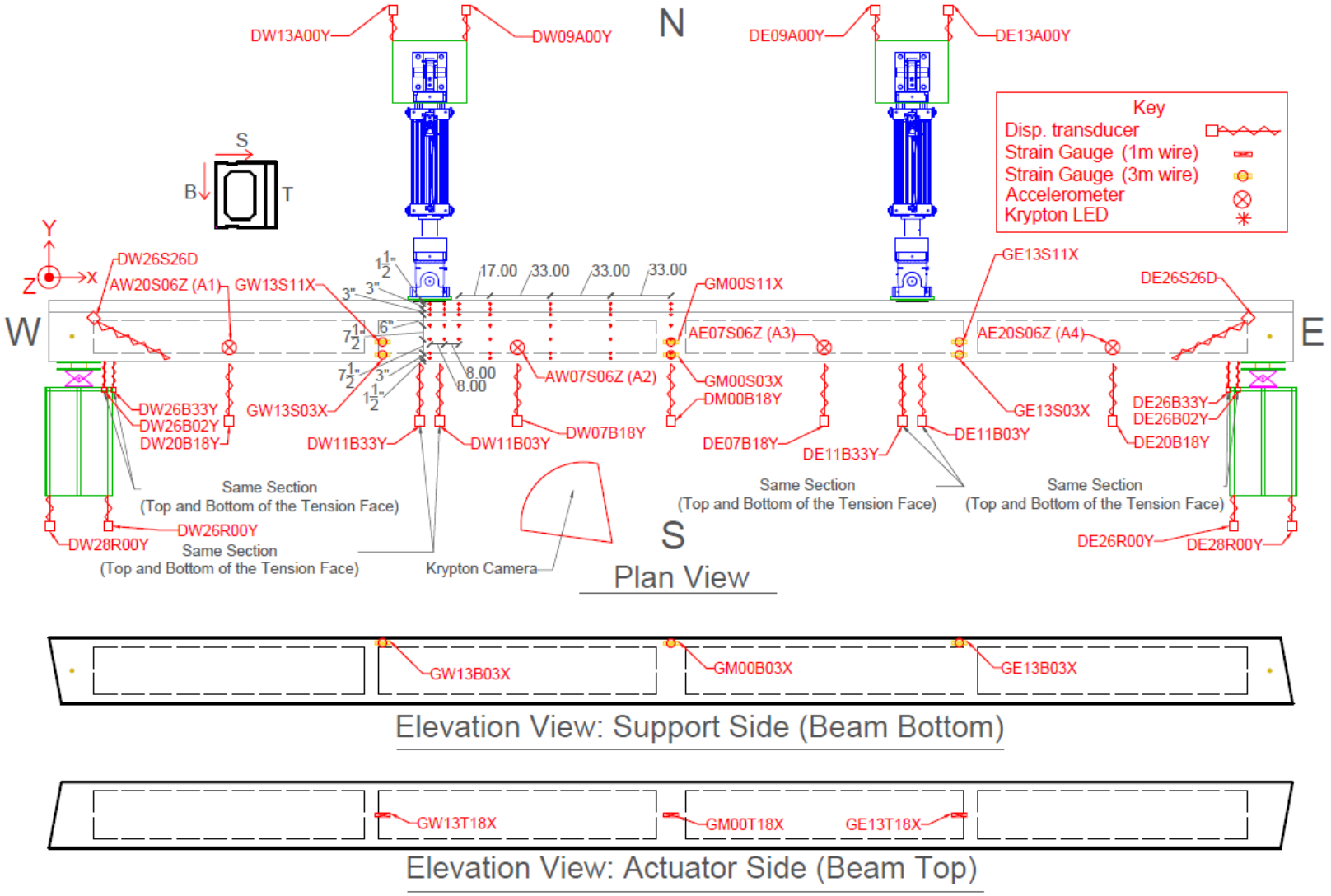

Figure 4-5 Beam 2 Instrumentation (service-level tests)

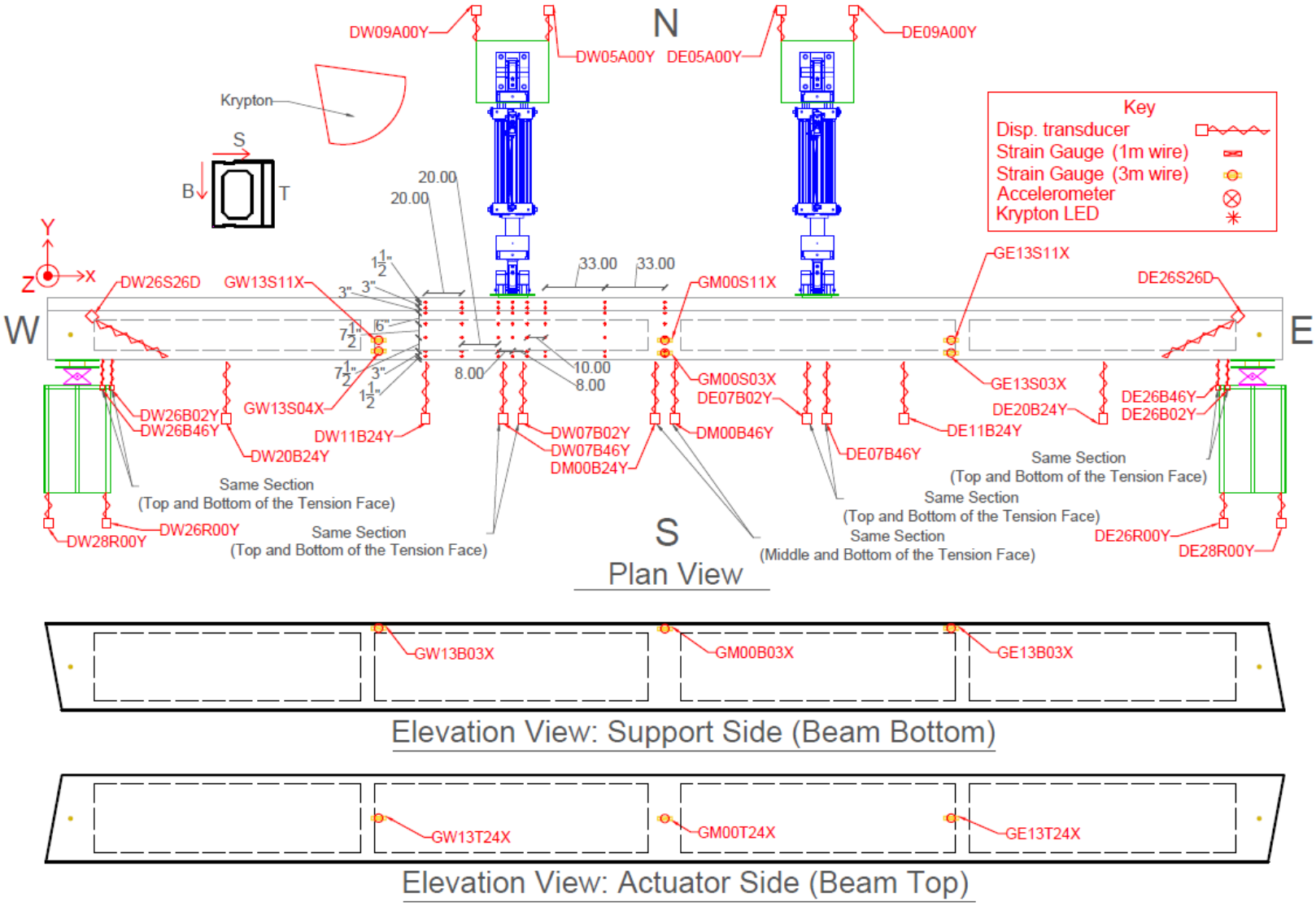

Figure 4-6 Beam 3 Instrumentation (service-level tests)

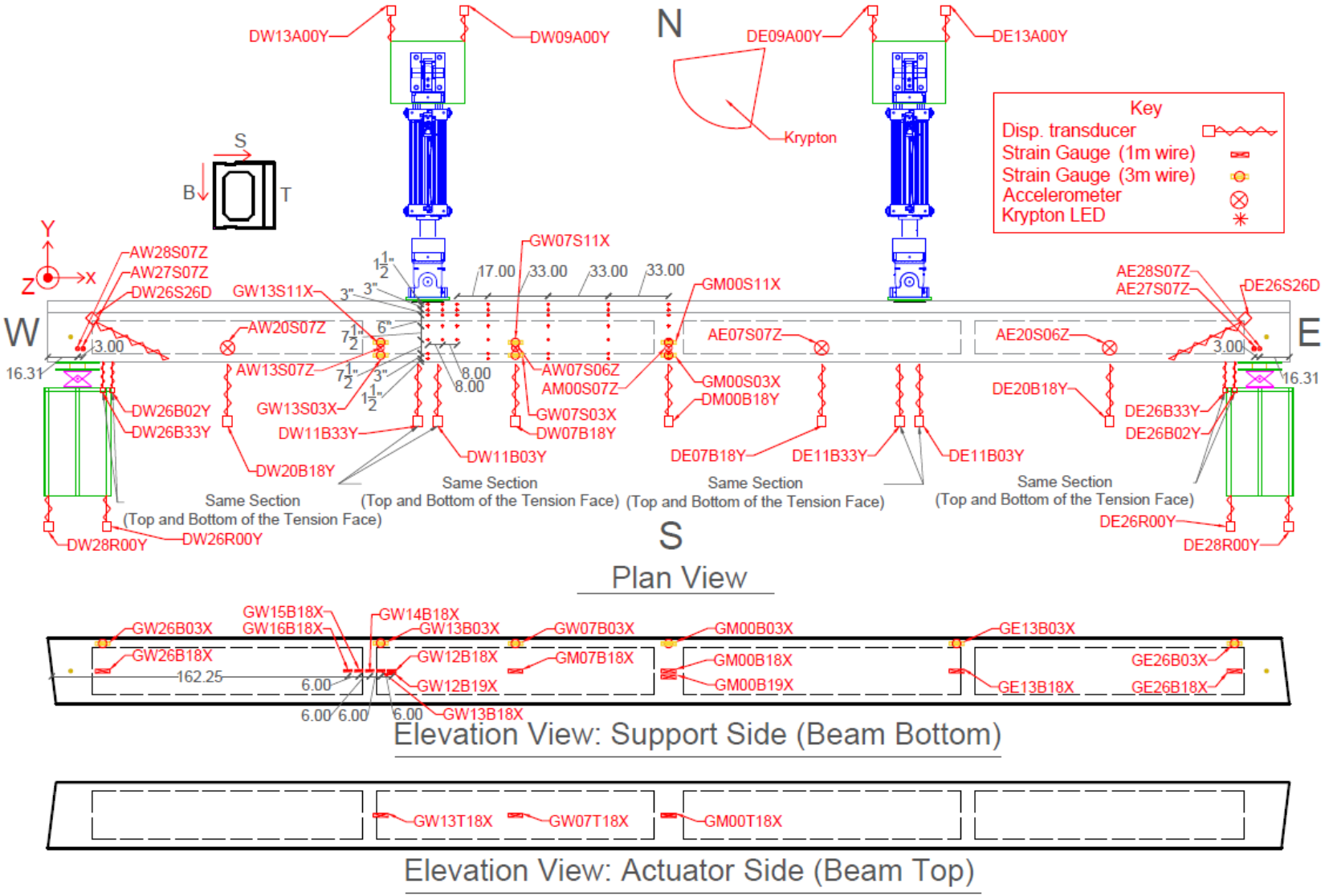

Figure 4-7 Beam 1 Instrumentation (capacity-level tests)

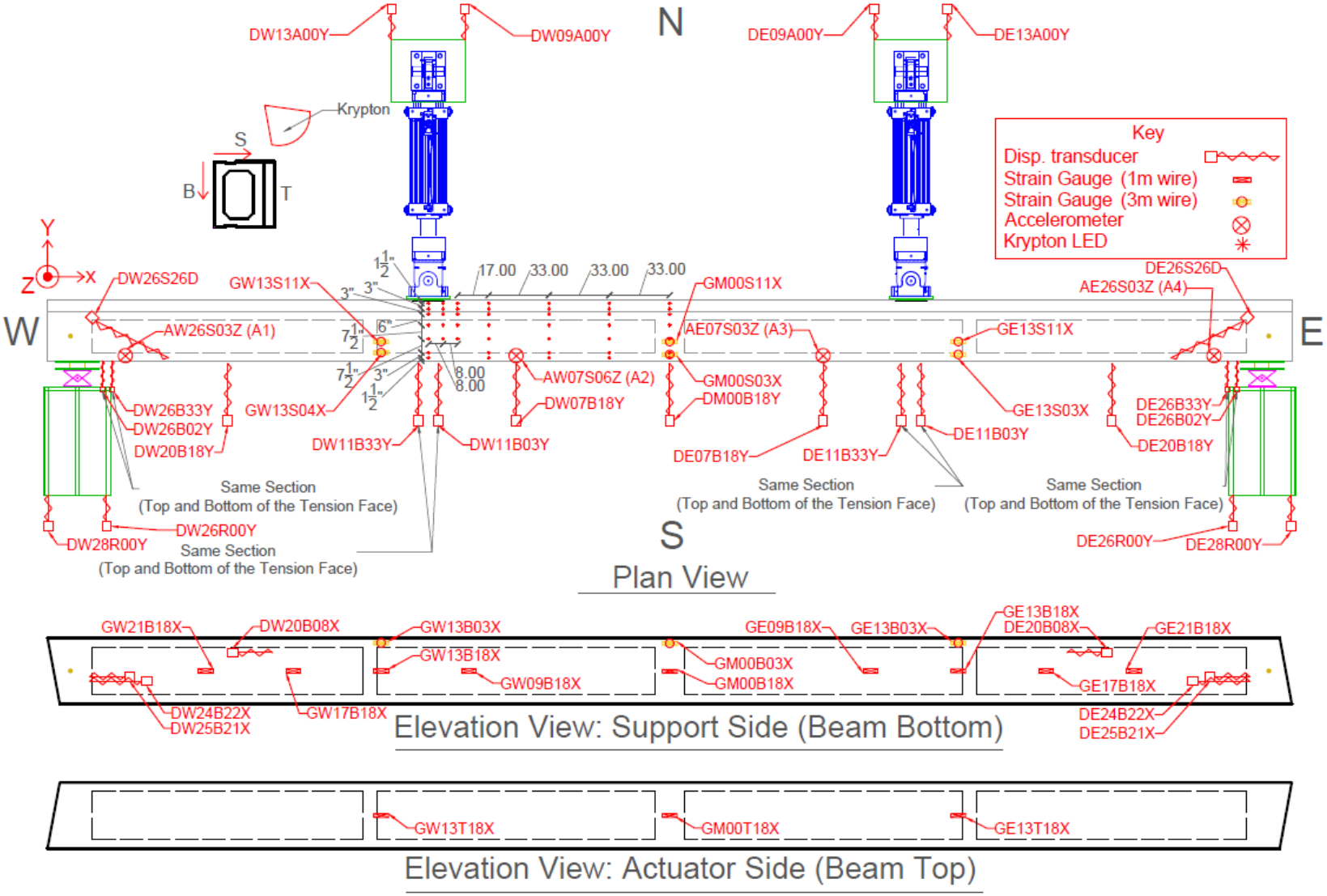

Figure 4-8 Beam 2 Instrumentation (capacity-level tests)

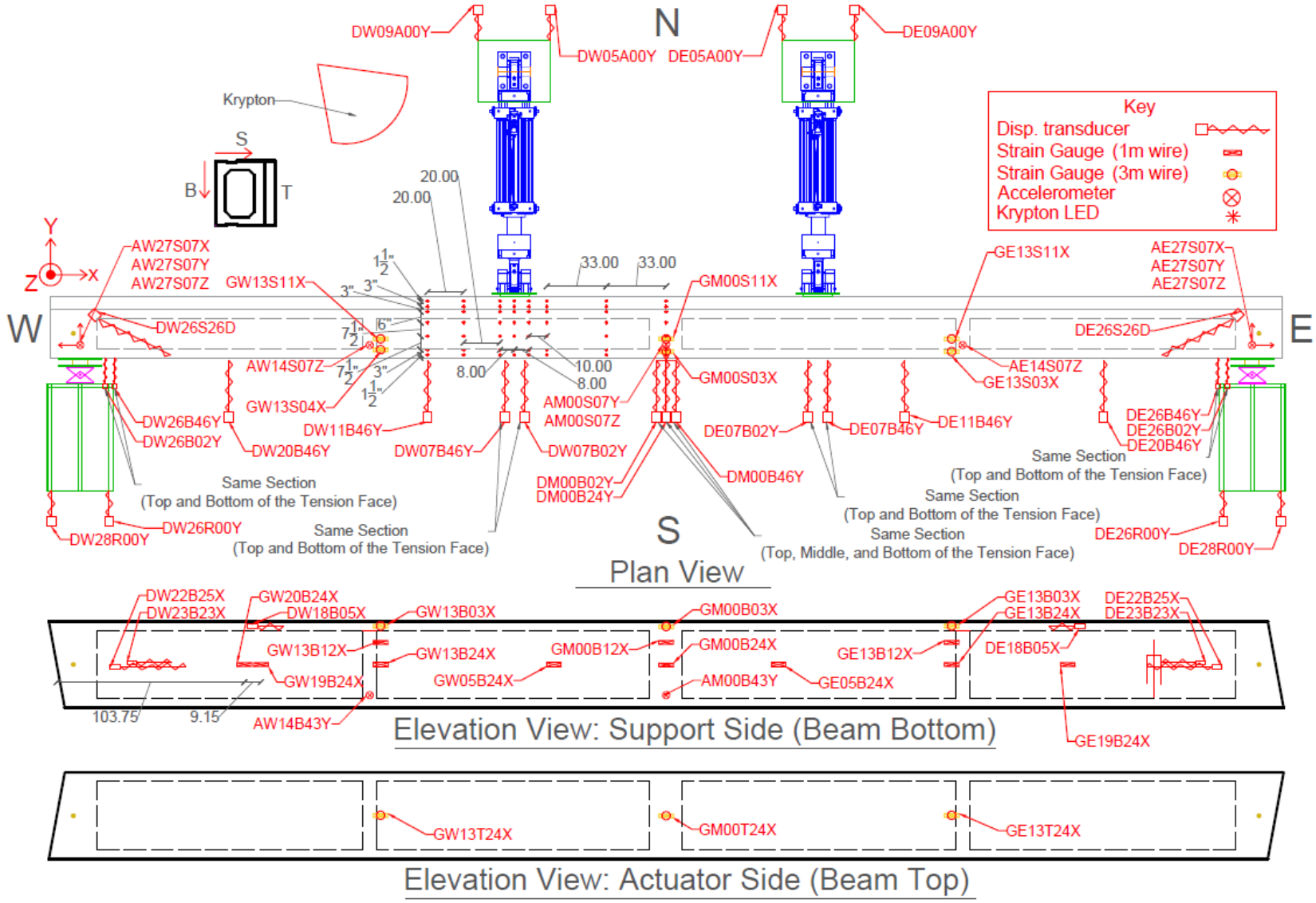

Figure 4-9 Beam 3 Instrumentation (capacity-level tests)

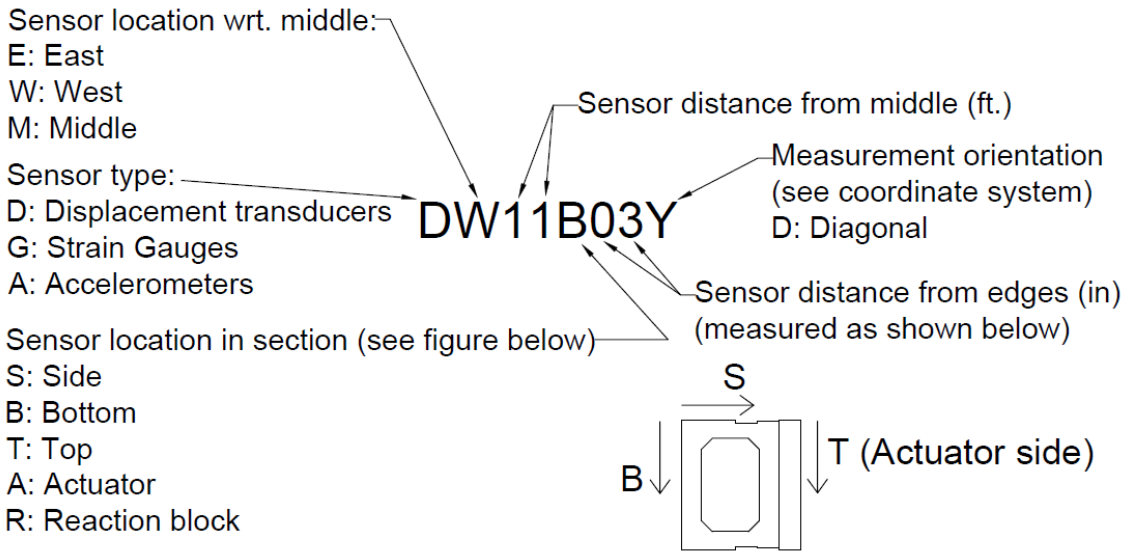

Figure 4-10 Instrumentation nomenclature

CHAPTER 5

TEST RESULTS

5.1 Beam 1

5.1.1 Service-level tests: Unretrofitted Beam

During the service-load tests the actuators were forced controlled, and each of the two actuators was set to apply the same loading profile to the beam to represent the design service load as discussed in a previous section. These tests were conducted to allow the comparison of the condition of the beams prior to the retrofit but also provide a measurement of the difference in the behavior under service loads due to the FRP application.

The history of the total force applied to Beam 1 during the service-level tests is presented in Figure 5-1. At the beginning of the first test, the actuators pushing the beam had to overcome the resisting friction between the gravity supports and the floor and moved the beam so that it came to full contact with the supports at the beam ends. The gaps introduced during the placement of the beam were unavoidable due to the weight, dimensions, and imperfections of the beam. In addition to translation, this motion involves rotation about the support with which the beam makes the first contact, causing fluctuations in the force as shown in Figure 5-1. Hence, the test was repeated. With the beam already in full contact with the supports place after the first test, the force profile is more stable and closer to the intended load protocol in the second test. Moreover, in the case of the repeated loading cycle, the recorded displacement of the beam mainly includes the deformation of the beam due to bending, whereas in the first test the recorded movement was a result of the combined translations and deformation of the beam. The force-displacement responses of the first and the second loading cycles are shown in Figure 5-2. The comparison of the responses indicates that the beam translation had a significant contribution to the displacement response recorded from the first test. The separation of this translation from the beam deformation, which is the parameter of interest, is not feasible. Therefore, the discussion of the service-level test focuses on the second cycle.

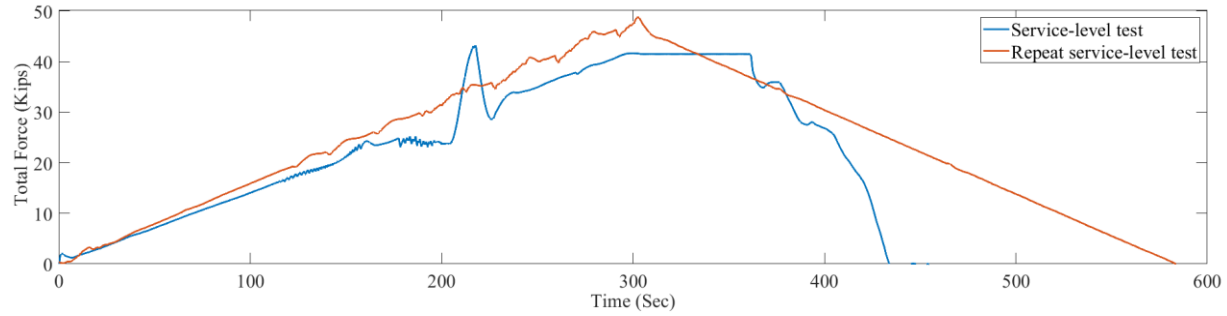

Figure 5-1 Total force time series during the service-level test of unretrofitted Beam 1

The strain was measured at four locations on the middle section of the beam and the results are presented in Figure 5-3. As expected, maximum tensile (positive) and compressive (negative) strains were recorded at the bottom and the top of the cross section, respectively. The strain profile at the peak force, shown in Figure 5-4, closely follows a linear variation of strain along the height of the section, which agrees with the kinematic assumption used in cross-section analyses that plane sections remain plane.

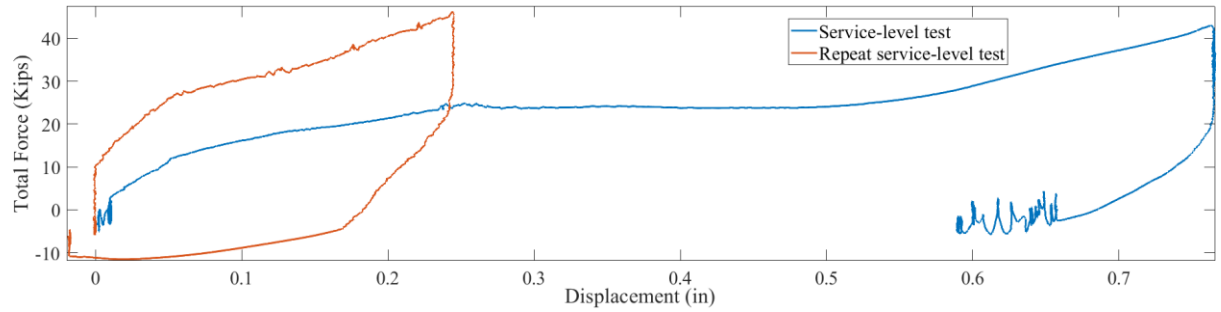

Figure 5-2 Total force vs. mid-span displacement during the service-level tests of unretrofitted Beam 1

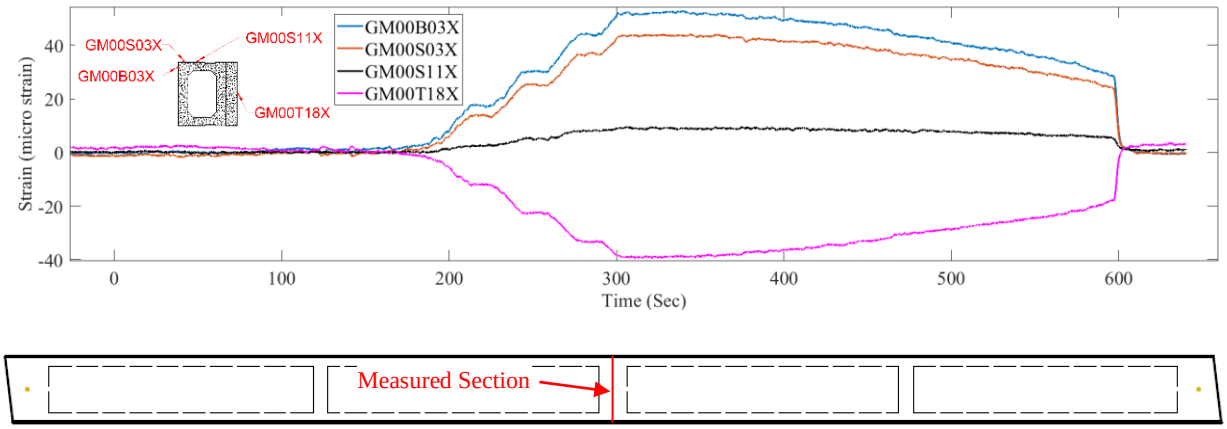

Figure 5-3 Strain time series during the service-level test of unretrofitted Beam 1

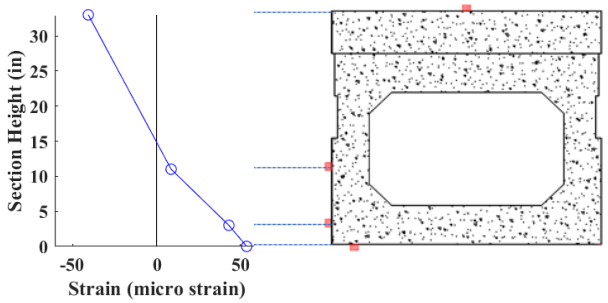

Figure 5-4 Strain profile at the peak force during the service-level test of unretrofitted Beam 1

5.1.2 Service-level tests: Retrofitted Beam

The variation of the total force applied to the retrofitted beam during the second cycle of the service-level test is presented in Figure 5-5. While the peak force is close to that achieved during the tests of the unretrofitted beam, a smoother loading profile is achieved, mainly as a result of adjustments made to the gravity supports to reduce the friction. The drop in the friction can be observed in the force-displacement response of the beam to the tests conducted prior to and after the retrofit as presented in Figure 5-6. The friction results in a trilinear response during both the loading and unloading stages of the unretrofitted beam. On the other hand, the friction is overcome at the onset of the loading and unloading of the retrofitted beam, resulting in a bilinear response. It can be observed from Figure 5-6 that the retrofitted beam displaces less than the unretrofitted for the same level of force. Moreover, the maximum mid-span displacement is reduced by approximately 2.5 percent as a result of the retrofit, indicating an increase in the stiffness of the beam.

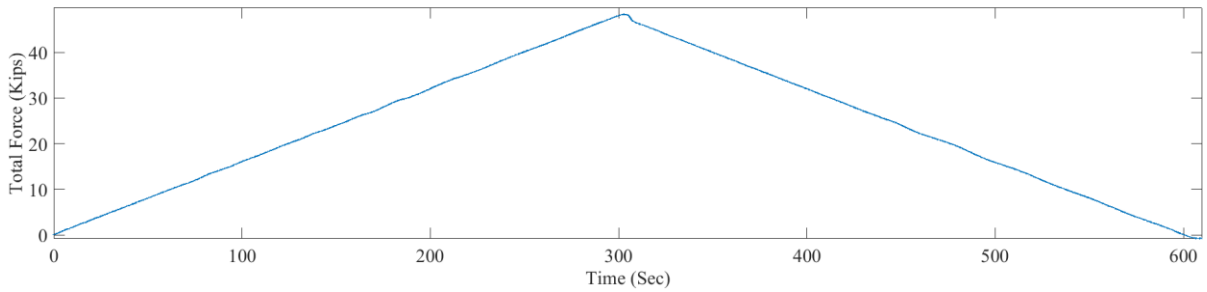

Figure 5-5 Total force time series during the repeat service-level test of retrofitted Beam 1

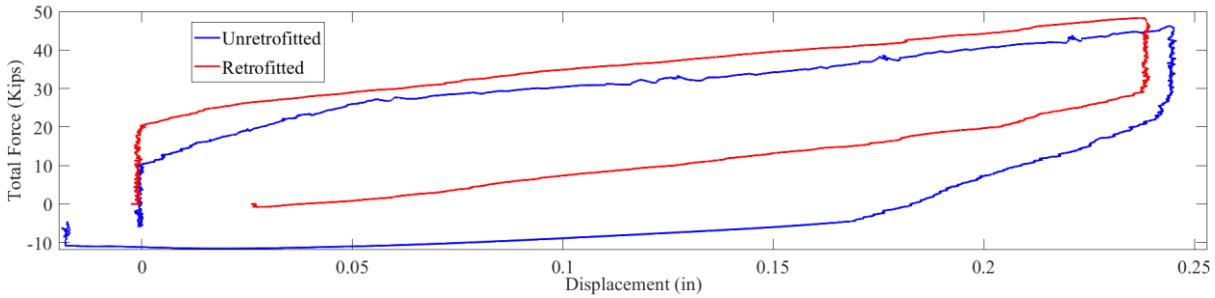

Figure 5-6 Total force vs. mid-span displacement during the repeat service-level tests of Beam 1

The strain measured from the concrete and the FRP laminate at the bottom face of the beam are compared in Figure 5-7. The measurements closely match each other, indicating an adequate bond between the FRP laminate and the concrete. The strain profiles at the peak force are plotted for three sections in Figure 5-8. Similar to that of the unretrofitted beam, the variation of strain along the height of each section is nearly linear. Figure 5-8 also indicates that the location of the neutral axis is similar between Sections a and c, while it is elevated in Section b. This can be justified by considering that Section c is a box section as shown in Figure 5-8 and therefore, its centroid is shifted toward the top of the section when compared to solid rectangular Sections a and b. This indicates that the concrete in the solid sections contributes to the tensile resistance of the section at this level of applied moment.

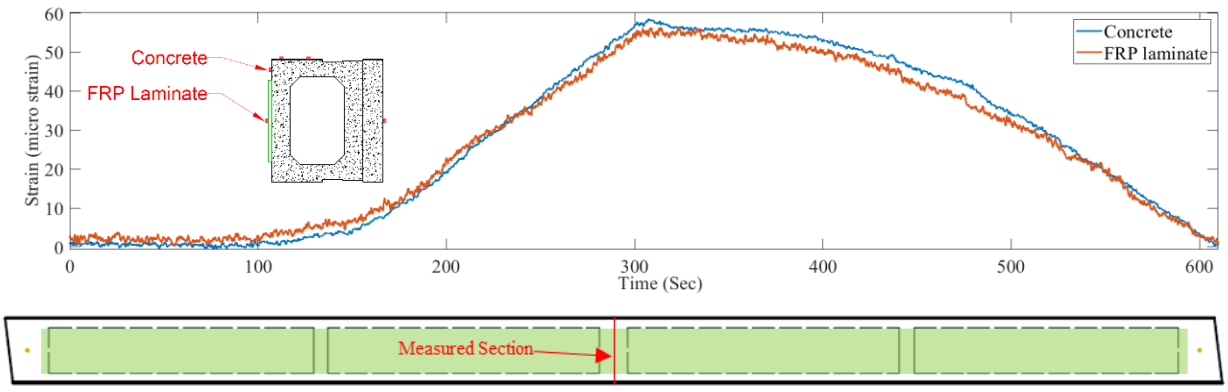

Figure 5-7 Strain time series during the service-level test of retrofitted Beam 1

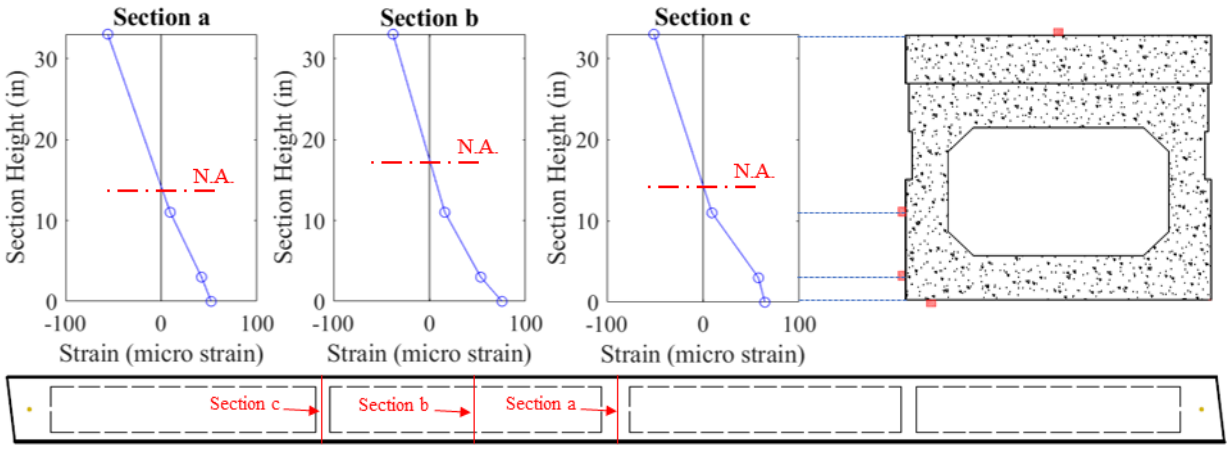

Figure 5-8 Total force time series during the repeat service-level test of retrofitted Beam 1

5.1.3 Capacity-level test

Following the service-level test and its repeat, the retrofitted beam was subjected to a displacement-controlled test until failure. The history of the total force applied to Beam 1 is presented in Figure 5-9. As discussed in a previous section, the applied force is resisted by beam deformation as well as the friction between the gravity supports and the floor. The latter has to be removed from the total force to obtain the force responsible for the beam deformation. The total friction force, estimated from the unloading branch of the repeat service-level test, is equal to 21.09 kips for Beam 1 and is deducted from the total force as shown in Figure 5-9 (as for the actuator force, half of the friction is deducted). Unless stated otherwise, the values of force and moment presented in this report will reflect the reduced level force due to friction.

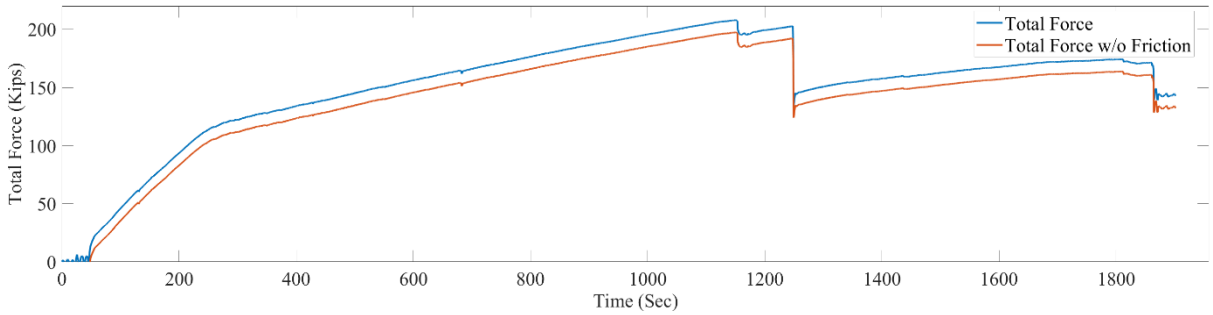

Figure 5-9 Total force time series during the capacity test of retrofitted Beam 1

The force applied by each actuator, shown in Figure 5-10, indicates that prior to the beam failure the east actuator had a significantly lower contribution to the total force compared to the west actuator, although the same displacement commands was given for both actuators. Once the test

was completed, the reason for this discrepancy was investigated. The investigation after the tests concluded that the observed difference was a result of an error in the measurements of the displacement of the east actuator.

This is presented in Figure 5-11, which shows that the actuator displacement reading, which was used by a controller to give displacement commands to the actuator, was exceeding the actual displacement due to a calibration error. Therefore, the east actuator was only displacing about 80% of the given command and consequently, it was applying lower force compared to the west actuator. This problem was fixed for the following tests.

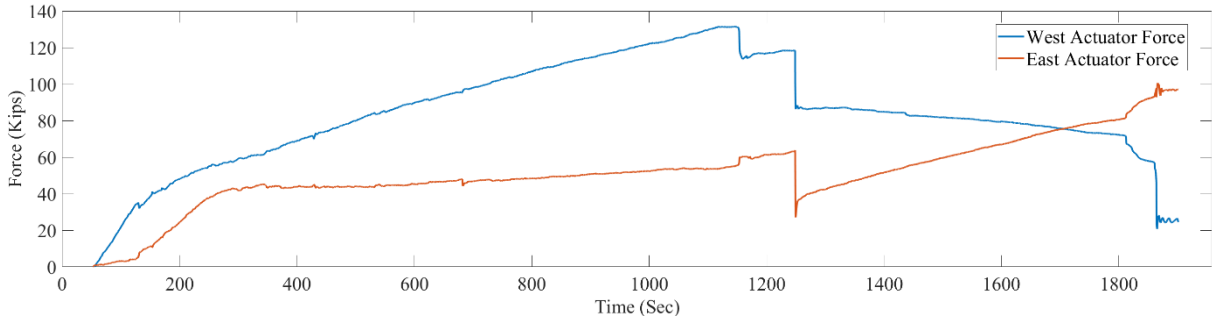

Figure 5-10 Actuator force time series during the capacity test of retrofitted Beam 1

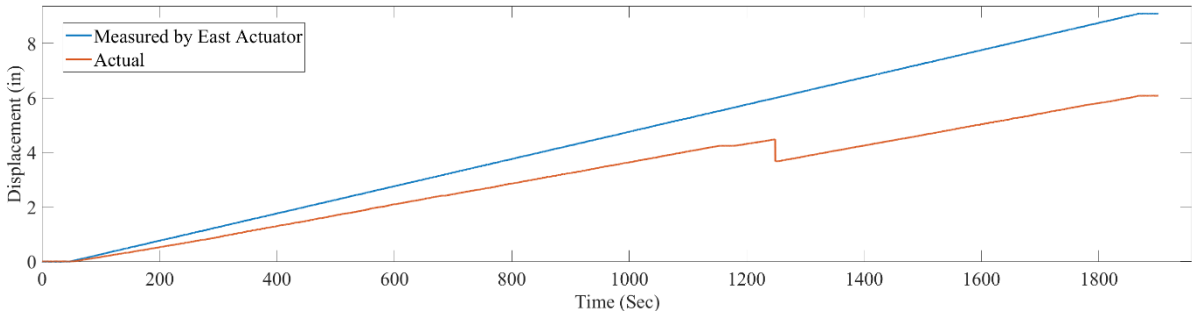

Figure 5-11 Error in the displacement read by the East actuator

The bending moment at the location of the actuators was calculated from the actuator forces and plotted against the corresponding beam rotations as shown in Figure 5-12. It should be noted that in a four-point-bending test, if the applied forces are equal, the bending moment is constant between the two actuators. In the case of uneven forces, the maximum moment occurs at the location of application of the higher force. In the case of Beam 1, the moment at the west actuator represents the maximum moment demand in the beam. As the demand increased, the concrete in tension reached its tensile strength and cracked. This led to a reduction in bending

stiffness as is evident from the change in the slope of the moment-rotation response curve. The concrete cracking can also be inferred from the comparison of the strain between the concrete and the FRP laminate at the bottom face of the beam, as shown in Figure 5-13. As the cracking moment was reached, the strain in the concrete started to rapidly deviate from that in the FRP Laminate. This indicates a crack was initiated within the boundaries of the strain gauge. This observation also suggests that the strains measured from the concrete in tension at moments beyond the cracking moment may not represent the state of strain as a crack may or may not cross the strain gauges. Therefore, the history of the tensile strain is obtained from the gauges installed on the FRP laminate as shown in Figure 5-14.

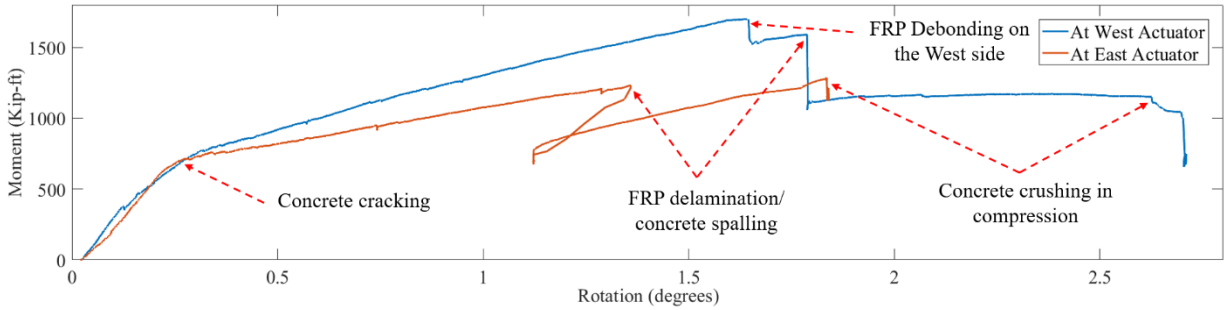

Figure 5-12 Moment vs. beam rotation during the capacity test of retrofitted Beam 1

Beyond the cracking moment, the beam resisted the increasing demand until debonding was initiated on the west side of the beam as shown in Figure 5-12. The debonding caused a drop in the strain on the west of the beam as illustrated in Figure 5-14. A smaller strain drop was recorded at the middle while a slight increase in the strain occurred on the East side. This observation indicates that the force along the FRP laminate was redistributed and therefore, the moment resistance started to increase following the debonding. This increase was interrupted by FRP delamination, concentrated mainly on the West side, as indicated by the drop in the moment and strain in Figures 5-12 and 5-14, respectively, marking the failure of the FRP system.

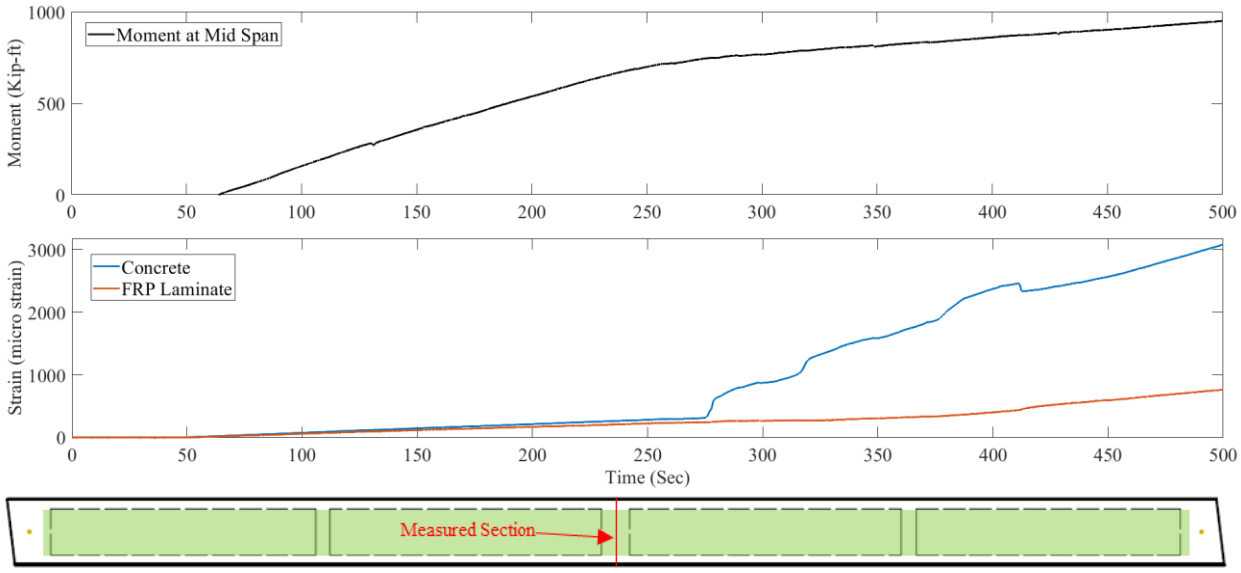

Figure 5-13 Strain time series measured at the onset of concrete cracking at the mid span

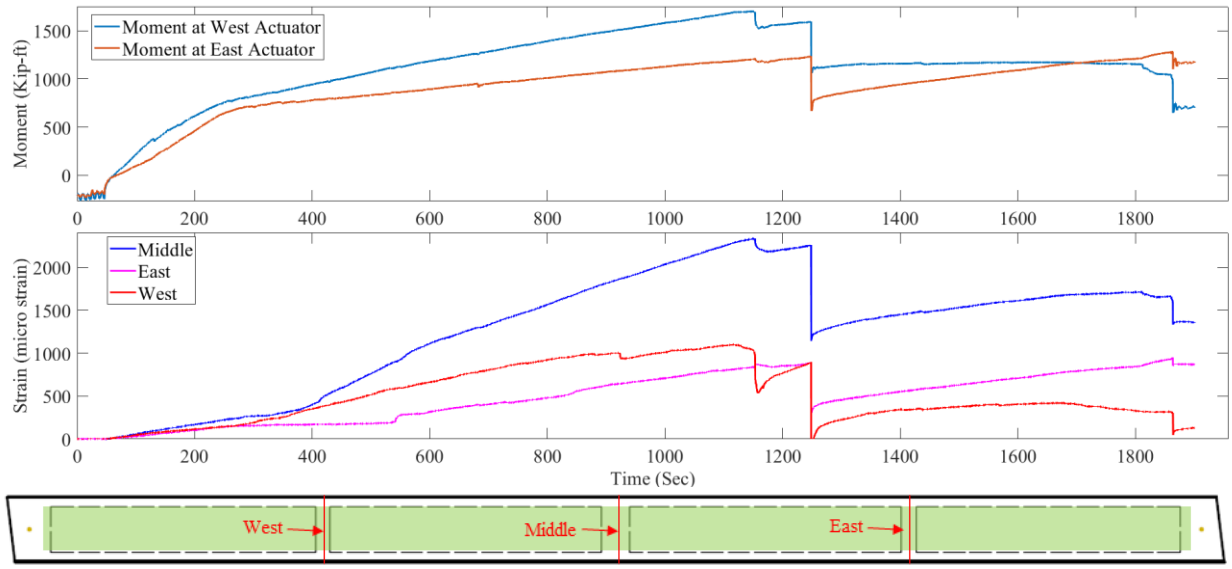

Figure 5-14 Strain variation on the FRP laminate during the capacity test of retrofitted Beam 1

Figures 5-15 through 5-17 present the state of the damage following the FRP failure. Spalling of concrete cover attached to the FRP was observed, exposing the prestressing strands. Also, the anchors on the west side of the beam were pulled out along with a cone of concrete surrounding them as shown in Figure 5-16. The FRP laminate slid relative to the concrete at the west end of

the beam, rupturing one anchor and leaving the other two in place as shown in Figure 5-17. The retrofit on the east side of the beam did not exhibit noticeable damage. It should be noted again that this difference in the state of damage between the east and west sides was most likely the result of the difference in the applied forces between the actuators that resulted in unsymmetric loading. Since the FRP system could not provide any resistance beyond its failure, the loading of the beam was continued, as this would allow to obtain the behavior of the unretrofitted beam. The loading stopped once the beam failed due to concrete crushing on the compression side.

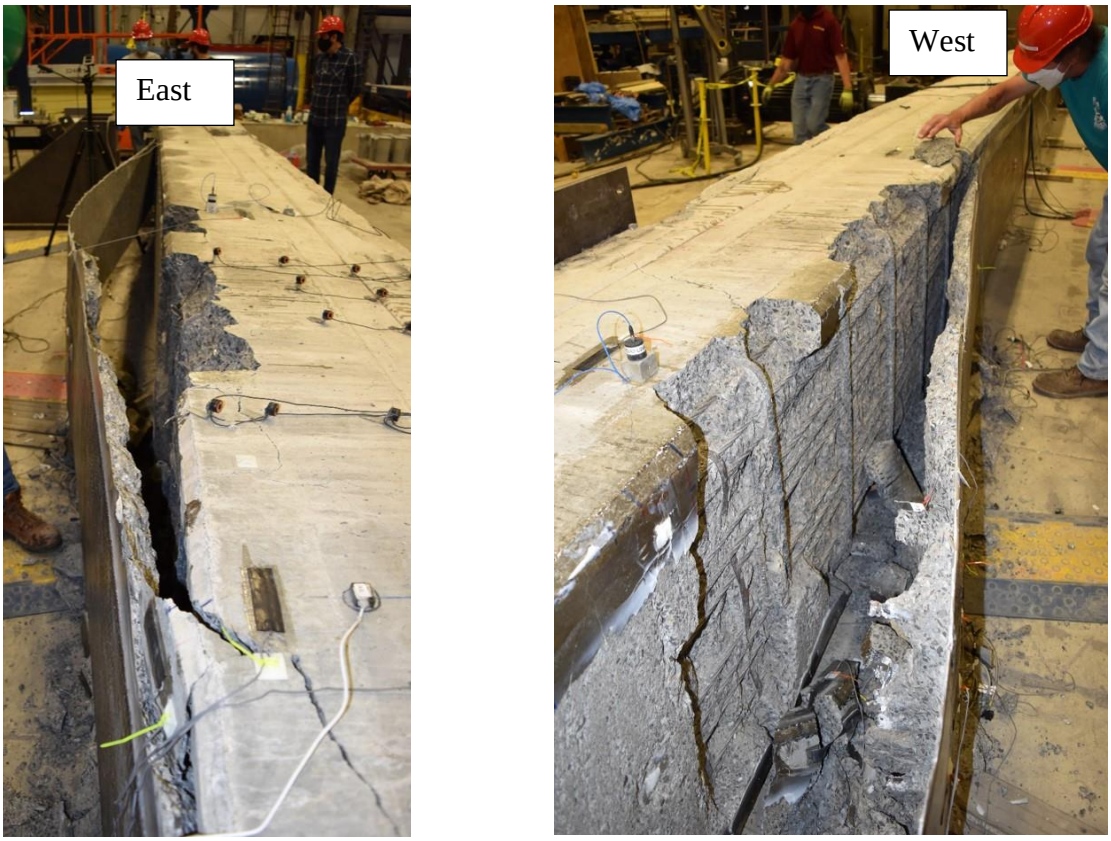

a) View toward East a) View toward West

Figure 5-15 Concrete spalling and FRP delamination at the west actuator location

a) spalled concrete cover b) anchors pulled out

Figure 5-16 State of damage following the failure of Beam 1

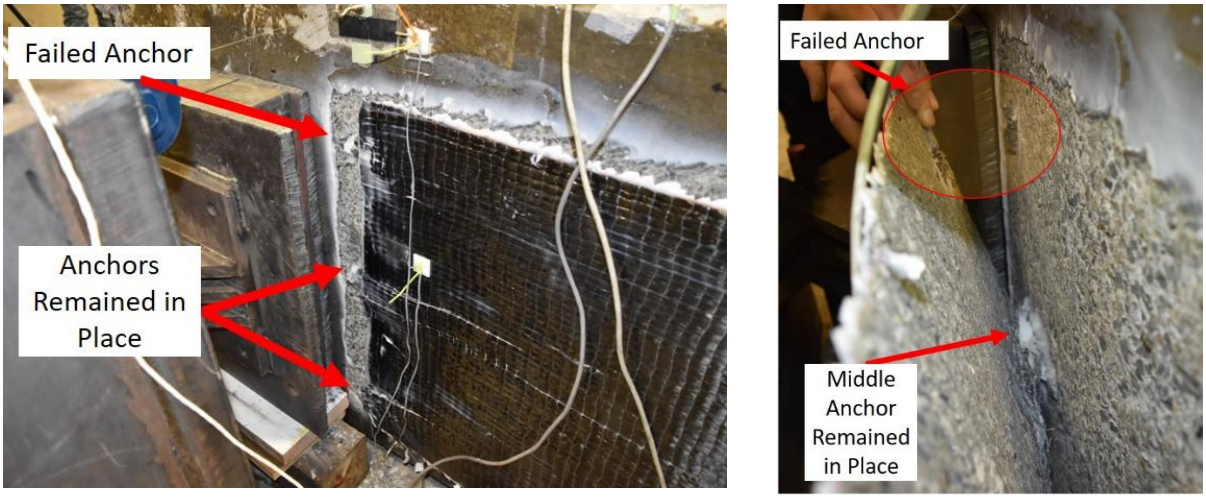

a) slid FRP laminate b) view to FRP-concrete interface

Figure 5-17 FRP sliding at the West end of Beam 1

5.2 Beam 2

5.2.1 Service-level test: Pre and Post Retrofit

The history of the total load applied to Beam 2 during the repeat service-level tests prior to and after implementing the retrofit is presented in Figure 5-18. Compared to the corresponding tests conducted on Beam 1, the variation of force is smoother in this case. Also, the similarity of the applied loading profile between the tests of the unretrofitted and retrofitted beam allows the assessment of the effect of the retrofit on the service-level response of the beam. This improvement is mainly due to the use of a roller system to transfer gravity loads to the floor as described in Chapter 4, leading to a reduction of friction force from 21.09 kips in Beam 1 to 10.73 kips in Beam 2.

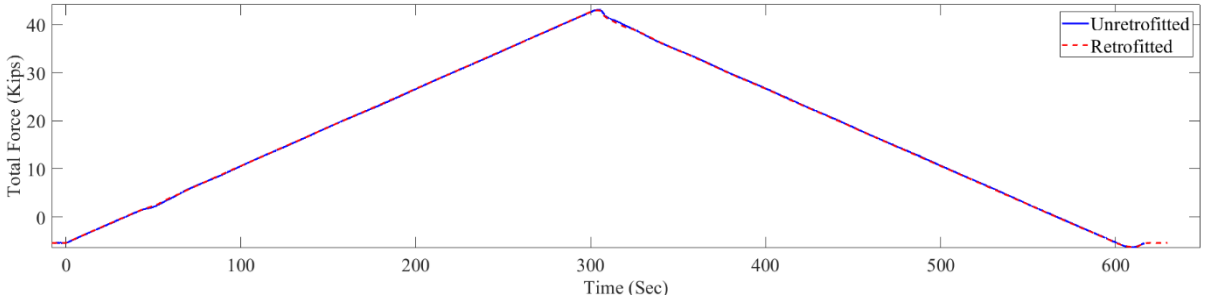

Figure 5-18 Total force time series during the service-level tests of Beam 2

The force-deformation of Beam 2 prior to and after the implementation of the retrofit is presented in Figure 5-19. The retrofit led to a 6.7 percent drop in the maximum displacement at the same peak force, indicating an increase in the stiffness of the beam. This increase is also reflected in the measured strains, an example of which is shown in Figure 5-20. In the figure, the strains corresponding to the tests prior to and after the retrofit are compared. The post-retrofit test resulted in lower strains, as indicated by all strain gauges in the section throughout the test. A similar trend is observed in the strain profiles obtained at the peak forces of the tests from three sections along the beam, as presented in Figure 5-21.

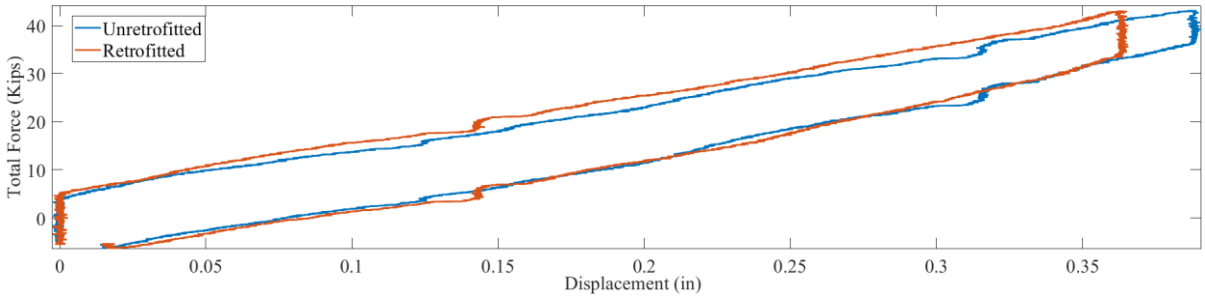

Figure 5-19 Total force vs. mid-span displacement during the repeat service-level tests Beam 2

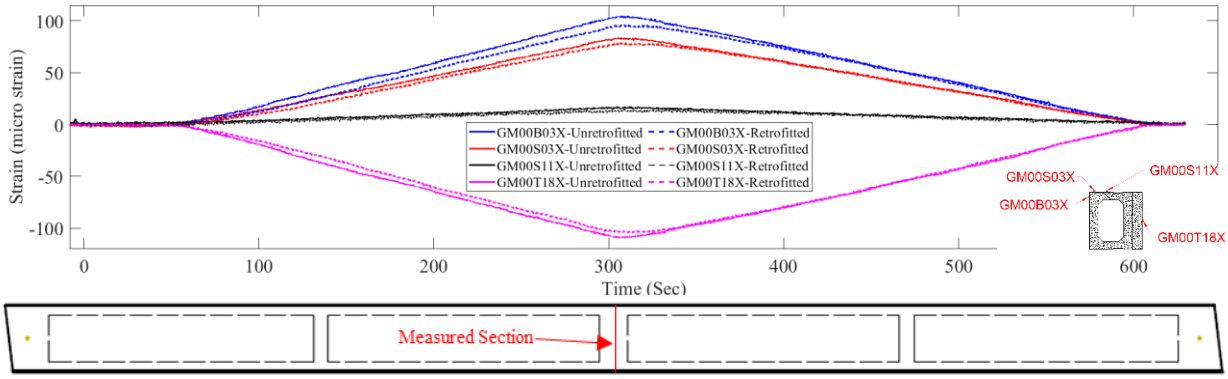

Figure 5-20 Strain time series during the repeat service-level tests of Beam 2

The comparison of strains between the concrete and the FRP laminate measured at the bottom face of three sections along Beam 2 is plotted in Figure 5-22. The strain variations in the FRP laminate tend to follow those in concrete in all sections. However, the values are lower in the FRP laminates. The difference is under 20 percent for the middle and west sections, while the east section indicates a difference of approximately 47 percent. The readings from the corresponding strain gauge on the east section were compared to a nearby strain gauge and the results are presented in Figure 5-23.

As discussed in the next sections, in all beams, it can be observed that the strains on the FRP laminate are consistently lower than the strains on the FRP. Hence, the assumption of strain compatibility assumed by ACI 440.2R-17 does not seem to hold. The reason for the reduced strain of the FRP could be the deformability of the epoxy connecting the FRP laminate and the concrete. The opening of cracks in concrete is not as likely to cause the difference between the strains measured on concrete and those measured on the FRP due to the low-level strain. More importantly, and the fact that the strains maintain a constant slope though out the loading and unloading phases. Moreover, no cracks were observed during the inspection of the specimen. Finally, as shown in Figure 5-13, the opening of cracks in concrete affects the strains dramatically. Such cracks are not observed in Beam 2 (Figure 5-22), nor in the case of Beam 3.

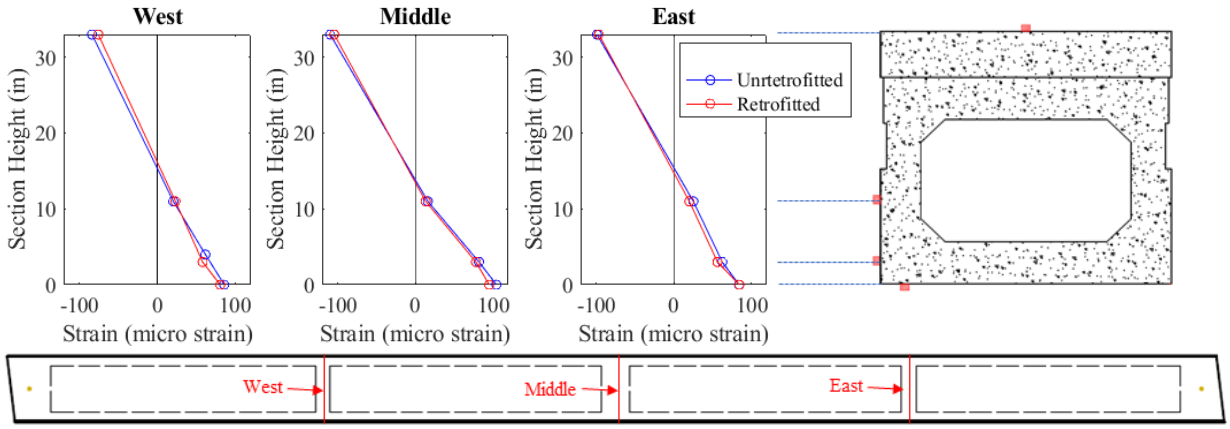

Figure 5-21 Strain profiles at peak force during the repeat service-level tests of Beam 2

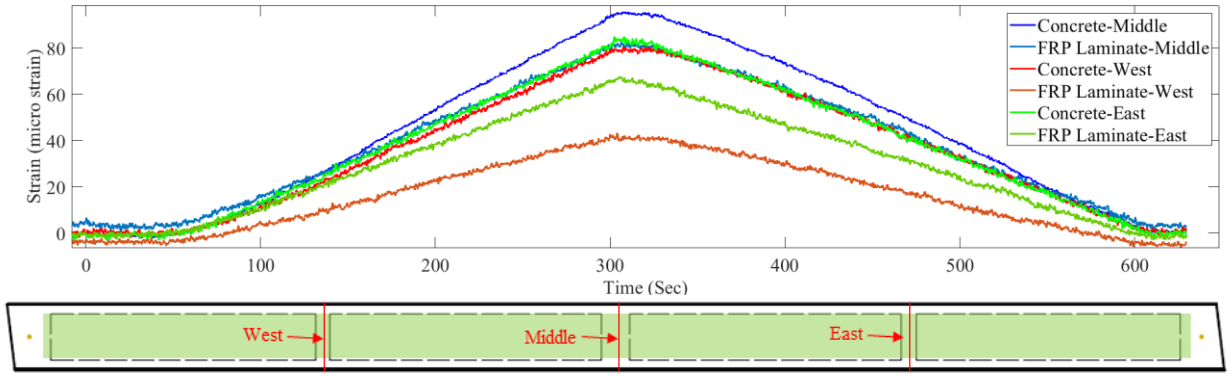

Figure 5-22 Comparison of strain variation between the FRP laminates and concrete at the bottom face of retrofitted Beam 2

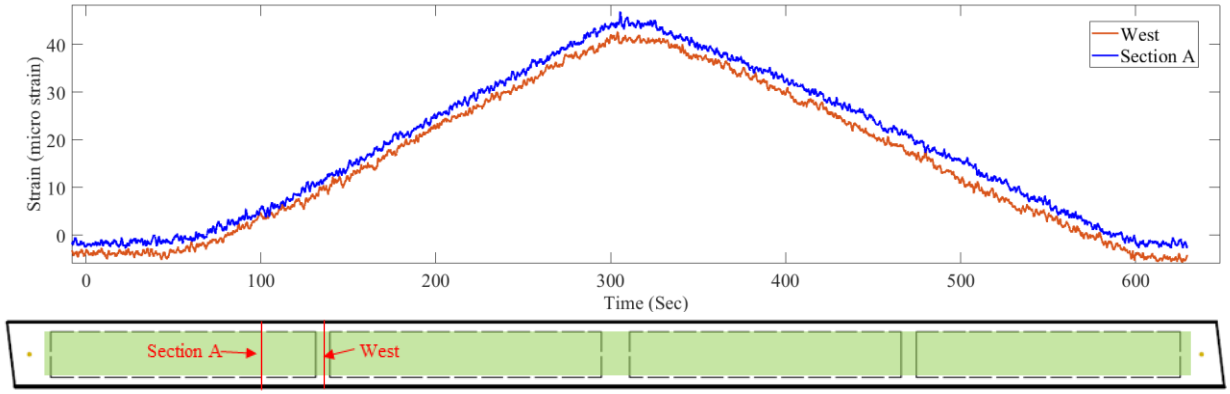

Figure 5-23 Comparison of strain readings on the west side of retrofitted Beam 2

5.2.2 Capacity-level test

The history of forces applied by each actuator during the displacement-controlled test to failure of Beam 2 is presented in Figure 5-24. The amplitudes of the actuator forces are similar up to the FRP failure, leading to a more symmetric moment distribution compared to that of Beam 1. This was expected after the replacement of the malfunctioning displacement transducer which was the source of error in the test of Beam 1. The total force resisted by Beam 2 is plotted against the mid-span displacement in Figure 5-25, while the moment-rotation response is presented in Figure 5-26. The change in the slope of the force-deformation and moment-rotation response curves indicates the opening of crack in concrete as confirmed from the strain measurements shown in Figure 5-27.

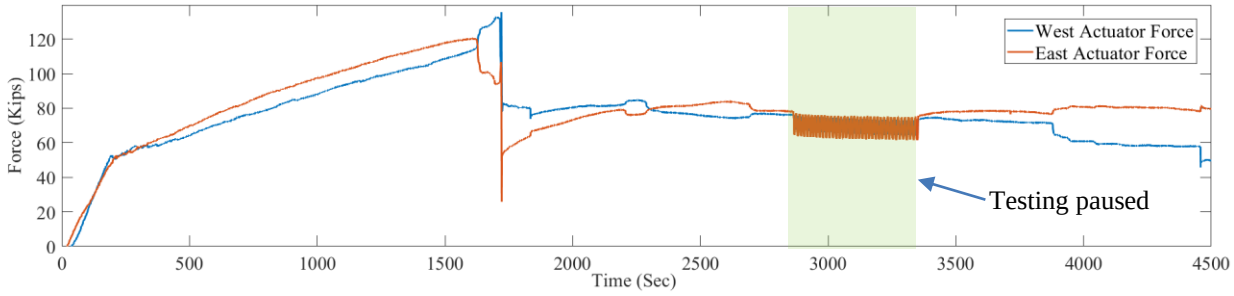

Figure 5-24 Actuator force time series during the capacity test of retrofitted Beam 2

Following the beam cracking, the applied load was resisted until debonding of FRP laminate was initiated on the East side of the beam as indicated in Figure 5-26. The debonding can also be inferred from the drop in the strain on the East of the beam as illustrated in Figure 5-28 and Figure 5-29. It can be also observed from Figure 5-29 that the strain in the laminate increased at the east end, indicating a redistribution of the force. Following this event, the total force resisted by the beam remained constant until debonding of FRP laminate occurred on the west side, which was shortly followed by FRP delamination and concrete spalling as the bond between the FRP and the concrete was strong enough to cause spalling of the concrete cover. This sequence of events can be observed in the plots of Figure 5-29 that focus on the failure region of response.

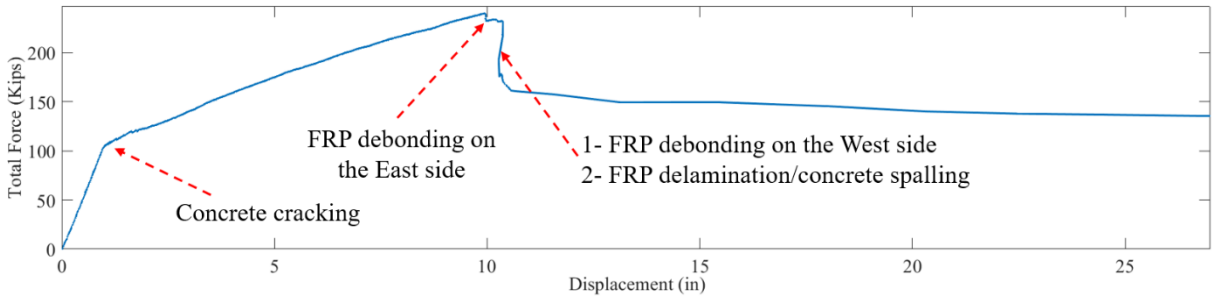

Figure 5-25 Total force vs. mid-span displacement during the capacity test of retrofitted Beam 2

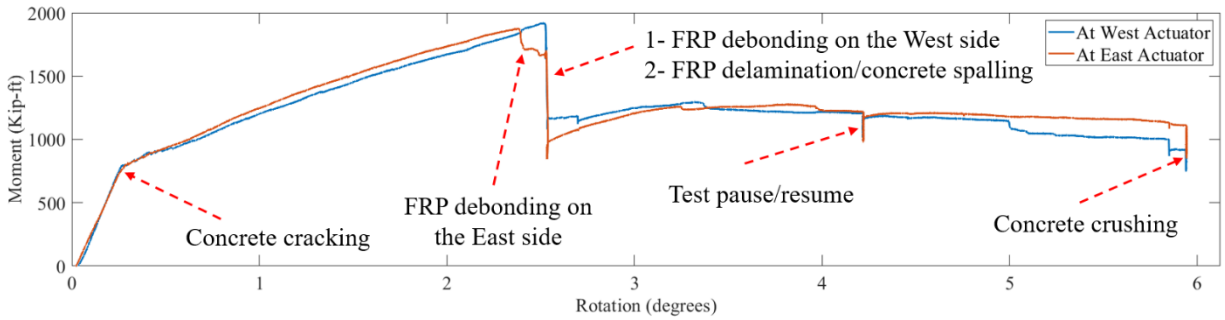

Figure 5-26 Moment vs. beam rotation during the capacity test of retrofitted Beam 2

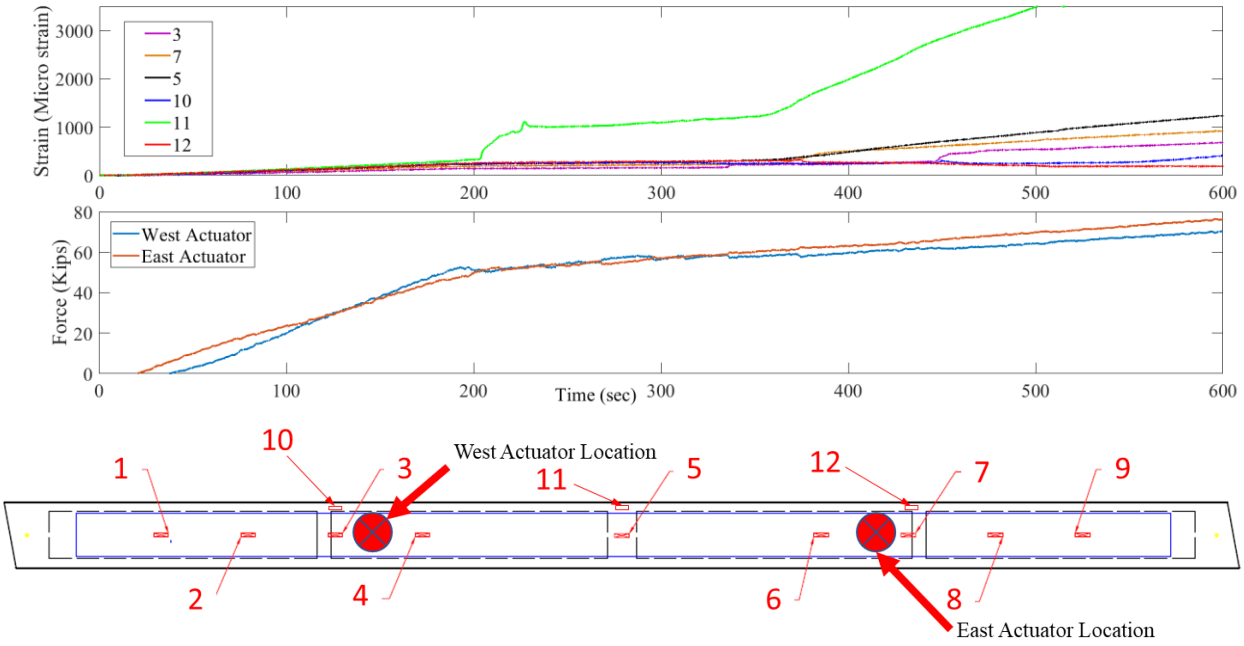

Figure 5-27 Strain variation at the concrete cracking region of response

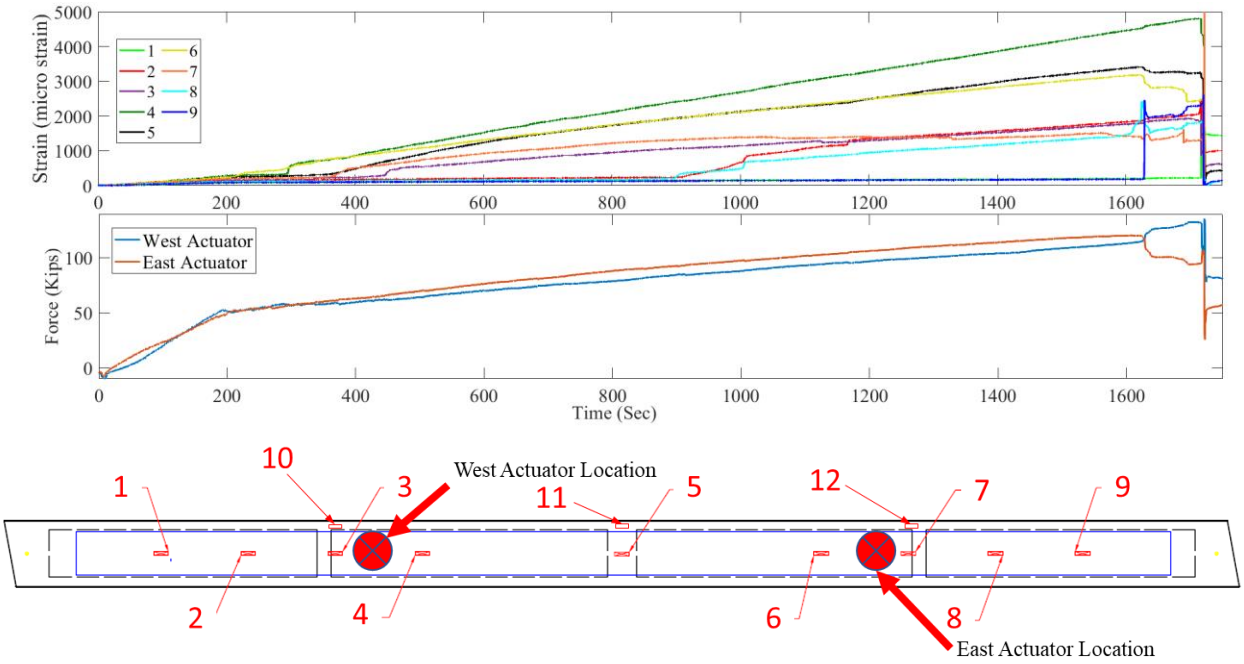

Figure 5-28 Strain time series measured on the FRP laminate

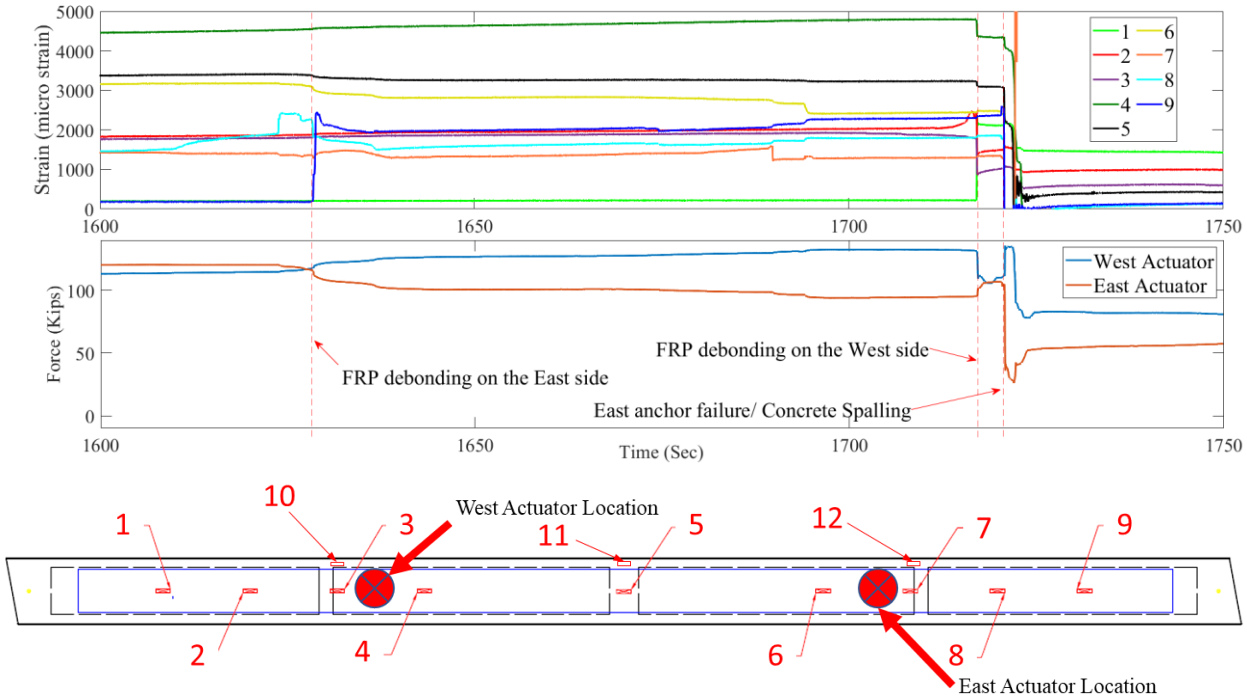

Figure 5-29 Variation of strain during the failure of the FRP retrofit

Figures 5-30 through 5-35 represent the state of the damage following the test. The cracks on the white epoxy in Figure 5-30 are indicative of the debonding that occurred on the West side of the beam. Closer to the middle of the beam where the moments were higher than the beam ends, the debonded FRP laminate transitioned into delaminated FRP as well as concrete spalling. This is shown in Figures 5-31 and 5-32. On the East side of the beam, the FRP was completely detached from the concrete substrate as shown in Figures 5-33 through 5-35. These figures also present the state of the anchors on the East side of the beam following the failure of the retrofit. As discussed in Chapter 4, compared to the West side, the anchors on the East were further distributed to investigate the effect of the anchor layout on the performance of the retrofit. Out of seven anchors embedded on this side, five were fractured at the interface of the concrete and the FRP laminate, indicating that the anchors reached their capacities. One of the anchors, located at the east end, was pulled out from the concrete which indicates a lack of adequate bond. Lastly, one anchor was found to be embedded less than an inch inside the concrete, due to mishandling during the application of the FRP system, eliminating its participation in resisting the loads. Overall, the distributed anchors seem to be less effective in prolonging the bond between the FRP laminate and concrete.

The test continued after the failure of the retrofit scheme. As shown in Figures 5-24 through 5-26, the resistance of the beam was stable as the actuator displacement increased. The test eventually stopped due to extensive concrete crushing at the location of the load application by the two actuators, after the midspan of the beam had been displaced by more than 26 in.

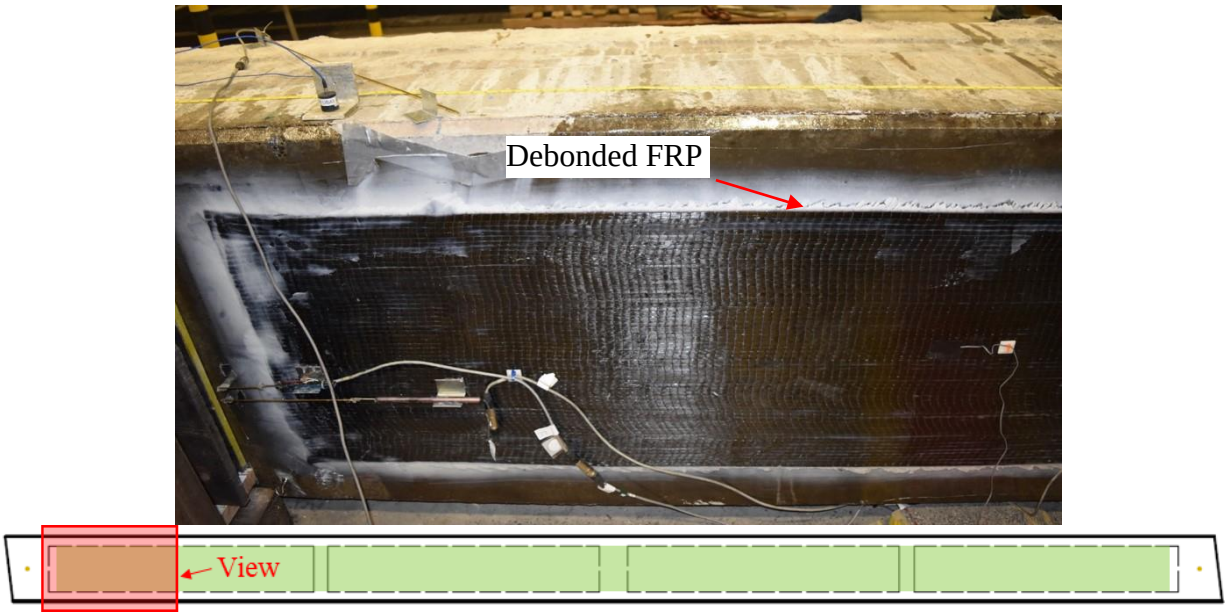

Figure 5-30 FRP Debonding at the West end

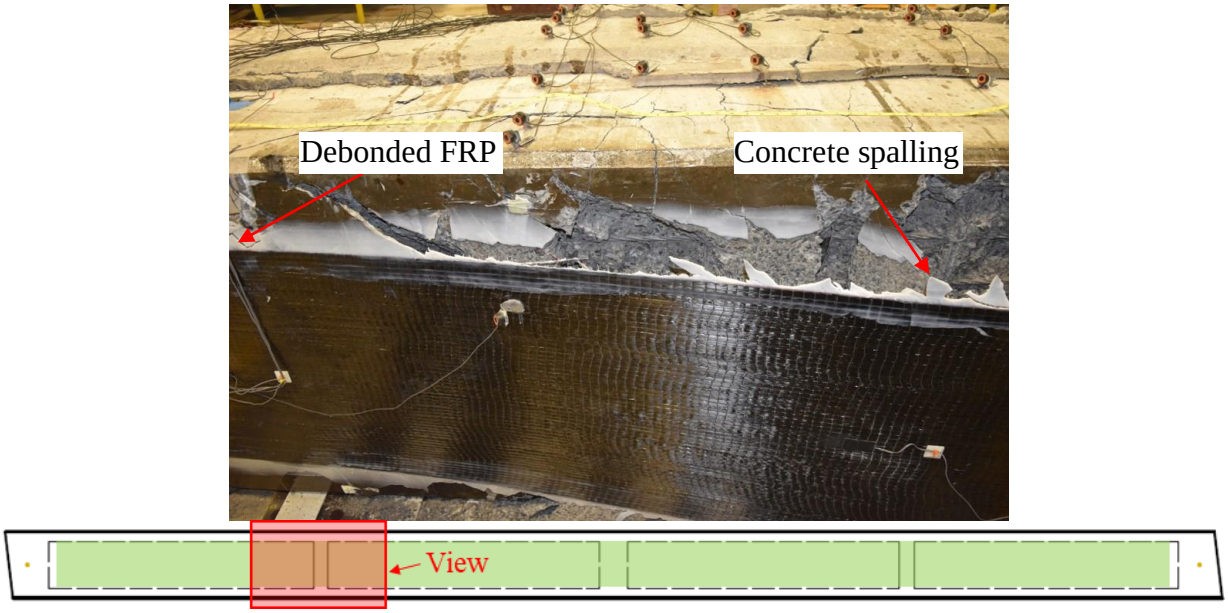

Figure 5-31 Transitioning from FRP debonding to concrete spalling at the West actuator location

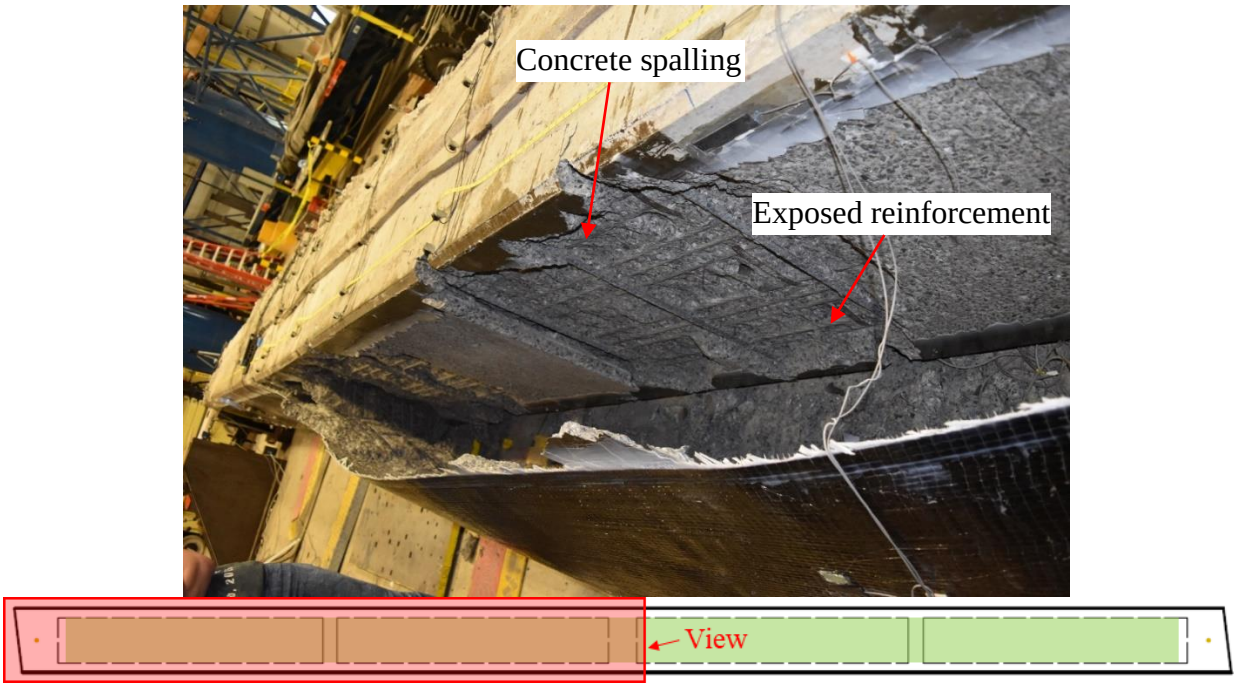

Figure 5-32 Concrete spalling at the maximum moment zone

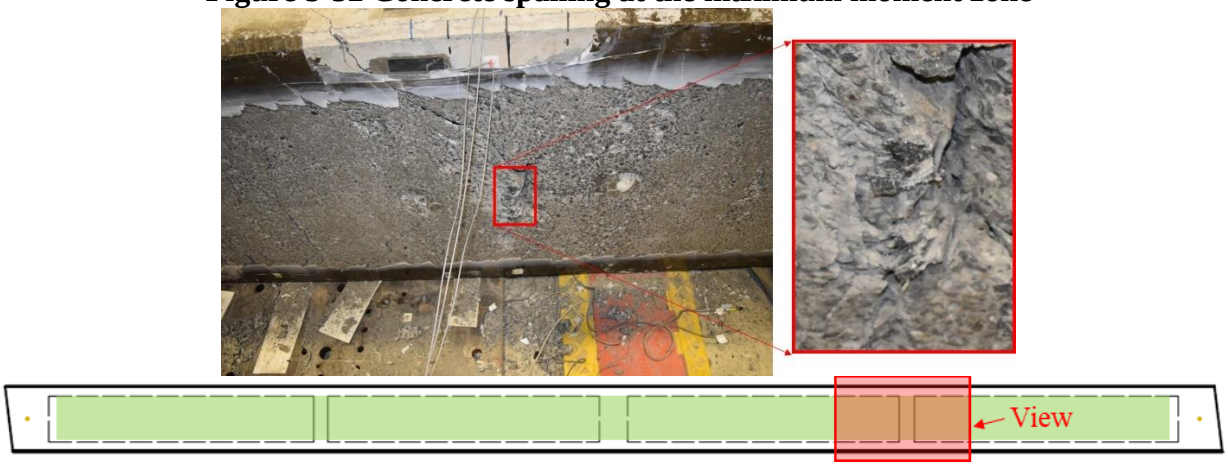

Figure 5-33 Anchor breakage at the east solid segment

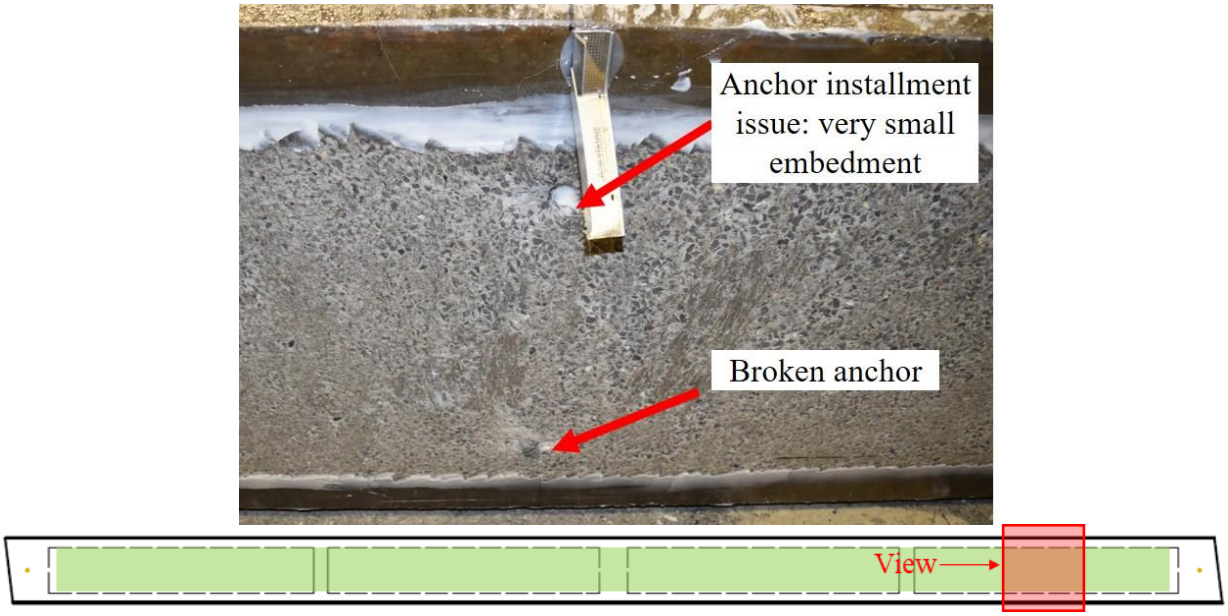

Figure 5-34 Status of Anchors at the east hollow segment

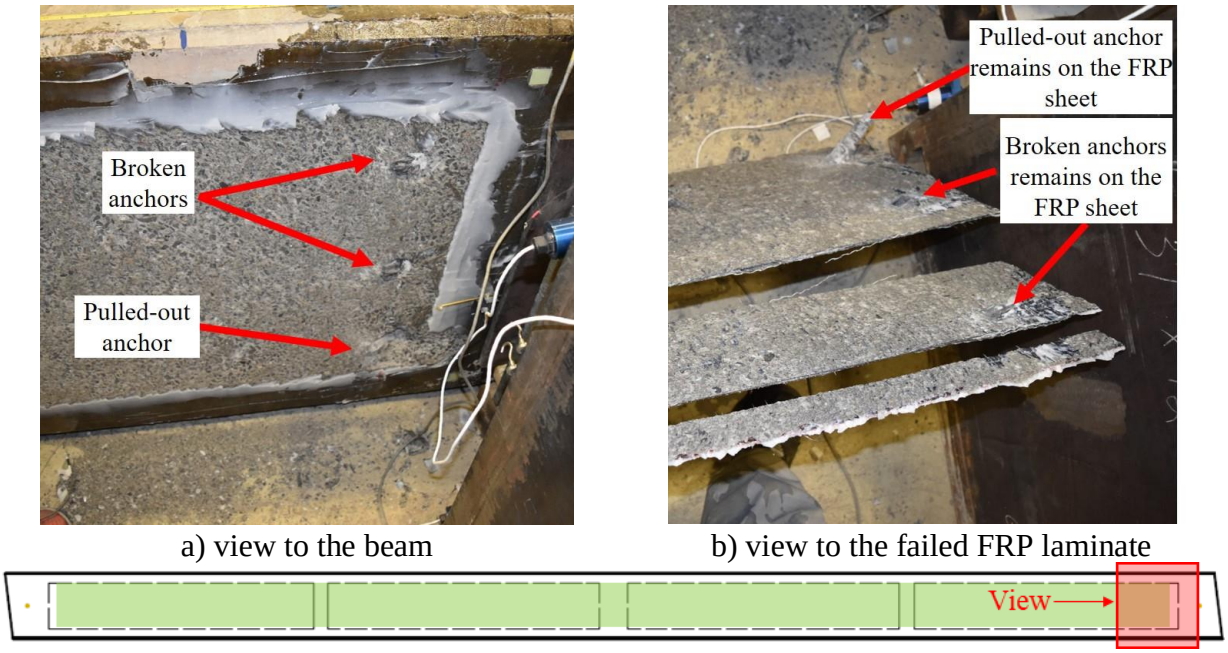

a) view to the beam

b) view to the failed FRP laminate

Figure 5-35 Status of Anchors at the east end

5.3 Beam 3

5.3.1 Service-level tests: Pre and Post Retrofit

The history of the total load applied to Beam 3 during the repeat service-level tests prior to and after implementing the retrofit is presented in Figure 5-36. It can be observed that the loading profile between the tests of the unretrofitted and retrofitted are practically identical.

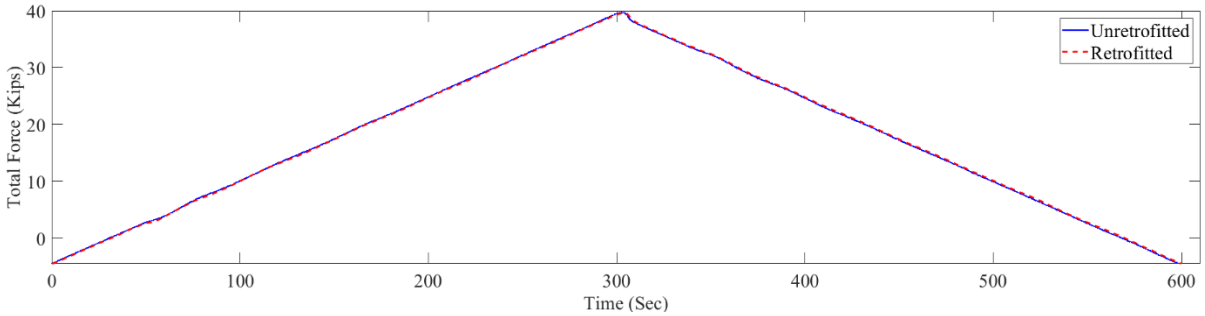

Figure 5-36 Total force time series during the service-level tests of Beam 3

Figure 5-37 compares the force-deformation response of the beam prior to and after the retrofit. A decrease of 2.9 percent in the maximum displacement at the peak force was observed due to the retrofit, indicating an increase in the stiffness of the beam. This is consistent with the observations from the tests on Beams 1 and 2. The strains measured at the mid-span section, as shown in Figure 5-38, also indicate a reduction of the beam deformation due to the retrofit at all locations along the section at every instant of the tests. A similar trend is observed in the strain profiles obtained at the peak forces of the tests from three sections along the beam presented in Figure 5-39.

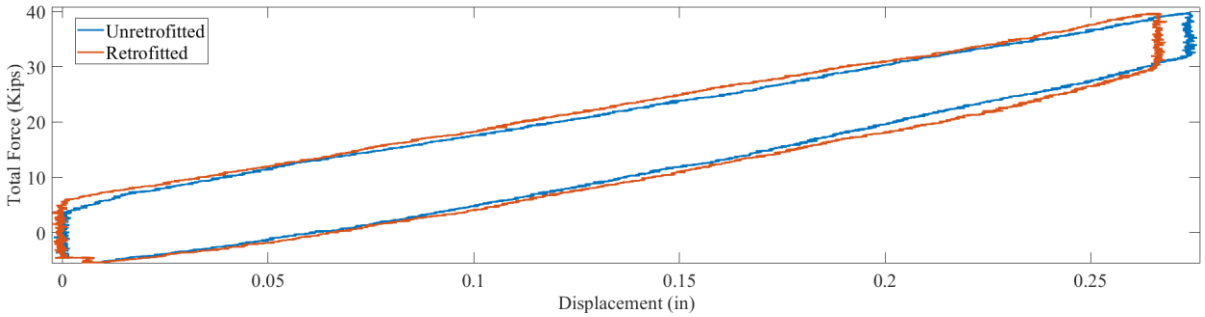

Figure 5-37 Total force vs. mid-span displacement during the repeat service-level tests Beam 3

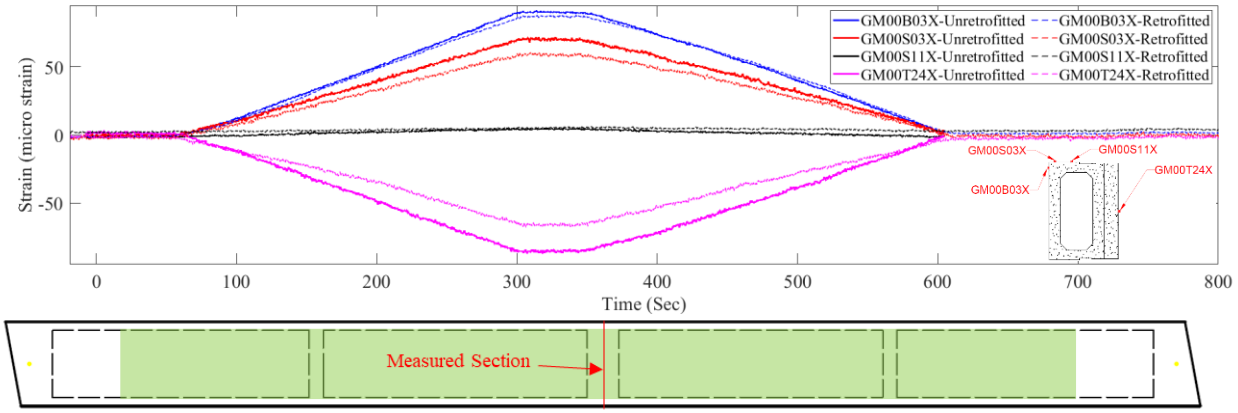

Figure 5-38 Strain time series during the repeat service-level tests of Beam 3

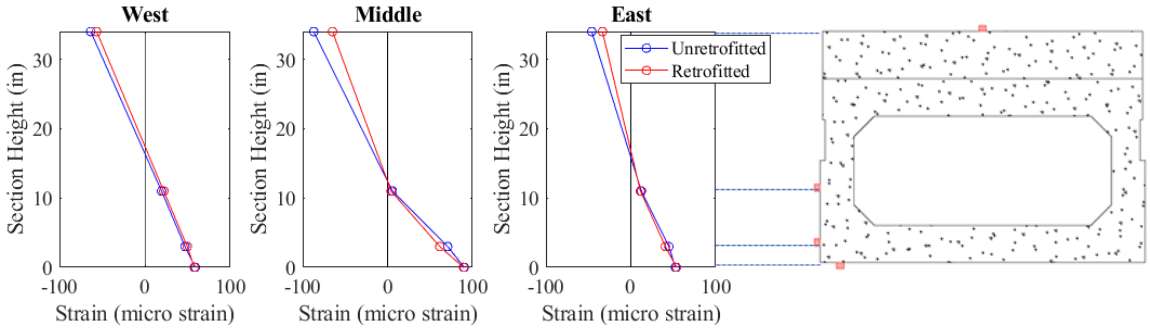

Figure 5-39 Strain profiles at peak force during the repeat service-level tests of Beam 3

The comparison of strains between the concrete and the FRP laminate measured at the bottom face of three sections along Beam 3 is presented in Figure 5-40. The strain variations in the FRP laminate tend to follow those in concrete in all sections. However, the strains are lower in the FRP laminates. This observation is consistent with the measurements on the other two beams as discussed in a previous section.

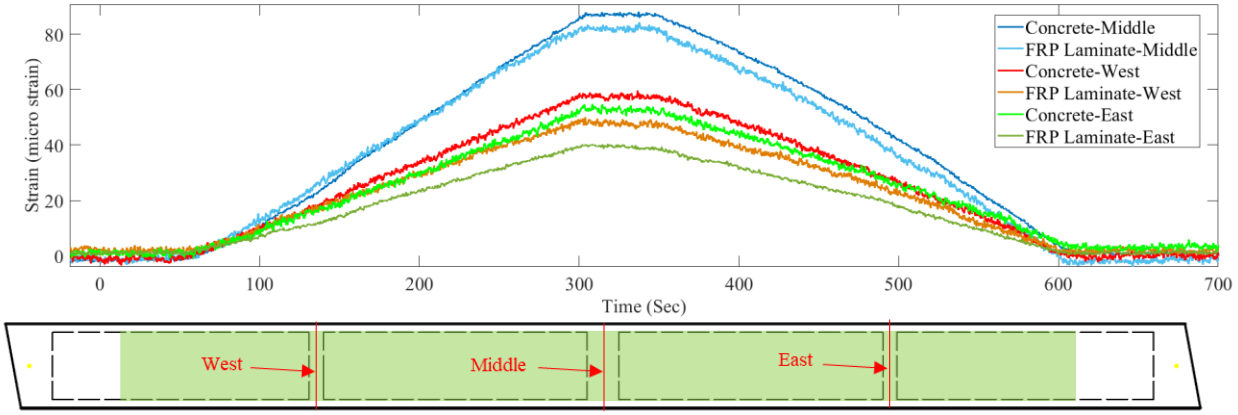

Figure 5-40 Comparison of strain variation between the FRP laminates and concrete at the bottom face of retrofitted Beam 3

5.3.2 Capacity-level test

The history of forces applied by each actuator during the displacement-controlled test of Beam 3 is presented in Figure 5-41. The amplitudes of the forces are close to each other prior to the FRP failure, leading to a symmetric moment distribution. The total force resisted by Beam 3 is plotted against the mid-span displacement in Figure 5-42, while the moment-rotation response is presented in Figure 5-43. As in the capacity tests of the other two beams, concrete cracking followed the elastic response of Beam 3. Moreover, the comparison of strains between the concrete and the FRP laminate, shown in Figure 5-44, indicates a drop in the concrete strain measurements as a result of strain relaxations at the location of the strain gauge due to the initiation of cracks surrounding the gauge.

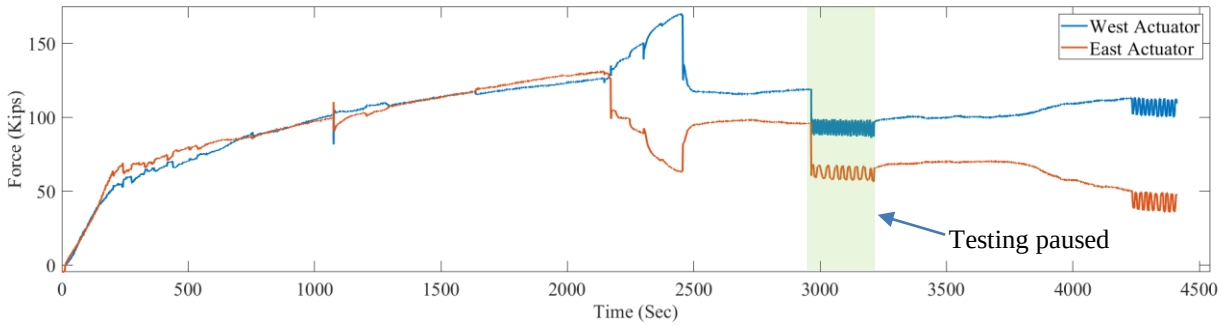

Figure 5-41 Actuator force time series during the capacity test of retrofitted Beam 3

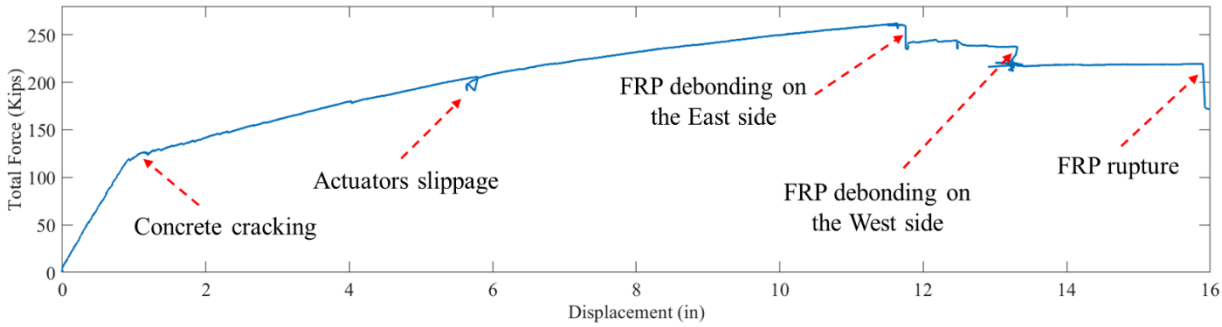

Figure 5-42 Total force vs. mid-span displacement during the capacity test of retrofitted Beam 3

Following the beam cracking, a minor slippage occurred at the actuator supports, resulting in a drop in the demand on the beam which was shortly recovered. As the displacement demand increased, debonding of FRP laminate on the east side of the beam was observed, leading to a drop in the resistance at a beam rotation of 2.5 degrees, as shown in Figure 5-43. The debonding can also be inferred from the drop in the strain measured by Gauge 3 as illustrated in Figure 5-45.

It can be also observed from this figure that strain read at Gauge 4, which was closer to the East end, increased and became closer to that of Gauge 3. This indicates a more uniform distribution of stress in the debonded FRP laminate after it debonded. Following this event, debonding occurred at the west side of the beam, as illustrated in Figures 5-43 and 5-45. These events resulted in a completely unbonded FRP laminate which continued to carry load transferred to it only through the anchors. Once the strain capacity in the FRP laminate was reached, it fractured at multiple points simultaneously, which led to the drop in the resistance as shown in Figure 5-43, at an angle of 3.5 degrees.

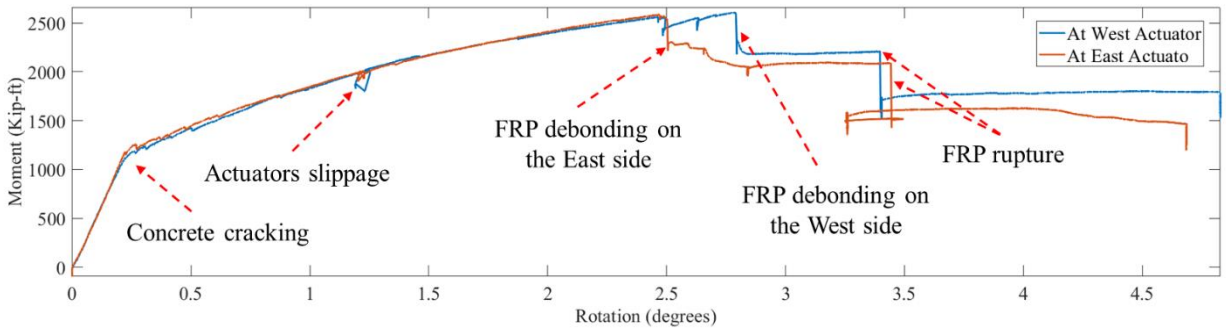

Figure 5-43 Moment vs. beam rotation during the capacity test of retrofitted Beam 3

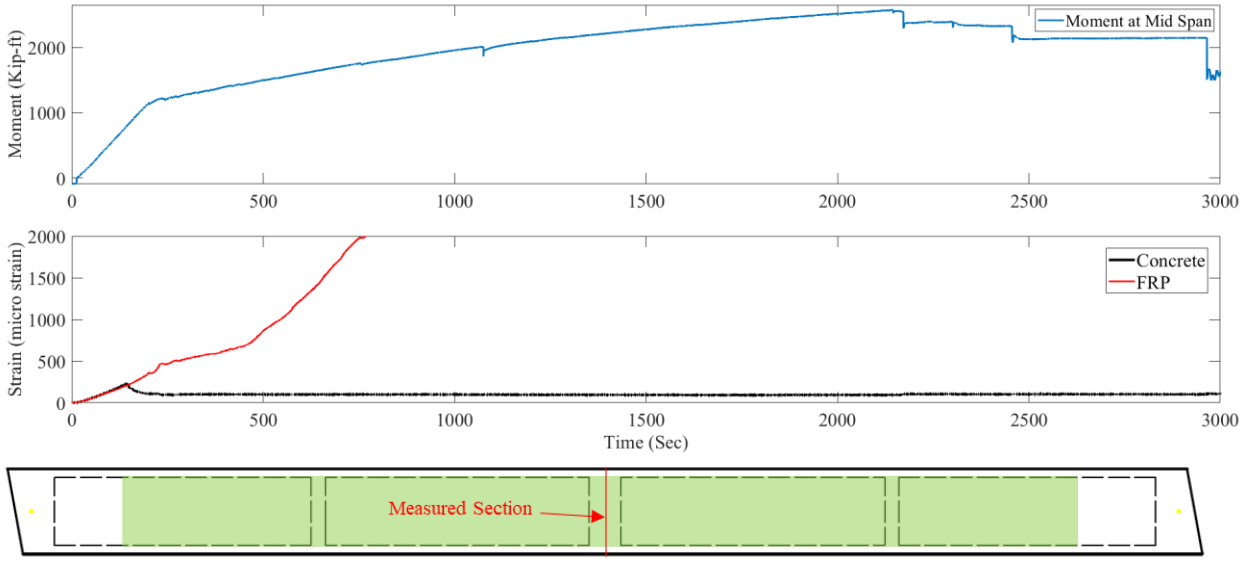

Figure 5-44 strain variation at the concrete cracking region of response

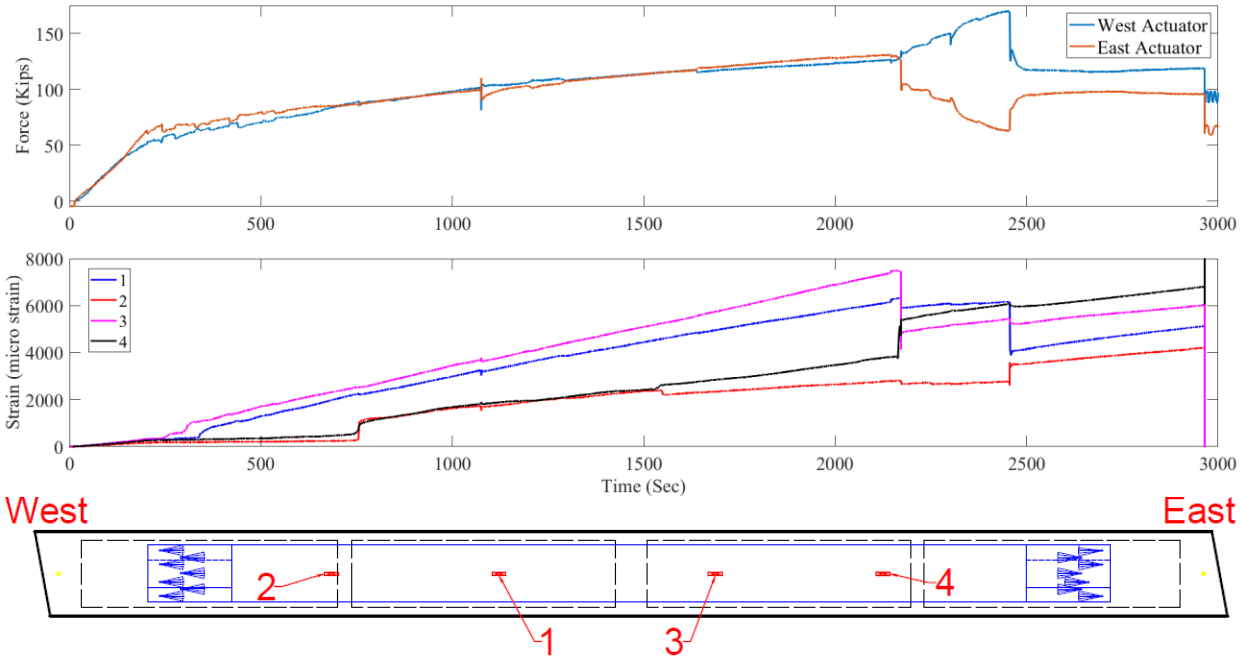

Figure 5-45 Strain time series measured on the FRP laminate

Figures 5-46 through 5-48 present the state of the beam following the capacity-level tests. Except for a small segment, the FRP laminate was fractured between its supports, as shown in Figure 5-46. The end zones, which included seven FRP anchors sandwiched between FRP laminates, remained in place and only partial FRP delamination was identified. The delaminated segments, shown in Figure 5-48, are to the right and left of the white lines marked on the West and East end zones, respectively. Also, the location of the anchors was marked with red and yellow stickers on the West and East end zones, respectively, showing that the anchored zone remained almost intact.

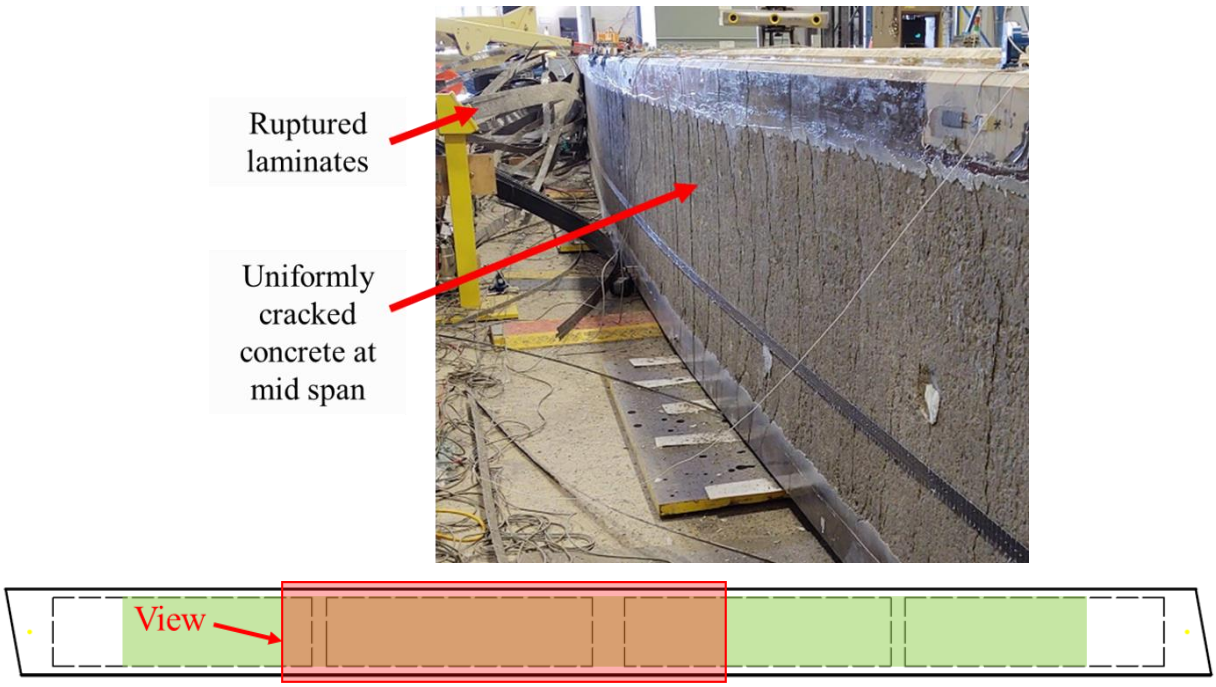

Figure 5-46 State of damage at the middle of Beam 3

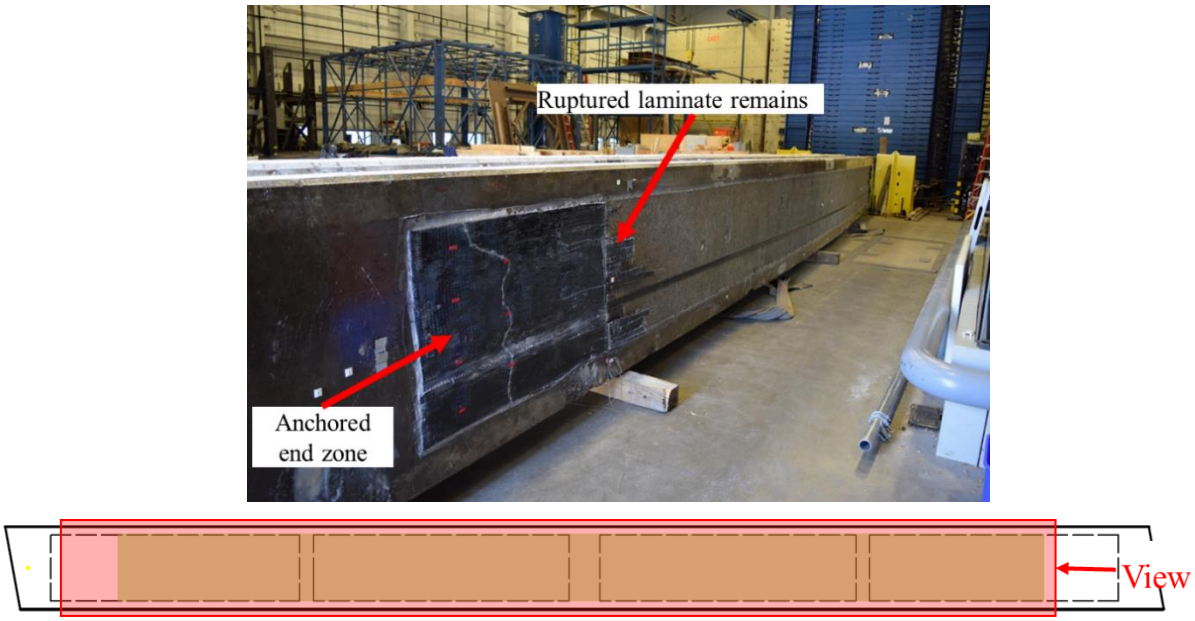

Figure 5-47 strain variation at the concrete cracking region of response

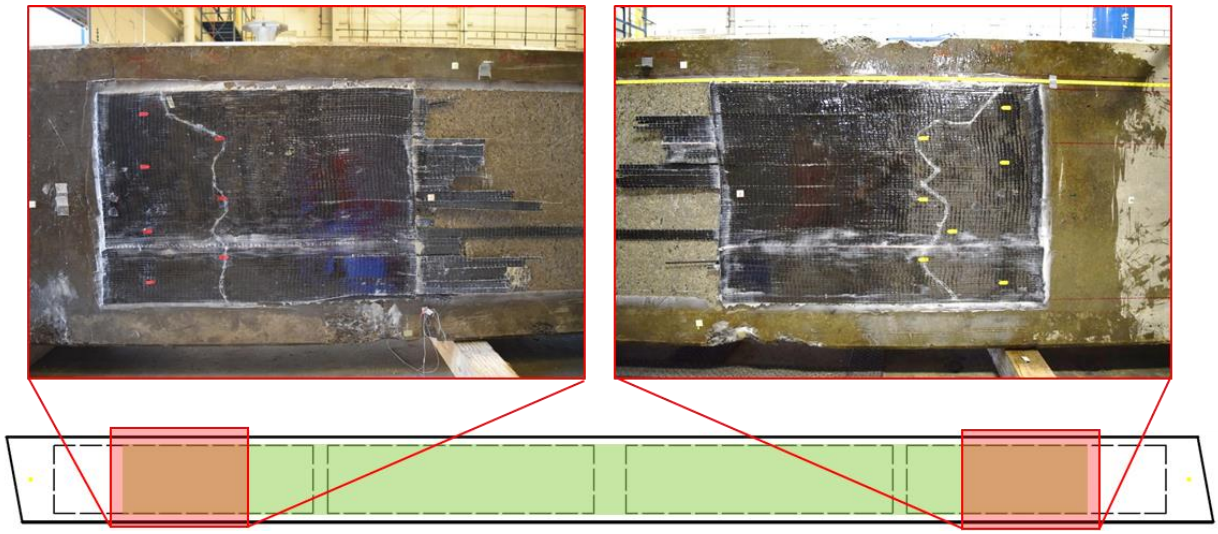

Figure 5-48 State of damage at the end zones of FRP laminate

CHAPTER 6
DISCUSSION AND COMPARISON OF RESULTS

6.1 Overall Performance

As stated in Chapter 2, the main objective of this project was to increase the flexural capacity of the beams. The moment-rotation response of the three tested beams, recorded at the west actuator, is shown in Figure 6-1. As discussed in Chapter 5, the post-retrofit-failure response represents the behavior of the unretrofitted beams which is confirmed by analytical calculations for the three beams. Therefore, comparing the strength achieved prior to and after the retrofit failure provides an estimate of the increase in the flexural capacity. All three the retrofitted beams exhibited significant capacity improvements ranging between 22 to 50 percent as summarized in Table 6-1. The strength at the onset of the retrofit failure is also compared to that achieved from the unretrofitted beams. This comparison, which takes into account the setbacks in the resistance due to the debonding of the FRP laminate, indicates improvements between 19 to 26 percent in the strength.

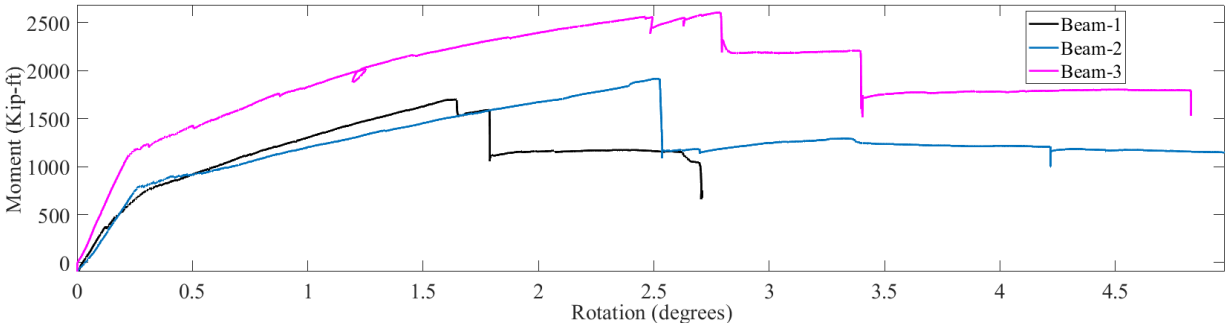

Figure 6-1 Comparison of the response of the beams

Table 6-1 Capacity improvements compared to the unretrofitted beam.

Specimen	Capacity improvement wrt. bare beam (at peak load)	Capacity improvement wrt. bare beam (at failure)
Beam 1	21.90%	18.60%
Beam 2	45.60%	40.50%
Beam 3	50.00%	25.70%

The mid-span displacement of the beams, which is normalized to the span length and plotted in Figure 6-2 shows maximum deformations of 0.96% prior to the retrofit failure of Beam 1. This parameter is increased to 1.60% and 2.45% in the response of Beams 2 and 3. Given the beams resisted forces at larger deformations following the retrofit failure, it can be concluded that the retrofit limited the deformation capacity of the beams. However, the deflections at the onset of the retrofit failure were evident visually, providing a warning of failure. Also, in the case of Beams 2 and 3, the deflections are beyond the common service-level limits (1/800 to 1/1000). An example of the deflected beam at the onset of retrofit failure is provided for Beam 3 in Figure 6-3.

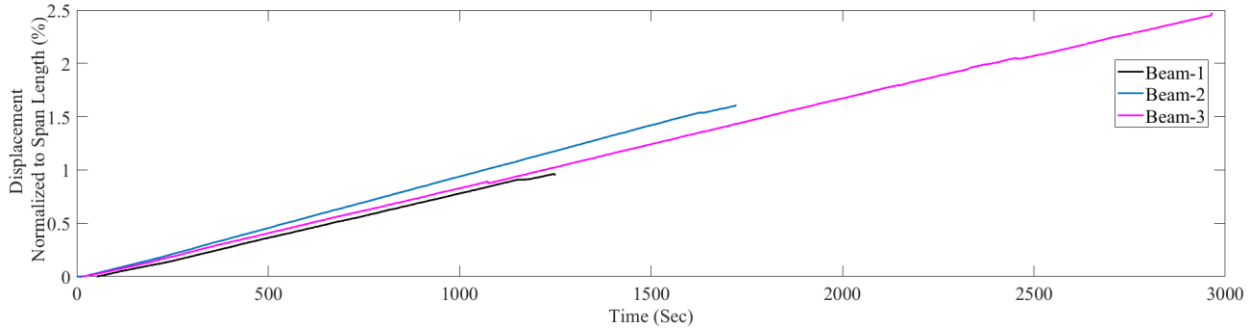

Figure 6-2 Displacement history of the beams at midspan (plotted up to the retrofit failure)

Figure 6-3 Deformation of Beam 3 at the onset of retrofit failure

The retrofit also slightly improved the bending stiffness of the beams, up to 7% as discussed in Chapter 5 based on the data from the service load level tests. Although this improvement was not an objective of this project, it indicates the potential of this retrofit system in addressing the serviceability issues related to beam deflection. This can be achieved by reducing the dead-load induced deflections prior to the application of the retrofit through methods like beam jacking. However, beam jacking involves practical challenges which are not studied here.

In terms of the failure mode, Beams 1 and 2 experienced an FRP delamination and concrete spalling which exposed the prestressing strands and the shear reinforcement at the regions of maximum moment. The retrofit of Beam 3 failed by fracture of the FRP laminate, while the concrete substrate, which exhibited uniform flexural cracking along the region of the maximum moment, remained in place. It should be noted that the debonding of the FRP laminate preceded the retrofit failure in all the beams, underscoring the role of anchors in mitigating a failure dominated by debonding. Also, the laminate debonding is visually identifiable and can provide an early warning of failure.

6.2 Comparison of response

In order to compare the responses of Beam 3 (4 ft. wide) and Beams 1 and 2 (3 ft. wide), the moment resistance per width of the beams is calculated. The resulted moment-rotation response is shown in Figure 6-4. Also, the total area of FRP laminate used at the maximum moment region of each beam is summarized in Table 3-1 and repeated in Table 6-2 for convenience. There's an inverse relationship between the peak strength of the beams, shown in Figure 6-4, and the laminate area. This observation is counterintuitive since higher strengths are expected as the utilized laminate area increases. A similar trend is observed between the laminate area and the demand at which FRP laminate debonding occurred in the beams. Moreover, the comparison of deformation capacities between the beams indicates higher ductility was achieved with less FRP laminate stiffness. These trends can be explained by considering the interaction between the FRP laminate and the concrete as well as the anchor arrangement.

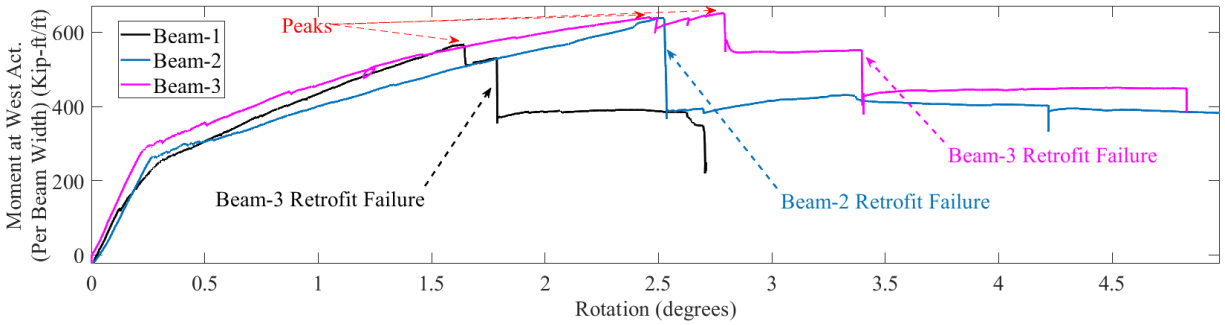

Figure 6-4 Moment-rotation response normalized to the unretrofitted beam capacity

Table 6-2 CFRP materials used for each beam.

Specimen	Beam width (ft)	Laminate area at midspan	Anchor area on each side	Laminate area per beam width	Anchor/laminate area ratio
	ft.	Sq. in.	Sq. in.	Sq. in./ft.	
Beam 1	3	5.76	3.08	1.92	0.53
Beam 2	3	3.84	3.08	1.28	0.80
Beam 3	4	2.56	3.08	0.64	1.20

6.2.1 Concrete-FRP Interface

The strain time-series responses during the service-level tests, provided in Chapter 5, indicate that the trends of the strains in the concrete substrate and the FRP laminate match closely due to the bond developed by the epoxy adhesive. On the other hand, the strains of the FRP laminate are smaller than those of the concrete substrate. This difference induces shear deformation in the epoxy at the concrete-FRP interface. As the transverse load increases, the shear stress reaches the shear strength of the epoxy, leading to the debonding of the FRP laminate. Therefore, as the thickness and cross section of the laminate increase, the shear strength of the epoxy is reached at a lower demand. This justifies the debonding trend observed in Figure 6-4, according to which as the thickness of the laminate increases, debonding occurs earlier.

6.2.2 Anchor Arrangement

The scheme of the anchors installed in each beam as well as the distribution of the strain along the length of the FRP laminate prior to debonding are presented in Figure 6-5. The strains for each beam were normalized to their maximum value. The corresponding beam deformation as well as the bending moment diagram are provided in Figures 6-6 and 6-7 respectively. Overall, the strains dropped with the decrease in the deformation as expected. However, in the case of

Beam 1, the rate of the drop was higher in the region of the anchor layers located closer to the middle (inner anchors), especially on the west side where moment demand is maximum. This drop was approximately 60% percent of the maximum strain. A similar trend can be observed in Beam 2 around the inner anchors. However, in the case of Beam 3, where all of the anchors were concentrated at the end regions of the FRP laminate, such a change in the rate of strain drop was not observed. The strain is directly related to the stress and therefore the force carried by the FRP laminates. Given the rate of drop in the measured deflections is not higher in those regions, the drop in the strain (Force) in Beams 1 and 2 is due to the transfer of the force to the concrete through the inner anchors. The remaining force in the laminate is transferred to the concrete through the epoxy and the anchors located at the outer layer(s).

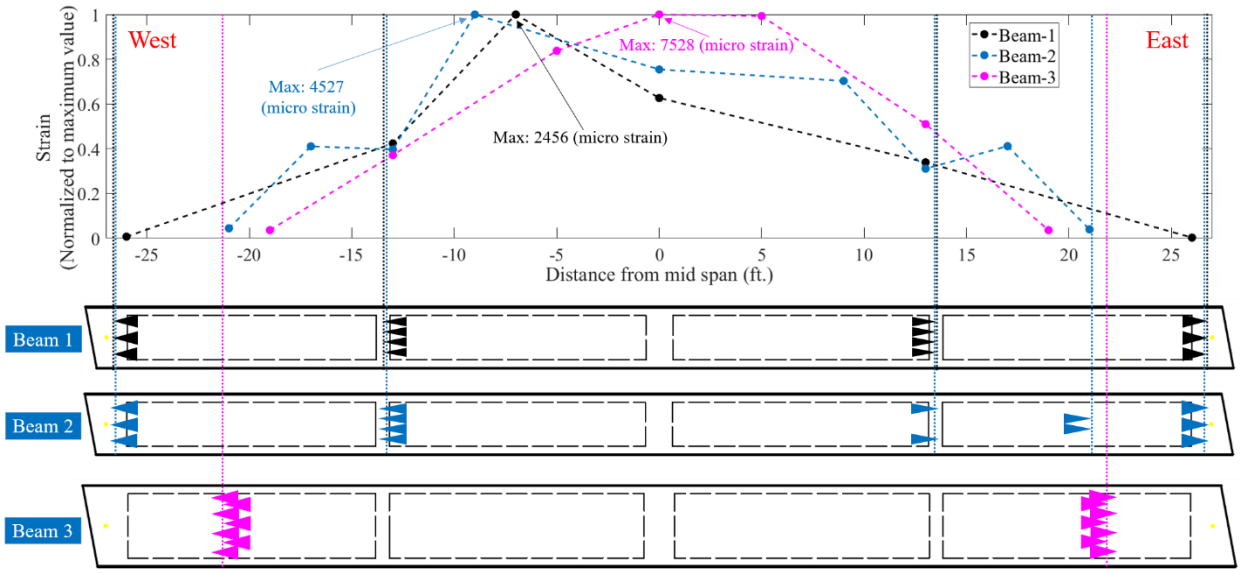

Figure 6-5 Strain distribution along the length of the laminate prior to debonding

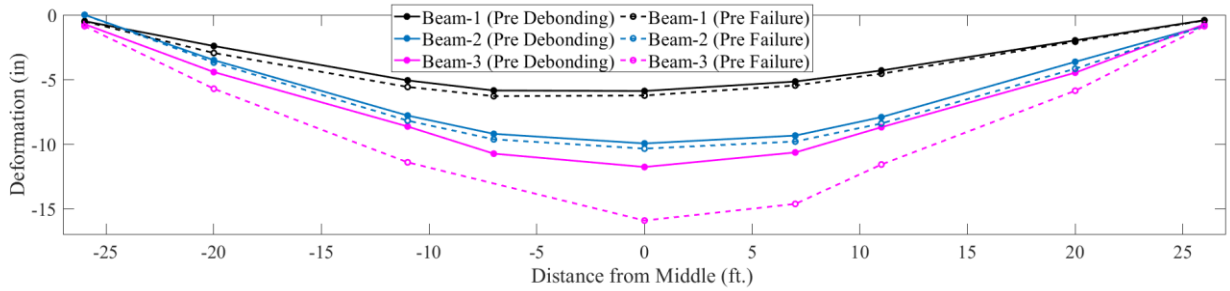

Figure 6-6 Deformation profile of the beams at the onset of debonding and failure

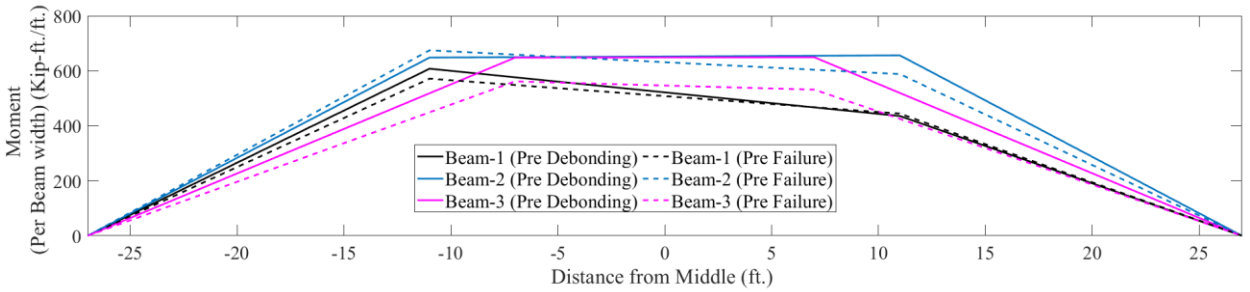

Figure 6-7 Bending moment diagram of the beams at the onset of debonding and failure

Figure 6-8 presents the distribution of the normalized strain along the length of the FRP laminate at the onset of the retrofit failure. Following the laminate debonding and consequently, the disruption of the load-transfer path through the epoxy, the strains increased in the outer layer(s). However, the inner anchors were still responsible for the largest drop in strain. Therefore, the tensile force in the laminate was not equally distributed between the anchors. Once the capacity of the anchors which sustained higher forces was reached, their failure resulted in a force redistribution among the remaining anchors. Due to the brittle nature of the failure in the anchors, this redistribution was not gradual. In the case of Beams 1 and 2, this redistribution resulted in the failure of the other anchors and ultimately the failure of the retrofit.

In the case of Beam 3, strain redistributions occurred following the FRP laminate debonding, which led to more uniform strains along the length of FRP as shown in Figure 6-8. It should be noted that the resulting strain distribution did not follow the beam deflection since the FRP laminate, and the concrete substrate were only connected at the end regions of the laminate. As discussed in Chapter 5, the retrofit failure occurred due to the fracture of the laminate which reached its fracture strain, leaving the anchors in place.

6.2.3 Conclusions

The changes in selected response quantities of Beams 2 and 3 with respect to those of Beam 1 are summarized in Table 6-3. The peak strength of the retrofitted beam at the onset of debonding was improved up to 31% after the application of smaller thickness of FRP laminates. This highlights the importance of reducing the bond stress to achieve higher capacities. In fact, similar to capacity design in RC frames, this can be considered as an additional check in the design procedure of ACI 440.2 R17, as it can determine the failure pattern of the retrofitted structure. In terms of the post-debonding behavior, the concentration of the anchors at the end regions of the

laminate in Beam 3 led to a relatively even distribution of forces in the laminate, while maintaining its ability to resist loads. This allowed the laminate to reach higher strains prior to failure compared to the other beams, resulting in a 90 percent increase in the deflection capacity at failure when compared to Beam 1.

Table 6-3 Performance improvements compared to Beam 1.

Specimen	Strength capacity improvement at peak	Strength capacity improvement at FRP failure	Deflection capacity improvement at peak	Deflection capacity improvement at FRP failure
Beam 2	25.70%	24.70%	44.80%	41.30%
Beam 3	31.20%	13.00%	50.90%	89.90%

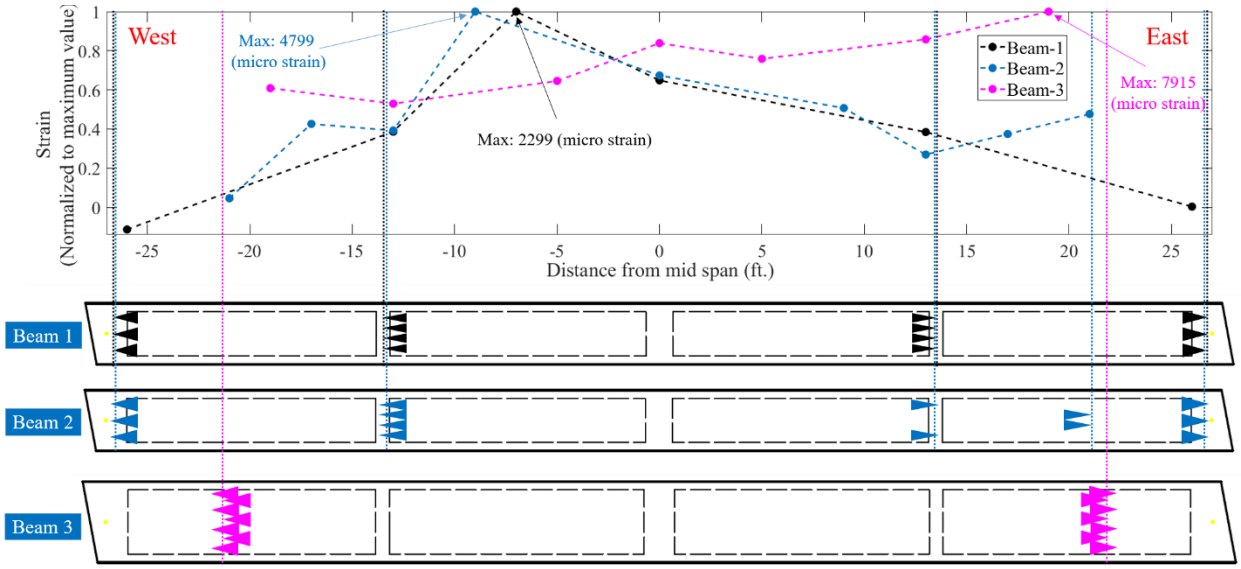

Figure 6-8 Strain distribution along the length of the laminate prior to failure

The research presented in this report provides much needed experimental data for the behavior of beams obtained from an actual bridge and retrofitted with FRP laminates and anchors. The tests indicate that the adopted retrofit scheme increases the stiffness, and mainly the strength of beams. Moreover, differences in the design of the retrofit scheme, i.e. the thickness of the FRP layer and the distribution of the anchors can lead to drastically different failure patterns.

6.2.4 Future Work for Code Implication

The results obtained from this experimental study can be further studied and combined and have an impact on the design methodology of the retrofit schemes for reinforced and prestressed

concrete structures. It is suggested to further complement this study with small scale tests on the behavior of anchors so that robust design guidelines can be developed for the anchor geometry and layout. These guidelines can include the required area of the anchors, as well as the length and overlap of the fans. Finally, the arrangement of the anchors needs to be further investigated with nonlinear finite element analyses and/or additional tests.

This research also indicated a strain incompatibility between concrete and the FRP, which was observed in the tests of all tree beams. This is contrary to the current design practice and requires further investigation with small-scale tests. These can determine the possible influence of the beam flipping during the application of the FRP, as the gravity loads were essentially negated. In needed, that could be achieved in the field with beam jacking, if deemed necessary.

Determining the desired failure pattern and quantifying the associated safety factors is another topic that can be further investigated, and changes can be introduced in the current design guidelines. That can include the design capacity to considered, as well as the strain limits on the FRP laminates.

REFERENCES

AASHTO (2017), LRFD Bridge Design Specifications, 8th Edition.

ACI Committee. (2014). Building code requirements for structural concrete (ACI 318-14) and commentary (ACI 318R-14), American Concrete Institute.

ASTM (2000). Standard Test Method for Tensile Properties of Polymer Matrix Composite Materials D 3039/D 3039M-00, American Society for Testing and Materials, West Conshohocken, PA.

ASTM (2013). Standard Test Method for Obtaining and Testing Drilled Cores and Sawed Beams of Concrete, ASTM C42/C42M-12, American Society for Testing and Materials, West Conshohocken, PA.

Avendano, A., Hovell, C., Moore, A., Dunkman, D., Nakamura, E., Bayrak, O., & Jirsa, J. (2013). Pretensioned box beams: Prestress transfer and shear behavior.

Brecht, H., Hanson, J., & Hulsbos, C. (1965). Ultimate shear strength tests of full-sized prestressed concrete beams.

Ceroni, F., Pecce, M., Matthys, S., & Taerwe, L. (2008). Debonding strength and anchorage devices for reinforced concrete elements strengthened with FRP sheets. Composites Part B: Engineering, 39(3), 429-441.

Computers and Structures Inc. (CSI) (2020), SAP2000 V. 21 software.

De Lorenzis, L., & Nanni, A. (2001). Shear strengthening of reinforced concrete beams with near-surface mounted fiber-reinforced polymer rods. Structural Journal, 98(1), 60-68.

Dias, S. J., & Barros, J. A. (2005). Shear strengthening of RC beams with near-surface-mounted CFRP laminates.

Fathelbab, F. A., Ramadan, M. S., & Al-Tantawy, A. (2014). Strengthening of RC bridge slabs using CFRP sheets. Alexandria Engineering Journal, 53(4), 843-854.

Harries, K. A. (2009). Structural testing of prestressed concrete girders from the Lake View Drive Bridge. Journal of Bridge Engineering, 14(2), 78-92.

Harries, K. A., Kasan, J., & Aktas, J. (2009). Repair methods for prestressed girder bridges.

Hassan, T., & Rizkalla, S. (2003). Investigation of bond in concrete structures strengthened with near surface mounted carbon fiber reinforced polymer strips. Journal of composites for construction, 7(3), 248-257.

International Concrete Repair Institute (ICRI) (2013). Selecting and Specifying Concrete Surface Preparation for Sealers, Coatings, Polymer Overlays, and Concrete Repair. Technical Guideline, St. Paul, MN.

Kim, Y. J., Green, M. F., & Fallis, G. J. (2008). Repair of bridge girder damaged by impact loads with prestressed CFRP sheets. Journal of Bridge Engineering, 13(1), 15-23.

Klaiber, F., Wipf, T., & Kash, E. (2004). Effective Structural Concrete Repair-Volume 2 of 3: Use of FRP to Prevent Chloride Penetration in Bridge Columns.

Larson, K. H., Peterman, R. J., & Rasheed, H. A. (2005). Strength-fatigue behavior of fiber reinforced polymer strengthened prestressed concrete T-beams. Journal of composites for construction, 9(4), 313-326.

Martin, J. A., & Lamanna, A. J. (2008). Performance of mechanically fastened FRP strengthened concrete beams in flexure. Journal of composites for construction, 12(3), 257-265.

Naito, C., Sause, R., & Thompson, B. (2008). Investigation of damaged 12-year old prestressed concrete box beams. Journal of Bridge Engineering, 13(2), 139-148.

National Bridge Inventory (NBI). (2020). "NBI ASCII files." https://www.fhwa.dot.gov/bridge/nbi/ascii2020.cfm

Obaidat, Y. T., Heyden, S., Dahlblom, O., Abu-Farsakh, G., & Abdel-Jawad, Y. (2011). Retrofitting of reinforced concrete beams using composite laminates. Construction and Building Materials, 25(2), 591-597.

Panchacharam, S., & Belarbi, A. (2002). Torsional behavior of reinforced concrete beams strengthened with FRP composites. Paper presented at the First FIB Congress, Osaka, Japan.

Parretti, R., & Nanni, A. (2004). Strengthening of RC members using near-surface mounted FRP composites: Design overview. Advances in Structural Engineering, 7(6), 469-483.

Rahimi, H., & Hutchinson, A. (2001). Concrete beams strengthened with externally bonded FRP plates. Journal of composites for construction, 5(1), 44-56.

Ritchie, P. A. (1989). External reinforcement of concrete beams using fiber reinforced plastic.

Rosenboom, O. A. (2006). Behavior of FRP repair/strengthening systems for prestressed concrete.

Shahawy, M., & Beitelman, T. E. (1999). Static and fatigue performance of RC beams strengthened with CFRP laminates. Journal of Structural Engineering, 125(6), 613-621.